

**LOW CAPACITY RELIQUEFIER FOR STORAGE OF
CRYOGENIC FLUIDS**

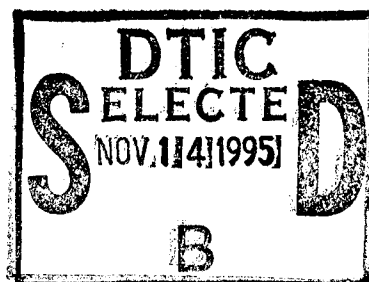
Woodrow Ellison
K. Randall Kohuth

General Pneumatics Corporation
Western Research Center
7662 E. Gray Road, Suite 107
Scottsdale, AZ 85260-6910

19951113 154

November 1993

Final Report



Distribution authorized to DoD components only; Proprietary Information; November 1993. Other requests for this document shall be referred to AFMC/STI.

WARNING - This document contains technical data whose export is restricted by the Arms Export Control Act (Title 22, U.S.C., Sec 2751 et seq.) or The Export Administration Act of 1979, as amended (Title 50, U.S.C., App. 2401, et seq.). Violations of these export laws are subject to severe criminal penalties. Disseminate IAW the provisions of DoD Directive 5230.25 and AFI 61-204.

DESTRUCTION NOTICE - For classified documents, follow the procedures in DoD 5200.22-M, Industrial Security Manual, Section II-19 or DoD 5200.1-R, Information Security Program Regulation, Chapter IX. For unclassified, limited documents, destroy by any method that will prevent disclosure of contents or reconstruction of the document.

DTIC QUALITY INSPECTED 8



PHILLIPS LABORATORY
Space and Missiles Technology Directorate
AIR FORCE MATERIEL COMMAND
KIRTLAND AIR FORCE BASE, NM 87117-5776

UNCLASSIFIED



AD NUMBER

AD- B205 187

NEW LIMITATION CHANGE

TO

DISTRIBUTION STATEMENT A -
Approved for public release; Distri-
bution unlimited.

Limitation Code: 1

FROM

DISTRIBUTION STATEMENT -

Limitation Code:

AUTHORITY

Janet E. Mosher, Phillips Lab., Kirtland AFB, N. M.

THIS PAGE IS UNCLASSIFIED

PL-TR--94-1133

This final report was prepared by General Pneumatics Corporation, Scottsdale, AZ. under Contract FO4611-89-C-0055, Job Order 21021002, with Phillips Laboratory, Kirtland Air Force Base, New Mexico. The Laboratory Project Officer-in-Charge was Capt Jeffrey Wiese (VTPT).

When Government drawings, specifications, or other data are used for any purpose other than in connection with a definitely Government-related procurement, the United States Government incurs no responsibility or any obligation whatsoever. The fact that the Government may have formulated or in any way supplied the said drawings, specifications, or other data, is not to be regarded by implication, or otherwise in any manner construed, as licensing the holder, or any other person or corporation; or as conveying any rights or permission to manufacture, use, or sell any patented invention that may in any way be related thereto.

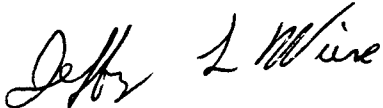
This report has been authored by a contractor of the United States Government. Accordingly, the United States Government retains a nonexclusive royalty-free license to publish or reproduce the material contained herein, or allow others to do so, for the United States Government purposes.

This report contains proprietary information and shall not be either released outside the government, or used, duplicated or disclosed in whole or in part for manufacture or procurement, without the written permission of the contractor. This legend shall be marked on any reproduction hereof in whole or in part.

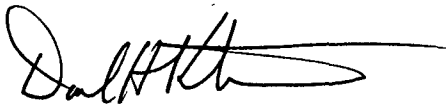
If your address has changed, if you wish to be removed from the mailing list, or if your organization no longer employs the addressee, please notify PL/VTPT, 3550 Aberdeen Ave SE, Kirtland AFB, NM 87117-5776 to help maintain a current mailing list.

This report has been reviewed and is approved for publication.

FOR THE COMMANDER



JEFFREY WIESE, Capt, USAF
Project Officer



DAVID KRISTENSEN, Lt Col, USAF
Chief, Space Power and Thermal
Management Division



HENRY L. PUGH, JR., Col, USAF
Director of Space and Missiles Technology

DO NOT RETURN COPIES OF THIS REPORT UNLESS CONTRACTUAL
OBLIGATIONS OR NOTICE ON A SPECIFIC DOCUMENT REQUIRES THAT IT BE
RETURNED.

The following notice applies to any unclassified (including originally classified and now declassified) technical reports released to "qualified U.S. contractors" under the provisions of DoD Directive 5230.25, Withholding of Unclassified Technical Data From Public Disclosure.

NOTICE TO ACCOMPANY THE DISSEMINATION OF EXPORT-CONTROLLED TECHNICAL DATA

1. Export of information contained herein, which includes, in some circumstances, release to foreign nationals within the United States, without first obtaining approval or license from the Department of State for items controlled by the International Traffic in Arms Regulations (ITAR), or the Department of Commerce for items controlled by the Export Administration Regulations (EAR), may constitute a violation of law.
2. Under 22 U.S.C. 2778 the penalty for unlawful export of items or information controlled under the ITAR is up to two years imprisonment, or a fine of \$100,000, or both. Under 50 U.S.C., Appendix 2410, the penalty for unlawful export of items or information controlled under the EAR is a fine of up to \$1,000,000, or five times the value of the exports, whichever is greater; or for an individual, imprisonment of up to 10 years, or a fine of up to \$250,000, or both.
3. In accordance with your certification that establishes you as a "qualified U.S. Contractor", unauthorized dissemination of this information is prohibited and may result in disqualification as a qualified U.S. contractor, and may be considered in determining your eligibility for future contracts with the Department of Defense.
4. The U.S. Government assumes no liability for direct patent infringement, or contributory patent infringement or misuse of technical data.
5. The U.S. Government does not warrant the adequacy, accuracy, currency, or completeness of the technical data.
6. The U.S. Government assumes no liability for loss, damage, or injury resulting from manufacture or use for any purpose of any product, article, system, or material involving reliance upon any or all technical data furnished in response to the request for technical data.
7. If the technical data furnished by the Government will be used for commercial manufacturing or other profit potential, a license for such use may be necessary. Any payments made in support of the request for data do not include or involve any license rights.
8. A copy of this notice shall be provided with any partial or complete reproduction of these data that are provided to qualified U.S. contractors.

D E S T R U C T I O N N O T I C E

For classified documents, follow the procedures in DoD 5200.22-M, Industrial Security Manual, Section II-19 or DoD 5200.1-R, Information Security Program Regulation, Chapter IX. For unclassified, limited documents, destroy by any method that will prevent disclosure of contents or reconstruction of the document.

DRAFT SF 298

1. Report Date (dd-mm-yy) November 1993		2. Report Type Final		3. Dates covered (from... to) 12-89 to 4-93		
4. Title & subtitle Low Capacity Reliquefier for Storage of Cryogenic Fluids				5a. Contract or Grant # F04611-89-C-0055		
				5b. Program Element # 62601F		
6. Author(s) Woodrow Ellison K. Randall Kohuth				5c. Project # 2102		
				5d. Task # 10		
				5e. Work Unit # 02		
7. Performing Organization Name & Address General Pneumatics Corporation Western Research Center 7662 E. Gray Road, Suite 107 Scottsdale, AZ 87117-5776				8. Performing Organization Report #		
9. Sponsoring/Monitoring Agency Name & Address Phillips Laboratory 3550 Aberdeen Ave SE Kirtland AFB, NM 87117-5776				10. Monitor Acronym		
				11. Monitor Report # PL-TR-94-1133		
12. Distribution/Availability Statement Distribution authorized to DoD components only; Proprietary Information; November 1993. Other requests shall be referred to AFMC/STI.						
13. Supplementary Notes						
14. Abstract The subject SBIR Phase II project addresses the tasks of generating cryocooling at 10 K and of reliquefying helium at a rate of 10 liters of liquid per day. The system designed is a combination of a four-stage Stirling cryocooler, a three-stage compressor, an anti-clogging Joule-Thomson cryostat, and a special drive mechanism which minimizes piston side forces and seal wear. A major task of the project was derivation of a multi-stage Stirling simulation computer program. The project resulted in the successful design, fabrication, and initial testing of a 10 K multi-stage Stirling cryocooler. The cryocooler employs an oil lubricated drive mechanism and rubbing piston seals to allow testing over the very low speeds necessary to reach 10 K, and a bolted structure to facilitate trouble-shooting and modification. As such, the machine is a versatile testbed for advancing multi-stage Stirling analysis, design, and regenerators technology, leading to higher efficiency, faster, smaller machines employing high reliability non-wearing drive mechanisms and seals.						
15. Subject Terms Cryocooler, Reliquefier, Helium, Stirling, Multi-stage, Joule-Thomson						
Security Classification of			19. Limitation of Abstract		21. Responsible Person (Name and Telephone #) (505) 846-2686	
16. Report Unclassified	17. Abstract Unclassified	18. This Page Unclassified	Limited	20. # of Pages 134		

**GOVERNMENT PURPOSE LICENSE RIGHTS
(SBIR PROGRAM)**

Contract Number: FO4611-89-C-0055

**Contractor: General Pneumatics Corporation
Scottsdale, AZ**

For a period of four (4) years after delivery and acceptance of the last deliverable item under the above contract, this technical data shall be subject to the restrictions contained in the definition of "Limited Rights" in DFARS clause at 252.227-7013. After the four-year period, the data shall be subject to the restrictions contained in the definition of "Government Purpose License Rights" in DFARS clause at 252.227-7013. The Government assumes no liability for unauthorized use or disclosure by others. This legend shall be included on any reproduction thereof and shall be honored only as long as the data continues to meet the definition on Government purpose license rights.

Accession For	
NTIS GRA&I	<input type="checkbox"/>
DTIC TAB	<input checked="" type="checkbox"/>
Unannounced	<input type="checkbox"/>
Justification	
By	
Distribution/	
Availability Codes	
Dist	Avail and/or Special
E-4	

PROJECT SUMMARY

Development of compact, efficient, long life cryocoolers capable of producing temperatures to below 10 K while dissipating heat at temperatures near 300 K has become a critically-pacing technology. The subject Small Business Innovation Research Phase II project addresses the tasks of generating cryocooling at 10 K and of reliquefying helium at a rate of 10 liters of liquid per day, and provides a basis for cryorefrigerators for less challenging temperatures. The report surveys the candidate types of cryocoolers, identifies why the Stirling cycle offers the best theoretic potential, and describes the successful analysis, design, fabrication, and initial testing of a 10 K multi-stage Stirling test bed cryocooler.

The system designed is a hybrid combination of a four-stage Stirling cryocooler, an integral three-stage compressor, an anti-clogging Joule-Thomson (J-T) cryostat, and a special drive mechanism which minimizes piston side forces and seal wear. A flow of helium from the compressor is cooled to 10 K by the Stirling cryocooler and is then expanded through the J-T cryostat, which liquefies a portion of the helium to return it to a storage dewar.

There are no established analytical models or empirical data for designing a multi-stage Stirling cryocooler to reach 10 K. The subject project endeavored to analytically determine and experimentally correlate the matching of displacements, regenerator characteristics, operating pressures and speeds for specific performance requirements at each stage. A major task of the project was derivation of a multi-stage Stirling simulation computer program, which will evolve and be refined interactively with the testing of the test bed cryocooler.

The fundamental development problem is that current Stirling and other regenerative cycle cryocoolers are inefficient and limited to very slow operating speed in reaching 10 K. Other types of cryocoolers, although capable of higher operating speeds, are even less efficient. Slow speed necessitates large drive forces and impedes the use of high reliability provisions such as non-rubbing bearings, seals, and linear motor drives. The multi-stage cryocooler fabricated in this Phase II project employs an oil lubricated drive mechanism and rubbing piston seals to allow testing over the range of very low speeds necessary to reach 10 K, and a bolted together structure to facilitate fabrication, troubleshooting, and modification. As such, the machine is a versatile test bed for advancing multi-stage Stirling analysis, design, and regenerators technology, leading to higher efficiency, faster operating speed, smaller machines employing high reliability non-wearing drive mechanisms and seals.

ACKNOWLEDGEMENT

The work reported herein was carried out at the Western Research Center of General Pneumatics Corporation, Scottsdale, Arizona during the period December 1989 through April 1993. The work was performed under a Small Business Innovation Research (SBIR) Phase II contact, F04611-89-C-0055, sponsored by the Strategic Defense Initiative Organization (now Ballistic Missile Defense Organization), and administered by the Air Force Phillips Laboratory.

The multi-stage Stirling computer model was derived under the direction of Dr. Graham Walker of Whitegaites, Inc., Scottsdale, Arizona.

The Ross drive mechanism was used with the permission and consultation of its inventor Mr. Andy Ross of Columbus, Ohio.

Regenerators design consultation and analyses using the REGEN computer programs were conducted by Dr. Ray Radebaugh of the National Institute of Standards and Technology, Boulder, Colorado.

Regenerators development was carried out at Energy Science Laboratories, Inc., San Diego, California, a leader in the development of new thermal energy storage materials for aerospace applications, under the direction of Dr. Timothy Knowles and Mr. Mike Fennell.

USE AND EXPRESSION OF UNITS

Both English and SI units were used for calculations and test data in the performance of this project. The values in this report are, however, expressed primarily in the International System of Units (SI) and customary units are provided in parentheses as appropriate for clarity.

CERTIFICATION OF TECHNICAL DATA CONFORMITY

The contractor, General Pneumatics Corporation, Western Research Center, hereby certifies that, to the best of its knowledge and belief, the technical data delivered herein under contract F04611-89-C-0055 is complete, accurate, and complies with all requirements of the contract.

November 30, 1993
Date

Steven G. Zylstra
Steven G. Zylstra, General Manager,
Western Research Center

TABLE OF CONTENTS

Report Documentation Page (DD Form 1473)	i
PROJECT SUMMARY	ii
ACKNOWLEDGEMENT	iii
USE AND EXPRESSION OF UNITS	iii
CERTIFICATION OF TECHNICAL DATA CONFORMITY	iii
TABLE OF CONTENTS	iv
LIST OF FIGURES	v
1.0 INTRODUCTION	1
2.0 CRYOREFRIGERATION OVERVIEW	1
3.0 PROJECT OBJECTIVES	8
4.0 ANALYSIS AND DESIGN	12
4.1 System Analysis and Design Overview	12
4.2 Compressor and J-T Cryostat Design	14
4.3 Multi-Stage Stirling Analysis and Design	22
4.4 Multi-Stage Stirling Computer Model	33
4.5 Regenerators	37
4.6 Drive Mechanism, Piston Guides and Seals	46
5.0 FABRICATION, ASSEMBLY, AND TESTING	53
5.1 Compressor and J-T Cryostat	53
5.2 Regenerators	53
5.3 Cryocooler Prototype	57
5.4 Assembly and Test	61
6.0 CONCLUSION AND CONTINUED DEVELOPMENT	71
BIBLIOGRAPHY OF RELATED WORK	74
APPENDIX A: Example Printout from Multiple Expansion Stirling Cryocooler Simulator Computer Program	
APPENDIX B: Preliminary Test Plan	

LIST OF FIGURES

<u>Figure No.</u>		<u>Page No.</u>
1	System Layout Design Derived in Phase I	9
2	System Drive Mechanism Schematic	11
3a	Cross Section of Phase II Prototype	15
3b	End-View Section Through Prototype Crankcase	16
4	Three-Stage Compressor Cross Section with Mating Scotch-Yoke Drive Mechanism	19
5	Anti-Clogging J-T Cryostat for Helium Liquefaction	20
6	J-T Cryostat for Prototype Helium Liquefier	23
7	Volumetric Heat Capacities of Various Materials	40
8	Counter-Rotating Dynamic Balance Wheels Arrangement	50
9a	Regenerator Mesh Stack in Boring Fixture	55
9b	Completed First Stage Regenerator Mesh Stack	55
10	Prototype Assembly and Major Coldhead Components	58
11a	Drive Mechanism Yoke, Piston Rods, Swinglink, and Crankshaft	59
11b	Drive Mechanism and Bellows Assembled into Crankcase	59
12a	Prototype System in Test Stand	63
12b	Coldhead with Test Heaters and Temperature Sensors	63
13	System Test Dewar	64
14	First Stage Heat Load Tests	67

LIST OF FIGURES (CONT'D)

<u>Figure No.</u>		<u>Page No.</u>
15	Second Stage Heat Load Tests	68
16	Third Stage Heat Load Tests	69
17	Fourth Stage Heat Load Tests	70

1.0 INTRODUCTION

Innovations related to the long term storage of cryogenic fluids for spacecraft systems were solicited in the 1987 Department of Defense Small Business Innovation Research program solicitation, Topic SDIO 87-6. In response, development was proposed of a small-scale cryocooler to reliquefy the boil-off vapor from, and thereby prolong the supply life of, cryogenic liquid storage dewars. Phase I of the project was to derive a detailed layout design for a combined multi-stage Stirling, Joule-Thomson (J-T) system for reliquefying the most difficult fluid, helium, at a rate of 10 liters per day. Phase I was conducted under contract F04611-88-C-0003 administered by the Air Force Astronautics Laboratory, and concluded in a final report, Low Capacity Reliquefier for Storage of Cryogenic Fluids, AFAL-TR-88-066, October 1988. Phase II, the detail design, fabrication, and test of a proof-of-principles prototype, was carried out under contract F04611-89-C-0055 administered by the Air Force Phillips Laboratory, and is reported herein.

The principal research of the project is that of employing a stepped displacer in a Stirling cryocooler to generate four successive stages of refrigeration down to a temperature of 10 K. Supporting research includes use of composite regenerators to achieve cryogenic thermal capacity with low thermal-fluid losses, incorporation of an anti-clogging J-T cryostat for long-term liquefaction of helium, design of a compact three-stage compressor to drive the J-T cryostat and pressurize the Stirling cryocooler, and use of the Ross drive linkage to minimize piston side forces and seal wear.

2.0 CRYOREFRIGERATION OVERVIEW

To date, the mission lives of spacecraft requiring cryogenic cooling for instrumentation or fuel have been very limited by dependence on stored cryogens, including (with normal boiling points as indicated): oxygen (90 K), argon (87 K), nitrogen (77 K), neon (27 K), hydrogen (20 K), and helium (4.2 K). Systems capable of 5 to 10 years of continuous orbital operation are needed for cooling a variety of instruments, shields, and cryogen

reservoirs. Some sensors require cooling to below 10 K, for which liquid helium is typically used. Space radiators do not provide heat sink temperatures (T) much below 300 K because their size varies inversely with T^4 . The power, weight, size and reliability of current cryocoolers are not suitable for spacecraft applications. Development of compact, efficient, long life cryocoolers capable of producing temperatures to below 10 K while dissipating heat at temperatures near 300 K has become a critically-pacing technology.

The research described herein addresses the tasks of generating cryocooling at 10 K and of reliquefying helium at a rate of 10 liters of liquid per day, and provides a basis for cryorefrigerators for less challenging temperatures.

To absorb heat at a low temperature and reject it to a higher temperature, i.e. generate refrigeration, requires the application of work on a thermodynamic medium. The medium may be fluid, elastic, magnetic, or electric, but in general only fluids (specifically gases) allow sufficient operating range to achieve a temperature change of more than a few tens of degrees Kelvin. Therefore, to generate cryogenic refrigeration with a heat sink in the range of 300 K requires the cyclic compression and expansion of a gas having a suitably low boiling point.

The Carnot cycle defines the theoretic minimum work required per unit of refrigeration, which is equal to $(T_H - T_L)/T_L$ where T_H and T_L are respectively the cycle maximum (sink) and minimum (refrigeration) absolute temperatures. However, the Carnot cycle is an unimplementable mathematical ideal. The cycle most closely approaching the performance of the Carnot cycle, upon which to base a cryorefrigerator with a sink temperature in the range of 300 K, is the Stirling cycle.

Progressively smaller, lighter Stirling cryocoolers have been developed over the past 40 years, principally for infrared night vision equipment and missile guidance systems requiring cooling in the range of 80 K. In competition with many other types of

cryocoolers, including Vuilleumier, Linde-Hampson, Brayton, Claude, Gifford-McMahon, and Solvay, Stirling cryocoolers have emerged as the choice for small systems, being smaller, lighter, lower in cost, and more efficient.

Recently, a new generation of miniature Stirling cryocoolers, typified by the Oxford cryocooler (Bib. 20) and the Standard Spacecraft Cooler, have been developed employing non-rubbing clearance seals, flexure suspensions, and resonant linear motors for greatly improved life and reliability. But there are fundamental problems in reaching temperatures much below 65 K with these machines. The principal advantages and disadvantages among various forms of cryocoolers are summarized below.

Stirling cryocoolers using pressurized helium as the working fluid and with a 300 K sink can achieve temperatures of 65 K with a single expansion stage and under 10 K with multiple stages. Current Stirling cryocoolers typically do not achieve net power efficiencies greater than 10% of Carnot. More importantly, they require close tolerance moving parts and cannot tolerate contamination of the working fluid by lubrication or wear debris, which to date has limited continuous unattended operation lifetimes to well under 3 years. Also, for size and weight efficiency the helium working fluid must be pressurized, such as to a charge pressure of 2 MPa, which requires perfect sealing or a reservoir of high pressure helium for long term operation.

Split-Stirling cryocoolers have the compressor piston and the displacer in separate cylinders interconnected by a single gas line. The piston and the displacer may be driven by separate motors, or the displacer may be pneumatically driven by the compressor piston. The latter case requires precise tuning of the displacer mass and damping to achieve proper cycle phasing and efficiency, which degrades with changes in friction over the operating life. The advantage of a Split-Stirling cryocooler is to minimize the mass and vibration at the cold (displacer) end. The disadvantage is that the interconnecting tube adds dead volume, flow losses, and stray heat loads which seriously reduce the efficiency.

Free-Piston Stirling machines have no mechanical linkage to the compressor piston or the displacer. The compressor piston is driven hydraulically or inductively and it in turn drives the displacer pneumatically. While eliminating the need for bearings, this arrangement requires precise resonant tuning of the drive and the piston and displacer dynamics, which varies with changes in temperature, friction, viscosity, clearances, etc., and does not provide the power or weight efficiency of a mechanically controlled Stirling machine.

Vuilleumier cryocoolers are essentially Stirling machines which use heat input, instead of mechanical work input, to generate a pressure cycle. As such, they are constrained to operate with pressure ratios of less than half that of mechanically driven Stirling machines and are proportionately bigger and heavier. Also, the high operating temperatures create material and wear problems. The principal advantage claimed for Vuilleumier cryocoolers, the potential for long life due to low forces on the bearings and seals, is a consequence of the low pressure ratio. A comparably derated mechanically driven Stirling cryocooler could have low pressure ratio and forces without the high temperature problems.

Pulse Tube cryocoolers are Stirling-like refrigerators with the advantage that a pressure wave in a tube substitutes for a moving mechanical displacer. They may be driven with a thermoacoustic wave generator, instead of a mechanical compressor, to have no moving parts. However, because they rely on irreversible heat transfer or expansion processes to generate the essential cycle phasing, pulse tube refrigerators are intrinsically less efficient and bulkier than conventional Stirling refrigerators. Pulse tube cryocoolers have reached temperatures below 35 K with 1 or 2 stages and below 10 K with 3 stages (Bib. 6, 21, 32).

Gifford-McMahon cryocoolers are commonly used in commercial applications where weight and power are not priorities. They are similar to Stirling machines except that they use actively-driven valves to control the compression/expansion cycle. This allows use of an oil-lubricated compressor and oil separator/filter system to generate a continuous supply of pressurized helium working fluid. The compressor can operate at high speed

with low bearing loads while the coldend displacer cycles with an ample pressure ratio at very low speed (e.g. 0.5 Hz) which facilitates reaching temperatures below 20 K. Gifford-McMahan machines can achieve operating lifetimes of several years with periodic maintenance of the oil supply, separator/filter, and helium charge. However, valving of the pressure cycle dissipates pressure work which imposes a serious power penalty. For flight applications, a Gifford-McMahan cryocooler would require approximately 3 times the power and weight of a Stirling machine.

Brayton cryocoolers operate at higher speeds with lower bearing loads and offer lower weight than other cryocoolers in capacities above 10 to 20 W at 80 K. Below this they have sharply increasing weight per unit of refrigeration with decreasing capacity and temperature, exceeding that of other cryocoolers. Overall, they require three to five times more power than Stirling cryocoolers.

Linde-Hampson cryocoolers employ Joule-Thomson cooling by isenthalpic expansion of a high pressure gas through a nozzle to liquefy part of the gas. Prior to expansion, the gas must be below its inversion temperature, above which expansion produces heating. With a 300 K sink, a single-stage cryocooler can achieve the temperature of boiling nitrogen (77 K at 0.1 MPa). Multi-stage cascade systems, using gases with successively lower inversion temperatures, can liquefy helium (4.2 K at 0.1 MPa). Linde-Hampson cryocoolers have typically not been used for long-life operation due to problems with compressor lubrication and wear and nozzle clogging. Power efficiency is inherently low due to losses in compressing the gas to high pressure and in expanding it through a nozzle without work recovery.

Rankine refrigerators are commonly used with freon working fluids in non-cryogenic applications. They differ from Linde-Hampson systems in that Rankine refrigerators expand a saturated liquid through a nozzle to produce a low boiling temperature fluid. To do so they must use a fluid which can be condensed at the heat sink temperature. Cryogenic temperature (but not below 63 K) can be reached with cascaded stages, each

of which employs a working fluid that can be condensed by cooling from the preceding stage, e.g. a xenon stage (normal boiling point 165 K) to cool a methane stage (112 K) which in turn cools a nitrogen stage (77 K). Because the heat transfers both into and out of the system are constant temperature (phase change) processes and a large portion of the working fluid is saturated liquid after expansion through the nozzle, a Rankine system can achieve higher power efficiency with lower operating pressures, but with more complexity (stages) than a Linde-Hampson system down to temperatures of about 65 K.

Sorption systems draw a gas at low pressure into a cool sorption medium, then drive the gas out with heat to pressurize it for expansion through a nozzle. To reach temperatures down to about 65 K, sorption systems typically employ cascaded Rankine stages to limit drive pressure and power requirements (Bib. 33). Lower temperatures require subsequent stages of neon (27 K), hydrogen (20 K), and helium (4 K). These gases cannot be condensed by cooling from a preceding stage and must therefore operate in the less efficient Linde-Hampson mode. Because they have few and simple moving parts, sorption systems offer the potential for very long operating life with minimal wear, vibration, and electromagnetic noise. However, they are bulky, and require actively controlled valves and a means to cyclically heat and cool each sorption medium, which is subject to thermal fatigue and gas contamination problems.

Thermoelectric and Thermomagnetic refrigerators ideally do not require moving parts. Real material properties, however, limit thermoelectric coolers to temperatures above about 150 K. The refrigeration generated, which is proportional to current, is offset by self-heating, which is proportional to current squared. Thermomagnetic cryocoolers employ superconducting magnets to avoid prohibitive power dissipation and are thereby constrained to operate over very low temperature range. Furthermore, since it is highly inefficient to cycle a superconducting magnet on and off, a moving mechanism is required to cycle the field applied to the magnetocaloric medium.

Non-rubbing magnetic or gas bearings, flexures, and close-tolerance clearance seals are desirable for long life, but are not without serious difficulties. They all require extremely high precision which complicates the design, and are very sensitive to debris, vibration damage, thermal and mechanical strains, and misalignments. Magnetic suspensions require highly complex control electronics. The low density and viscosity of helium necessitate extremely tight clearances in gas bearings. Non-contacting seals allow leakage past pistons in proportion to the clearance gap cubed, which wastes power and lowers compression ratio, necessitating a larger cryocooler for a given refrigeration capacity.

In general, such low wear features require sufficient operating speed such as for fluid dynamic effects in gas bearings and clearance seals or for power efficiency in resonant linear motor drives. As will be discussed further in subsequent sections, reaching temperatures below 20 K may require operating speeds which are problematically low for such provisions.

It is apparent from the foregoing comparative summary that Stirling cryocoolers offer the best potential for applications where thermodynamic efficiency, mechanical simplicity, and minimum size and weight are priorities. However, there are no established analytical models or empirical data for designing a multi-stage Stirling cryocooler to reach 10 K. Even the optimization of single-stage Stirling cryocoolers, which typically operate near 80 K, is not well understood. Dr. J. E. Zimmerman, while working at the National Bureau of Standards, experimentally demonstrated that a stepped displacer in a Stirling cryocooler could reach temperatures down to about 7 K (Bib 41). But Dr. Zimmerman's simple displacer depended on the minimal regenerative thermal capacity inherent in the walls and the helium gas in the annular gap between the displacer and cylinder, and generated only enough refrigeration to balance the parasitic losses.

The current project endeavors to analytically determine and experimentally correlate the matching of displacements, regenerator characteristics, operating pressures and speeds

for specific performance requirements at each stage. The multi-stage cryocooler thus fabricated employs an oil lubricated drive mechanism and rubbing piston seals to allow testing over the range of very low speeds necessary to reach 10 K, and a bolted together structure to facilitate fabrication, trouble-shooting, and modification but which does not minimize weight, size, and long-term leakage. As such, the machine is a versatile proof-of-principles test bed for continued investigations in the analysis and design of multi-stage Stirling cryocoolers and regenerators, and is not a flight prototype.

3.0 PROJECT OBJECTIVES

A multi-stage Stirling cryorefrigerator using helium as the working fluid can achieve temperatures under 10 K with a sink of 300 K (Bib. 38). However, to reach a helium liquefaction temperature of approximately 4 K, an all-Stirling machine would require a final displacer stage operating at an internal pressure of less than 0.1 MPa, as described by Zimmerman et al. (Bib. 41), so that the boiling point of the helium working fluid within it would be below the normal boiling point of 4.2 K. This would severely limit the system refrigeration capacity, which is proportional to the mean pressure of the working fluid, or would necessitate the complexity of a second, separately sealed Stirling system for the final stage to avoid the requirement for reduced pressure throughout the system.

The system derived in Phase I, shown in Figure 1, is a hybrid combination of a four-stage Stirling cryocooler, an integral three-stage compressor, and an anti-clogging J-T cryostat. A flow of helium from the compressor is cooled to 10 K by the Stirling cryocooler and is then expanded through the J-T cryostat, which liquefies a portion of the helium to return it to a storage dewar. The same compressor which feeds the helium flow to the J-T cryostat also pressurizes the Stirling helium working fluid in an arrangement which minimizes the number of moving parts and the peak loading on the drive. This system is mechanically rugged, doesn't require complex electronics, allows very simple intake and return of helium boil-off from the storage dewar, and would not be incapacitated should a leak develop.

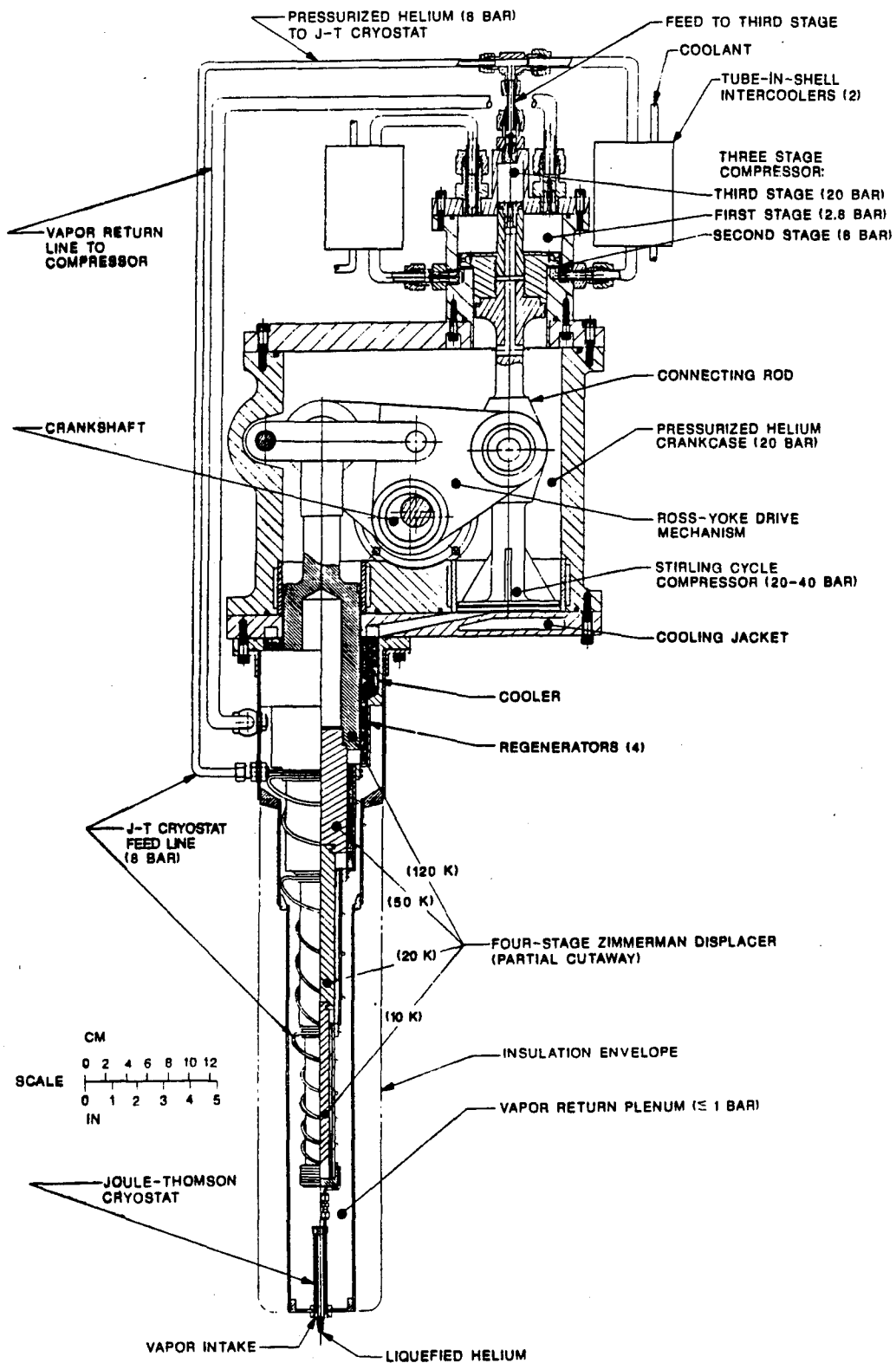


FIGURE 1. SYSTEM LAYOUT DESIGN DERIVED IN PHASE I

The Stirling cryocooler employs a stepped displacer to generate 4 successive stages of refrigeration at temperatures of 120 K, 50 K, 20 K, and 10 K. Helium boil-off vapor at 0.1 MPa and 4.2 K from a storage dewar is compressed and circulated by the three-stage compressor. After each stage of compression the helium is cooled to 300 K by an external coolant loop. Helium at 0.8 MPa from the compressor second stage is further cooled by the incoming boil-off vapor and the Stirling cryocooler stages, and is then liquefied and returned to the storage dewar by expansion through the J-T cryostat. The J-T cryostat is a unique, anti-clogging design for long-term operation. The Stirling cryocooler is pressurized to 2 MPa by the helium compressor third stage to maximize the Stirling thermodynamic effectiveness. The regenerators for the 4 Stirling stages consist of specially tailored materials to achieve high effective heat capacity with low axial conduction losses, void volume, and susceptibility to clogging. The three-stage compressor is an innovative single-piston design which minimizes the number of moving parts and the peak loading on the drive. As diagrammed in Figure 2, the compressor and the Stirling pistons are mutually driven by a mechanism known as the Ross linkage, which was specifically developed for Stirling machines. The Ross linkage drives the Stirling pistons with optimum cycle phasing to maximize thermodynamic efficiency, and with straight line motion to minimize piston side forces, which are the principal cause of seal wear. In addition, the straight line motion of the Ross linkage facilitates the use of metal bellows to seal the pistons from the crankcase and preclude contamination of the helium working fluid by bearing lubricant or drive motor outgassing.

System performance and sizing analyses, design configuration studies, layout design, and preliminary materials, fabrication and test plans were completed in Phase I. The objectives of Phase II were to carry out analyses refinement, detail piece parts design, fabrication, assembly, and basic performance testing of a proof-of-principles prototype of the system. The testing was planned to evaluate the analyses, design, and basic performance of the prototype system.

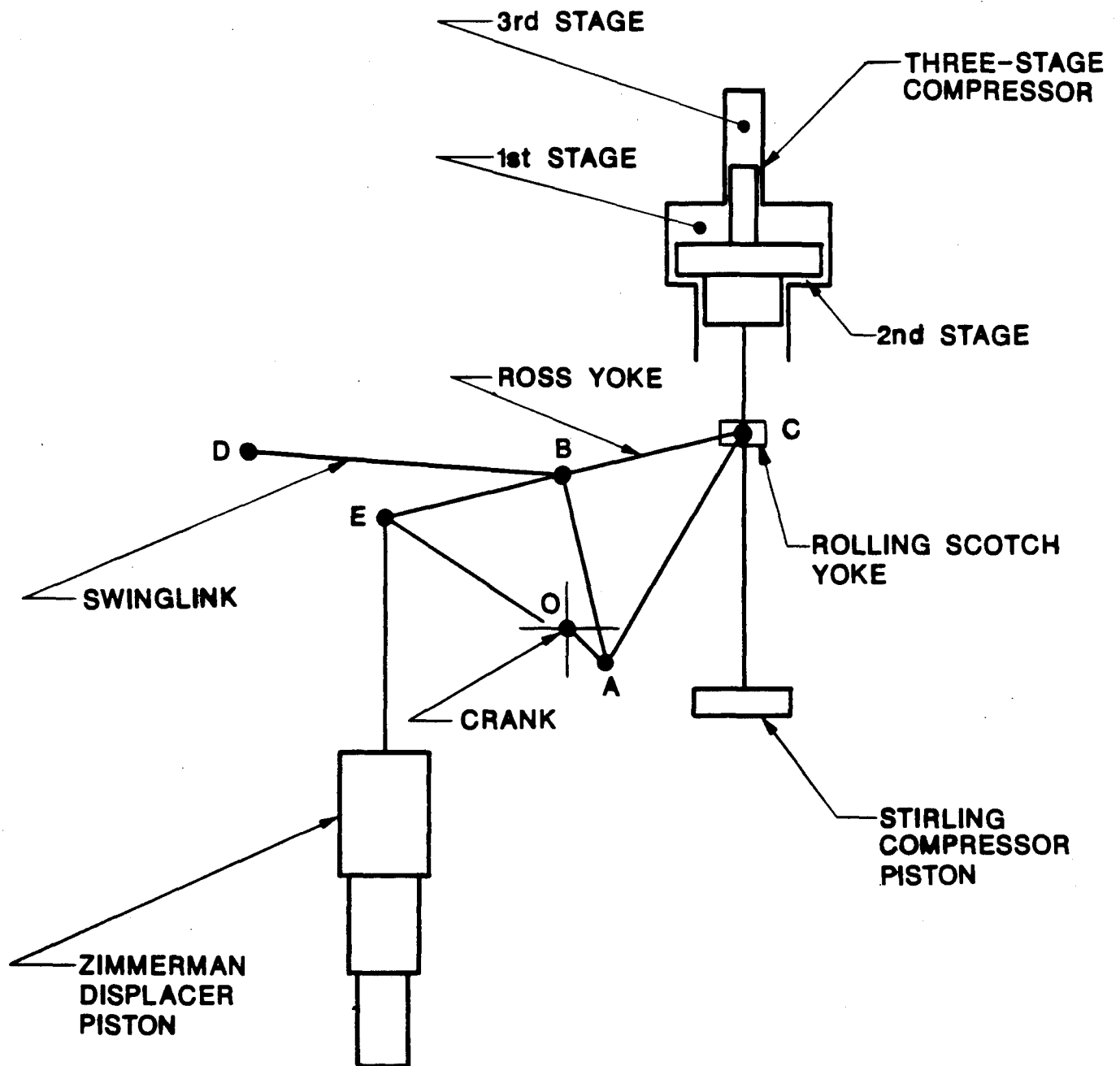


FIGURE 2. SYSTEM DRIVE MECHANISM SCHEMATIC

4.0 ANALYSIS AND DESIGN

4.1 System Analysis and Design Overview

The system sizing is based on producing 10 liters of liquid helium per day from storage dewar boil-off at approximately 0.1 MPa pressure with an external coolant supply at 300 K.

The density of liquid helium at 4.2 K and 0.1 MPa is 128.6 kg/m^3 and the latent heat of vaporization is 21.91 kJ/kg . The volume and mass flow of 10 liters of liquid helium per day is therefore 0.01 m^3 and 1.28 kg per day. This is equivalent to 0.015 g/sec and a refrigeration rate of 0.33 watts .

The J-T cryostat is sized for a liquid yield of 10% of the mass flow. Therefore, the required mass flow from the compressor to the cryostat to yield 10 liters of liquid per day is 0.15 g/sec or 9 g/min . Dividing by the density of helium at standard temperature and pressure (25°C , 0.1 MPa), 0.16 g/l , the required volumetric flow is approximately 60 standard liters per minute (SLPM), which is the basis for sizing the compressor.

The temperature distribution of 120 K, 50 K, 20 K, and 10 K for the 4 Stirling cooling stages was chosen to correspond with approximately equal Carnot coefficients of performance between the stages in order to distribute the sensitivity to regenerators ineffectiveness. Actual temperatures will depend on actual loads at each stage. The refrigeration required of the Stirling stages is that needed to make up for insufficiency of the incoming helium boil-off vapor in recuperatively cooling the pressurized flow to the J-T cryostat, plus parasitic heat loads. Counter-flow gas heat exchanger effectiveness is not precisely predictable, though better than 95% is commonly achieved. For design margin a heat exchanger effectiveness of 90% was assumed for the cooling from the incoming boil-off vapor flow. This resulted in required net refrigeration capacities for the Stirling stages of 1.0 W at 10 K, 4.5 W at 20 K, 17 W at 50 K, and 55 W at 120 K.

Based on the above refrigeration capacities and a temperature-entropy (T-S) chart of helium properties, preliminary estimates of the required helium mass and volume displacement rates for sizing each expansion stage were calculated assuming a charge pressure of 2 MPa, a cycle pressure ratio of 2:1, regenerative heat exchange at constant pressure, 10% temperature overlap between stages, and 10% of theoretic cycle efficiency. The resulting helium mass displacement rates were 0.8 g/s at 10 K, 1.5 g/s at 20 K, 2.5 g/s at 50 K, and 3.1 g/s at 120 K. These are close to those derived from an isothermal work estimation of $\text{refrigeration/mass} = 0.1 RT \ln (\text{pressure ratio})$.

As can be seen, design of the subject helium reliquefier is an iterative balancing of thermodynamic and mechanical factors, beginning with the helium flow and pressures required for the desired liquefaction rate. The 0.15 g/sec at 0.8 MPa flow to the J-T cryostat is determined by helium properties for isenthalpic expansion and the 10 K precooling generated by the Stirling cryocooler. The Stirling cryocooler capacity increases with helium charge pressure, chosen to be 2 MPa, which is limited by the work, structure, and complexity required to produce, withstand, and seal it. The refrigeration needed at each of the 4 Stirling cryocooler stages depends on the temperature distribution chosen and the recuperative cooling derived from the incoming helium boil-off vapor, which is limited by the size and complexity of the heat exchanger arrangement. The sizing of the 4 Stirling displacer stages to produce the required refrigeration depends on the helium charge pressure, cycle pressure ratio, regenerators effectiveness, estimated cycle efficiency (which allows for thermo-fluid parasitics and other non-idealities), and displacer stroke. The Stirling compressor sizing to produce the cycle pressure ratio depends on the displacer sizing, stroke, and dead volume such as that associated with the regenerators. Since they are linked by the Ross drive mechanism, the sizing of the three-stage compressor to produce the Stirling charge pressure and the pressure and flow to the J-T cryostat depends on the speed and strokes derived for the Stirling compressor and displacer.

As the system analysis and design evolved, it became increasingly evident that integration of the compressor and J-T subsystem with the multi-stage Stirling imposed too many design constraints and compromises for this stage of development. Detail designs for the J-T cryostat and the compressor were carried out and the J-T cryostat was fabricated and component tested, but compressor fabrication was not completed.

In concert with analysis and design, a comprehensive survey was conducted of prospectively applicable cryogenic developments, materials, bonding and sealing methods, and lubricants. Cross sections of the multi-stage Stirling assembly which was arrived at in Phase II are shown in Figures 3a and 3b.

4.2 Compressor and J-T Cryostat Design

The three-stage compressor is designed to intake helium at approximately 0.1 MPa and 300 K, generate the 0.8 MPa flow to the J-T cryostat, and maintain the 2.0 MPa pressurization of the Stirling cryocooler and crankcase with a minimum of internal leakage and wear. Cooling to dissipate the heat of compression to the 300 K external coolant is provided by tube-in-tube heat exchangers connected between the first and second stages and between the second and third stages. Flow required from the third stage is only enough to maintain the Stirling pressurization against leakage and does not require discrete cooling.

A three-stage compressor design with 3 equal compression ratios of 2.8:1 was chosen for several advantages over a two-stage design which would require an 8:1 first stage and a 2.5:1 second stage. The 3 equal compression ratios allow use of simple check valves for inlet and outlet instead of mechanically driven valves. Three stages allow more even distribution of drive loads about a shaft revolution than do 2 unequal stages. The high, 8:1, compression ratio in the first stage of a two-stage design would result in much higher temperature, less effective intercooling, and more compression work input.

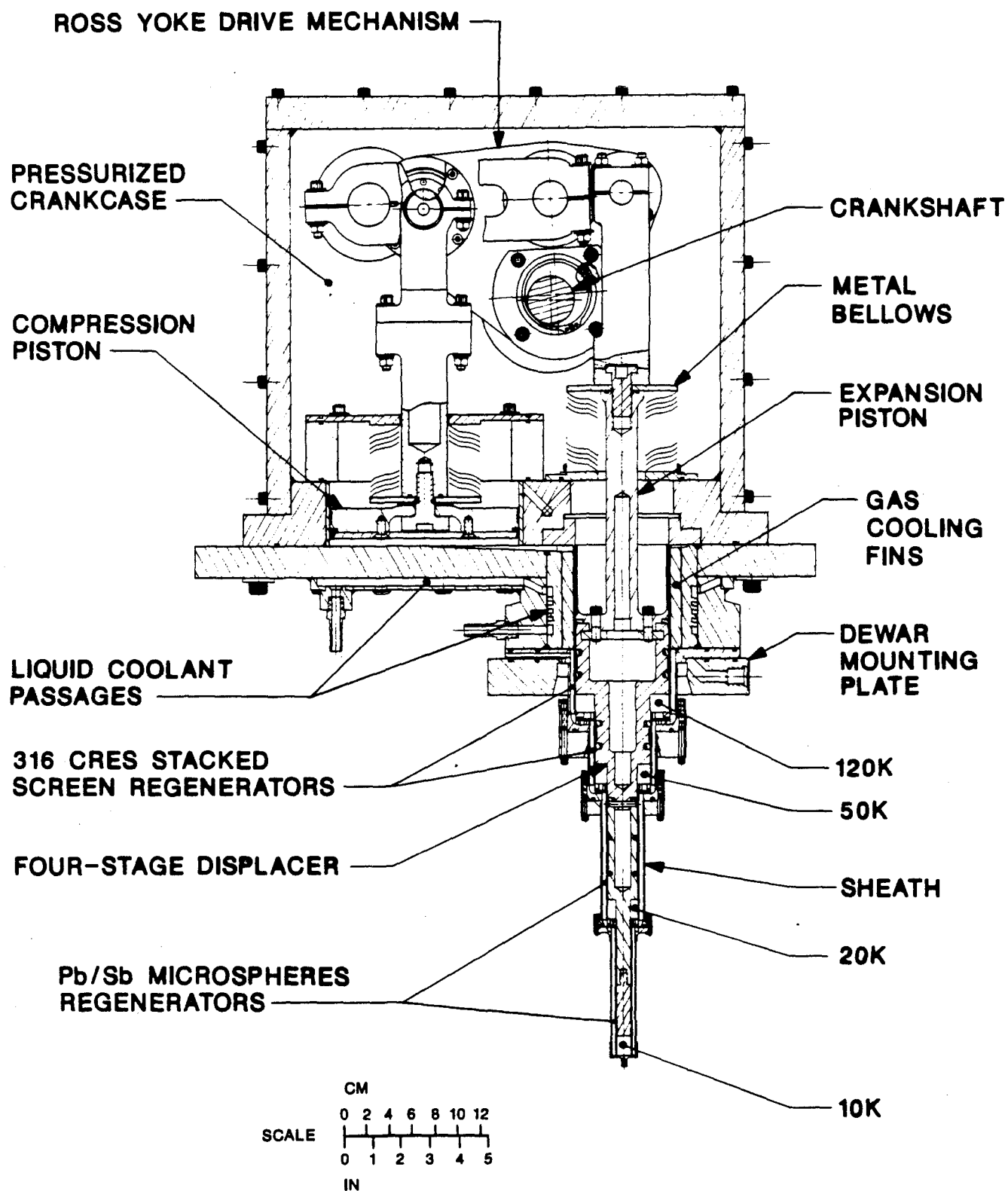


FIGURE 3a. CROSS SECTION OF PHASE II PROTOTYPE

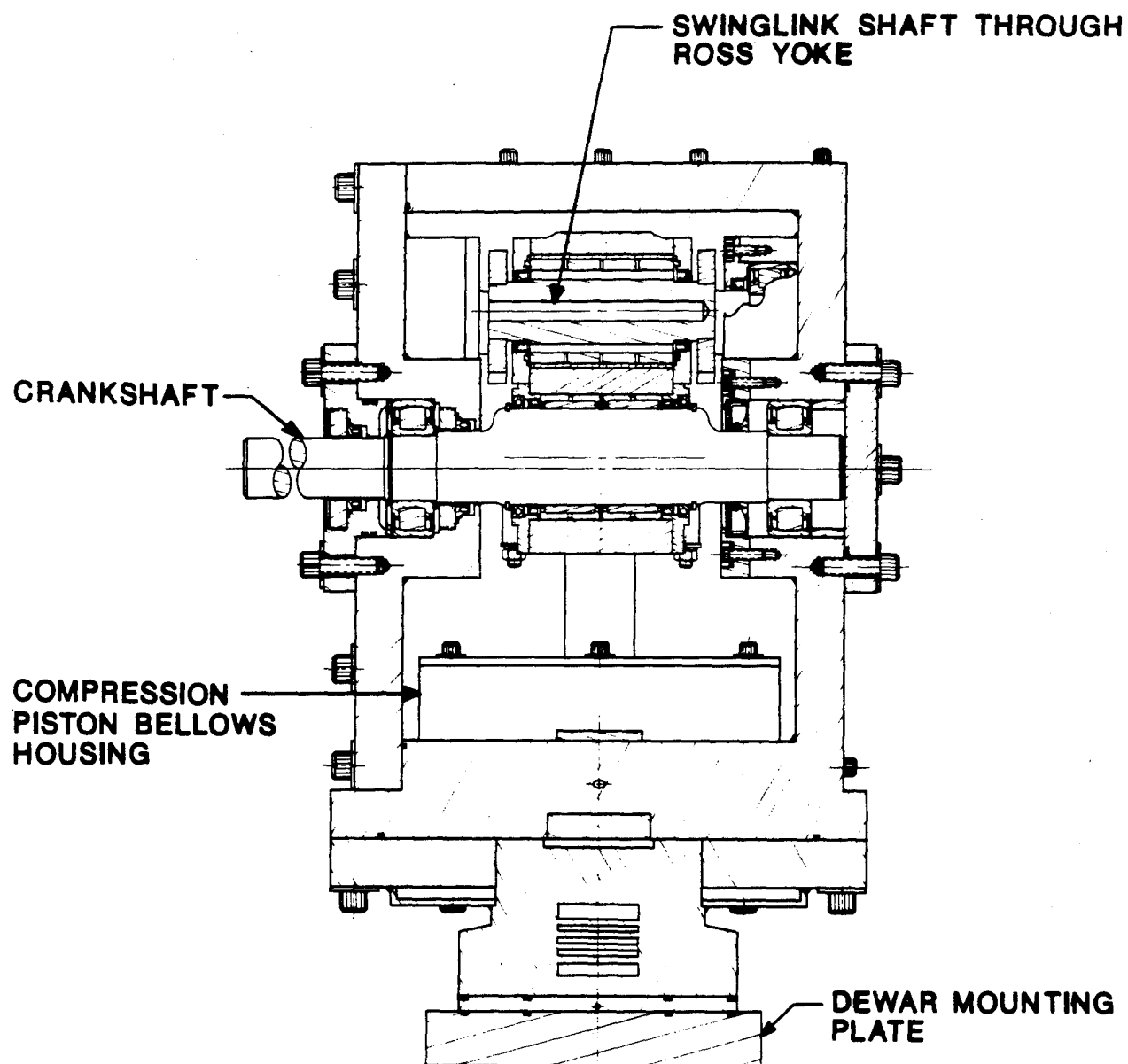


FIGURE 3b. END-VIEW SECTION THROUGH PROTOTYPE CRANKCASE

The helium working fluid for the Stirling section is pressurized to approximately 2 MPa by the compressor third stage to promote high Stirling refrigeration capacity, which is proportional to the mean pressure of the working fluid. This is accomplished by connecting the compressor third stage inlet into the 0.8 MPa J-T cryostat feed line from the second stage. The third stage is sized for a volumetric compression ratio of 2.8:1 and a displacement rate of 20% of the flow from the second stage. The outlet of the third stage is through check valves into each the crankcase and the Stirling system working space. In this way the flow through the third stage decreases from a maximum of 20% of the flow at 0.8 MPa from the second stage to zero as the pressure in the crankcase and Stirling system is brought up to 2.2 MPa.

The 3 stages of compression are accomplished by an innovative single-piston design with minimum moving parts and piston seals, which was to be integrated with the Stirling cryocooler as shown in Figure 1. The compressor was originally (Phase I) sized at 20 Hz operating speed for 60 SLPM at 0.8 MPa to the J-T cryostat, 20 SLPM at 2 MPa to charge the Stirling system and crankcase, and 20 SLPM (25%) allowance for volumetric inefficiencies, for a total first-stage displacement of 100 SLPM. (Details of the compressor sizing analyses are given in the Phase I final report.) Further analyses of the Stirling system in Phase II indicated that it might have to operate as slow as 5 Hz. Faced with enlarging the compressor for operation at 5 Hz, it was recognized that the 60 SLPM to the J-T cryostat and the 20 SLPM to charge the Stirling system would not be needed simultaneously, and the compressor need only be sized for 60 SLPM plus 15 SLPM (25%) allowance for inefficiencies. This resulted in the compressor design summarized as follows:

Operating speed	= 5 Hz
Volumetric efficiency	= 80%
Mechanical efficiency	= 75%
Isothermal efficiency	= 65%
Stroke	= 1.9 cm
Intake	= 75 SLPM at 0.1 MPa

Compression ratio per stage	= 2.8:1
First stage outlet pressure	= 0.28 MPa
piston diameters	= 14 cm o.d., 2.16 cm i.d.
power dissipation	= 237 watts
Second stage outlet pressure	= 0.78 MPa
piston diameters	= 14 cm o.d., 10.8 cm i.d.
power dissipation	= 237 watts
Third stage outlet pressure	= 2.2 MPa
piston diameter	= 2.16 cm
peak power dissipation	= 48 watts

The detail piece-parts designs for the compressor were completed, including a mating drive mechanism for testing it separately, as shown in Figure 4, and parts fabrication was begun. Heat transfer and fluid flow requirements for the compressor intercoolers were determined and suitable tube-in-tube heat exchangers were selected. However, the analysis and design of the multi-stage Stirling system and low temperature regenerators became increasingly consuming and dominant as Phase II progressed. Because the compressor was relatively established technology and could be replaced by a pressure-regulated tank of compressed helium for system testing with the advantage of avoiding the complex interactions of speed, pressures, refrigeration capacities and loads, compressor fabrication was suspended to focus the limited resources on the main development challenge, the multi-stage Stirling cryocooler.

The J-T cryostat for the subject system, shown in Figure 5, is based on General Pneumatics' (GP) exclusive anti-clogging nozzle design which was developed to overcome the reliability problems inherent in conventional J-T cryostats. In conventional J-T cryostats, the nozzle is a very small diameter circular orifice and is easily clogged by contaminants in the flow. At temperatures below 10 K, anything other than helium in the flow becomes a solid contaminant with the potential to clog the nozzle. The GP cryostat design has a tapered annular nozzle which is highly resistant to blockage due to a large

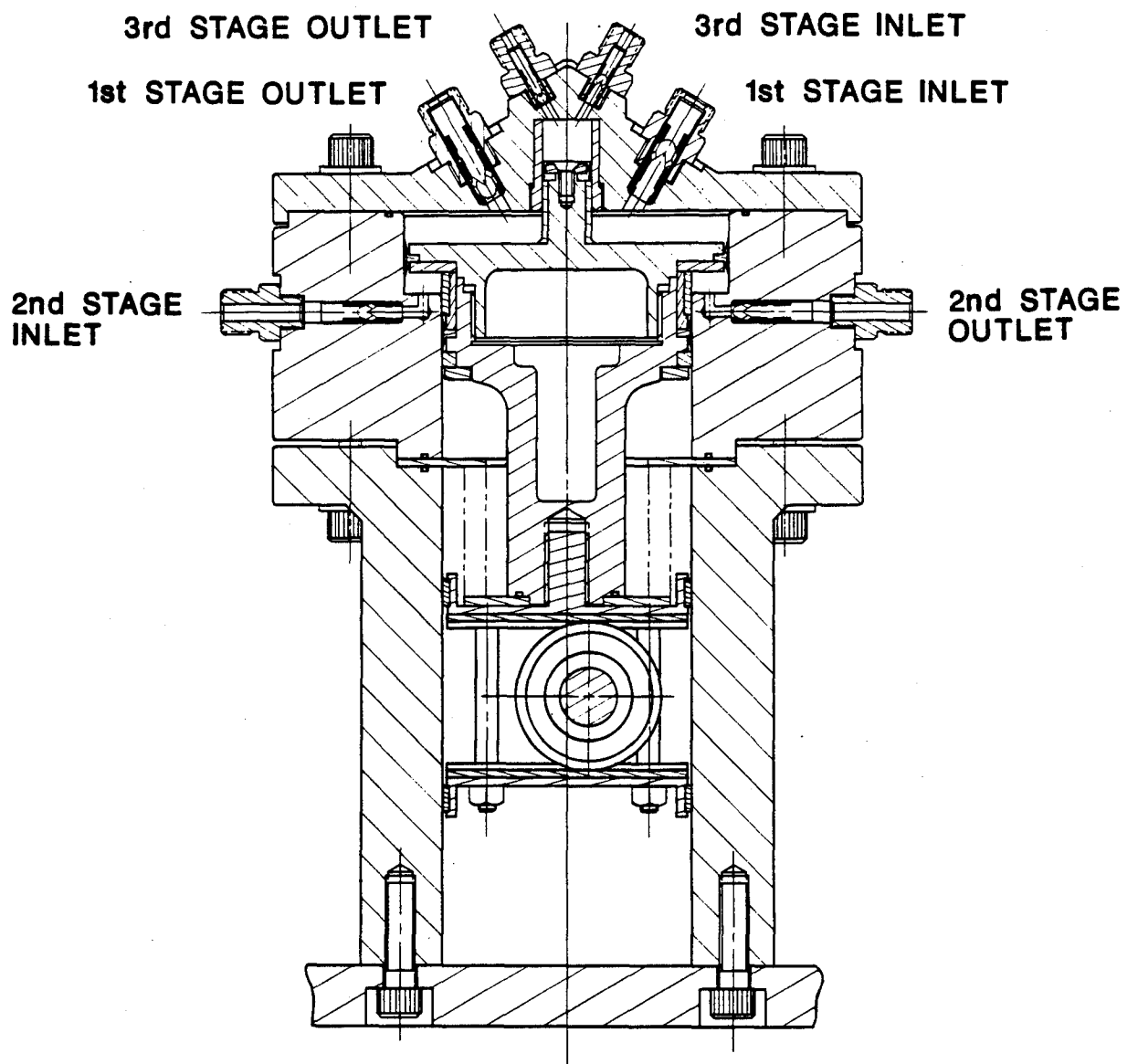


**FIGURE 4. THREE-STAGE COMPRESSOR CROSS SECTION
WITH MATING SCOTCH-YOKE DRIVE
MECHANISM**

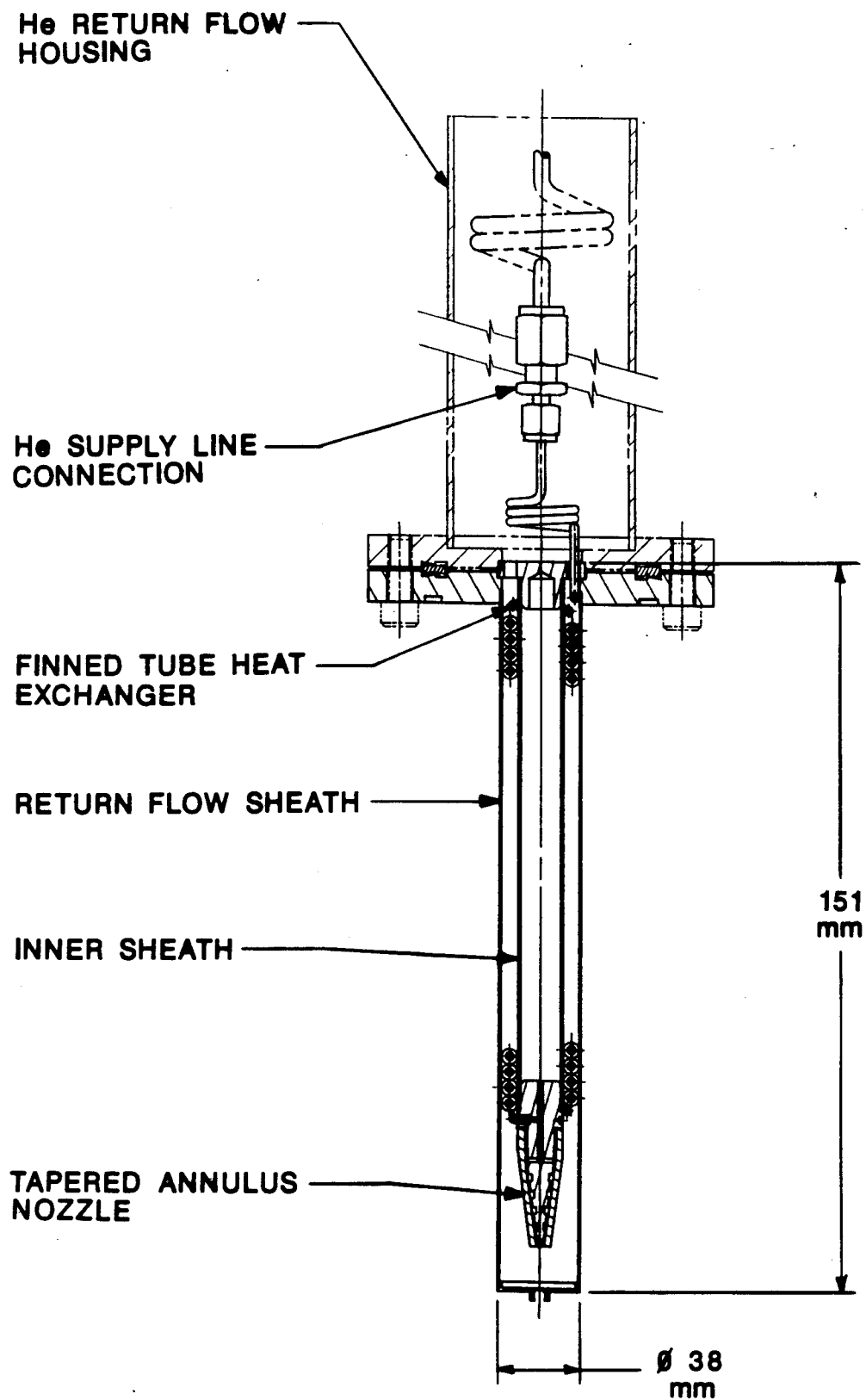


FIGURE 5. ANTI-CLOGGING J-T CRYOSTAT FOR HELIUM LIQUEFACTION

ratio of circumference to flow area. Labyrinth flow spoiler grooves in the nozzle increase flow friction to allow wider, less clog-susceptible passages while providing turbulent voids to continuously break up and clear contaminants from the flow. GP anti-clogging cryostats have demonstrated sustained operation with gas contaminant levels which quickly clogged conventional cryostats, while effectively maintaining a very stable cold tip temperature.

To liquefy the helium, the J-T cryostat provides for near-isenthalpic expansion from the 0.8 MPa compressor pressure to the 0.1 MPa storage dewar pressure at the 0.15 g/s flow rate. The 0.8 MPa pressure is chosen based on helium thermodynamic properties to result in the highest liquefaction rate per unit of compressor power.

The cryostat also provides for essential recuperative cooling of the pressurized helium flow to below the 10 K generated by the Stirling system. The helium flow at 0.8 MPa must be cooled to below approximately 7.4 K before expansion through the nozzle or no liquefaction will result. This is accomplished by passing the pressurized helium flow through a coiled finned tube heat exchanger around which flows the boil-off vapor which is initially at 4.2 K as it leaves the liquid helium storage dewar. The boil-off vapor is drawn into the system by the compressor suction through a thin-wall stainless steel sheath which encloses the coiled finned tube heat exchanger as shown in Figure 5. Finned tubing is similarly coiled around the Stirling cooling stages (as shown in Figure 1) to fully utilize the recuperative cooling potential of the incoming cold boil-off gas. Approximately 90% of the cooling required for the pressurized helium flow prior to expansion through the J-T nozzle must be derived from the incoming boil-off gas.

It might seem that a system should be able to 'bootstrap' its way down from 300 K using only recuperative cooling from incoming boil-off vapor without need for cooling from the Stirling cryocooler. Such a system would be a pure Linde-Hampson system and would require much more power than the subject hybrid system. This is because some form of power consuming refrigeration is required to transfer the latent heat of vaporization of

the helium boil-off, as well as system parasitic heat loads, to the 300 K sink. The Stirling cycle is inherently much more power efficient than the Linde-Hampson cycle and is therefore used to provide as much of the refrigeration as practical. A J-T stage is required to finally reliquefy and return the helium to 4.2 K because of practical limitations for a Stirling system to reach much below 10 K as mentioned in Section 3.0 and further described in Sections 4.3 and 4.5.

Key design parameters of the J-T cryostat are sizing of the nozzle cone angle and flow annulus to produce the required pressure drop at the proper flow rate, and effectiveness of the coiled finned tube heat exchanger. For design margin, the J-T cryostat was sized assuming a 10% liquefaction rate. If the heat exchanger effectiveness approaches 95%, as is probable in this type of heat exchanger, then the liquefaction rate should be close to 50%.

Fabrication, pressure, leak, and flow testing of the J-T cryostat, shown in Figure 6, were completed in Phase II, but it was not yet integrated with the system in order to facilitate basic performance testing of the multi-stage Stirling cryocooler.

4.3 Multi-Stage Stirling Analysis and Design

To reach temperatures much below 80 K from 300 K, the various types of cryorefrigerators require multiple stages due to the thermodynamic properties of the working media and to overcome external and internal parasitic losses. A Linde-Hampson system requires at least 3 stages to reach below 10 K as dictated by the boiling and inversion temperatures of the applicable gases. A Gifford-McMahon cryocooler can reach below 15 K with only 2 stages because the displacer can operate at very low speed (e.g. 0.5 Hz) and ample pressure ratio (e.g. 4:1), but with lower power efficiency than a Stirling system. Single-stage Stirling cryocoolers can routinely reach 65 K, but to reach 10 K from 300 K a hypothetical single-stage Stirling cryocooler with no external heat loads would require a regenerator effectiveness of better than 99.3%, which is not feasible. Multi-

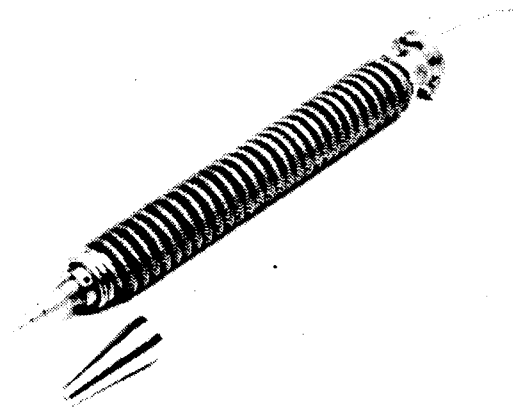


FIGURE 6. J-T CRYOSTAT FOR PROTOTYPE HELIUM LIQUEFIER

staging allows distributing the regenerators to operate over smaller temperature differentials, which lowers the effectiveness required, and provides more power efficient interception of heat loads. To reach much below 10 K requires compromises in operating speed and pressures which impose severe penalties on the upper stages.

Although there is a lot of analytical and empirical data available on the design of single-stage Stirling cryocoolers for operation near 80 K, there are no established guidelines for designing a multi-stage Stirling cryocooler to have particular refrigeration capacities at each stage. Zimmerman's experiments demonstrated that a stepped displacer could produce the effect of multiple expansion stages in reaching temperatures below 10 K, but provided little data for sizing the stages for specific capacities or optimizing performance.

Thermodynamically the subject system can be modeled as four single-stage refrigerators either in parallel or series with the same ideal (Carnot) heat absorbed, dissipated, and power required. But both arrangements are physically infeasible. The parallel arrangement would require that single stages operate from 300 K to temperature extremes of 10 K, 20 K, or 50 K, which is not realizable. The series arrangement would require that the compression space of each stage be cooled by the next higher stage, which is highly impractical at best. In the subject stepped-displacer system, all stages share a common compression space and stream of helium through the regenerators. This affects regenerator sizing to allow for flow and heat transfer of helium to lower stages, and introduces major uncertainties in determining the ratios of expansion space displacements to compression space displacement and to dead volumes, which are basic parameters in the design of single-stage Stirling machines.

The theoretic (Carnot) total work input required by either the parallel or series model is identical for the same external heat loads, but the sizing of the individual stages is not. The parallel model requires each stage to absorb only its external heat load and reject it directly to 300 K. The series model requires each stage to absorb its external heat load plus all the heat absorbed and the work dissipated by lower stages. For comparison, the

theoretical net refrigeration capacities prescribed for the stages of the subject system by parallel vs series modeling are: 1.0 vs 1.0 W at 10 K, 2.4 vs 4.4 W at 20 K, 6.4 vs 17.5 W at 50 K, and 13.1 vs 55.2 W at 120 K. Of course the difference between 13.1 W and 55.2 W refrigeration capacity for the 120 K stage can make a big difference in the sizing of the expansion space and regenerator for that stage.

The external heat loads are based on cooling the 0.15 g/s helium flow to the J-T cryostat, and the temperatures are design assumptions based on a 300 K sink, a 10 K fourth stage, and approximately equal Carnot coefficients of performance between stages.

The compression and expansion spaces and pressures were originally estimated in Phase I using single-stage formulae and Cryoweiss (Bib. 37) computer model analyses. Diameters, lengths, stroke and speed were proportioned in approximate correlation with temperature vs density and comparison with previous machines. Early in Phase II, mass displacements for each expansion stage were calculated from a helium T-S diagram, assuming a pressure cycle of 2 MPa to 4 MPa, constant-pressure regeneration, 10% temperature overlap between stages, and net refrigeration equalling 10% of theoretical.

The refrigeration required at each stage to cool the 0.15 g/s helium flow to the J-T was calculated to be 13.1 W at 120 K, 6.4 W at 50 K, 2.4 W at 20 K, and 1.0 W at 10 K, which is 10% of the total enthalpy change from 300 K to 10 K and assumes that the remaining 90% of the cooling is provided by the incoming boil-off vapor flow. It was further assumed that each stage must absorb the heat and work dissipated by lower stages (the parallel stages model). The required net refrigeration capacities for each stage were thus calculated to be 1.0 W at 10 K, 4.4 W at 20 K, 17.5 W at 50 K, and 55.2 W at 120 K.

The corresponding mass displacement rates derived from the helium T-S diagram, assuming net refrigeration equalling 10 % of theoretical, were 0.8 g/s at 10 K, 1.5 g/s at 20 K, 2.5 g/s at 50 K, and 3.1 g/s at 120 K. Those calculated from 10% of ideal isothermal expansion, given by heat absorbed per unit mass = $0.1 RT \ln (P_{\max}/P_{\min})$,

were 0.7 g/s, 1.5 g/s, 2.4 g/s, and 3.2 g/s, respectively. Note, these mass displacements are not the same as the total mass flow through each regenerator, which is the sum of the mass displacements for the corresponding stage and all lower stages. The gross refrigeration required for each stage depends on the expected losses.

The fundamental issues which governed the physical sizing and detail design of the machine were as follows.

In principle, Stirling machines produce more refrigeration per unit volume with increasing charge pressure and cycle pressure ratio. A charge (cycle minimum) pressure of 2 MPa and cycle maximum of 4 MPa were chosen as limited by structural practicality, sealing difficulty, and drive mechanism loads. Increasing pressure leads to thicker walls with increasing conducted parasitic heat loads. Decreasing pressure requires a larger, heavier machine for the same refrigeration capacity.

For a given pressure cycle, the refrigeration generated at each expansion stage is proportional to the product of speed, stroke, and diameter squared (i.e. displacement rate). All stages must operate with the same pressure cycle, speed, and stroke. Speed is limited by low heat transfer rates into sufficient regenerator mass in the lower stages, due to poor material specific heat capacity below 20 K. Stroke and diameters are limited by shuttle and conduction losses in the upper stages, driven by large stage-to-stage temperature differentials and otherwise relatively large diameters. The warmer stages favor faster speeds to limit diameter and stroke and the associated conduction and shuttle losses across the large temperature differentials.

Other losses include pumping loss, flow friction loss, and void volume losses. Pumping loss is caused by flow of working gas to and from the clearance space between piston and cylinder walls. Pumping loss increases with speed, diameter, and radial clearance, while shuttle loss is suppressed by radial clearance. Flow friction losses increase with speed and with attempts to minimize void volume, particularly in regenerators. Void

volume not only lowers the pressure cycle ratio but results in internal heat transfer and work losses from the compression/expansion of the working gas, especially in regenerators. Void volume is most detrimental in the coldest stages due to the gas density and limited regenerator heat capacity which is loaded by the compression/expansion internal heat flows.

Based on extrapolation from single-stage Stirling design guidelines, the ratio of dead volume, including regenerator void, to expansion space swept volume should be no more than 3:1 for the 10 K stage, decreasing to no more than 1:1 for the 120 K stage. The ratio of compression space swept volume to total expansion space swept volume should be in the range of 2:1 to 3:1. This may only be valid for single-stage cryocoolers in the 80 K range with dead/expansion volume ratio of 1:1. A literature review indicated that a compression/expansion volume ratio of 5:1 to 6:1 may be required for a cryocooler to operate down to 10 K, due to the gas density increase from 300 K to 10 K. Idealized Schmidt analysis for a 300 K sink prescribed ratios of compression space to expansion space swept volume of from 2.3:1 at 120 K to 11:1 at 10 K. The actual requirements for a multi-stage Stirling machine with a common compression space and distributed dead volumes are far more complex than can be precisely analyzed. An overall compression/expansion swept volume ratio of 5.5:1 was chosen as the best estimate.

The Stirling compression space sizing is driven by the total displacement of the expansion spaces, the dead volumes such as regenerator void (in proportion to the density of gas within them), and the corresponding compression space swept volume required to generate the pressure cycle. The speed must be the same as the expansion stages and the stroke must be similar in trade-offs with system layout and drive mechanism design. Thus, if nothing else, the physical sizing of the compression space limits the amount of refrigeration capacity margin for which the expansion stages can be practically designed.

Diameters, stroke, and speed are derived from the required mass displacement rates for each stage and proportioned according to loss trade-offs. Speed is limited by heat

transfer rates in the lower stage regenerators, due to poor specific heat capacity. Diameters and stroke are limited by conduction and shuttle losses in the upper stages, driven by large stage-to-stage temperature differentials. Piston-to-cylinder radial running clearance is key to suppressing shuttle loss to allow long stroke, small diameter, slow speed, at the cost of increased pumping loss. Stage-to-stage lengths must allow spaces for regenerators of sufficient heat capacity and heat transfer area without necessitating excessive diameter (conduction loss). Excess length suppresses conduction and shuttle losses but increases void volume. It was intended that the stage lengths accommodate conventional as well as thermal composite regenerators.

Regenerator volumes were estimated for the purpose of calculating void volumes and the compression piston displacement required for a 2:1 system volumetric compression ratio. The regenerators were initially sized to have 10 times the heat capacity of the helium working fluid assuming 300 series CRES screen for the upper 2 stages and lead shot for the lower 2, all with 60% void. This yielded excessive regenerator void volume (211 cm^3) and compression piston displacement (258 cm^3), so the regenerators were reduced to 132 cm^3 void volume (6:1 heat capacity ratio), which allowed the compression piston displacement to be reduced to 212 cm^3 (13.4 cm dia X 1.5 cm stroke) for a 2:1 system volumetric compression ratio. It should be noted that this sizing method does not ensure a 2:1 pressure cycle since the void volumes at colder temperatures contain gas at higher densities, and thus can have a proportionately greater effect on system performance than the larger, warmer void volumes. Also, previous analyses of loss trade-offs for conventional regenerators have indicated that the ratio of regenerator heat capacity to that of the working gas displaced each cycle should be as low as approximately 2:1.

Due to the poor heat capacity of all but a few exotic materials below 20 K, lead is not expected to add much more effectively coupled regenerative capacity to the coldest stage than that provided by the walls of the displacer and cylinder and the helium contained in the annulus. A lead regenerator was sized for the fourth stage anyway to allocate space for a thermal composite regenerator and to serve for analytic and test reference.

Dr. Radebaugh, of the National Institute of Standards and Technology (NIST), conducted computer analyses of the regenerators and expansion spaces sizing using the NIST programs REGEN, REGEN2, and REGEN3 (Bib. 1) to address real matrix and gas properties, limited heat capacity and transfer rate, thermo-fluid losses, void volume, and geometry (e.g. plates, mesh, microspheres, dimensions, thickness, spacing). The REGEN analyses consisted of stage-by-stage iterations as follows.

For chosen gross refrigeration, temperature, pressure cycle, operating speed, and regenerator material, idealized regenerator geometry was obtained from REGEN, which was then forced to a practical (producible) geometry by fixing key dimensions such as material thickness and flow gap. REGEN results were then used with REGEN2 in a preliminary pass at mass flow, expansion displacement, and simplified regenerator losses to yield net refrigeration. REGEN2 analysis was then repeated with mass flow from the preliminary pass added to mass flow from lower stages to account for regenerator sizing and losses to handle the total flow. These results were then submitted to REGEN3 for analysis of additional losses not accounted for by REGEN2. An unanticipated result of the REGEN analyses was that the optimum displacer stroke should be much shorter than the assumed design choice of 12.5 mm. The first series of analyses prescribed a stroke of 1.7 mm, as a function of displacement, to allow adequate heat transfer surface area in the fourth stage regenerator, which is known to be a problem below 20 K. This illustrated a basic design trade-off between locating the regenerator inside the displacer, as is common in split-Stirling and Gifford-McMahon cryocoolers, or arranging it around the cylinder wall as shown in Figure 1. Containing the regenerator matrix inside the displacer can make effective use of space which must otherwise be filled or sealed to avoid introducing overwhelming void volume, and which is a parasitic heat path anyway. However, this makes gas displacement and the regenerator cross section needed to handle it both a function of displacer diameter, which can severely limit the allowable stroke to match gas displacement with regenerator heat transfer capacity in very cold stages. When the fourth stage regenerator was configured around the cylinder to provide surface area independent of stroke, a second series of REGEN analyses arrived at a

stroke of 3 mm due to the need to limit shuttle loss, which is proportional to stroke squared, in the first stage. Longer stroke would require sizing the first and possibly second stage for more gross refrigeration (and power input) to make up for shuttle loss.

Based on a review of loss and drive mechanism design trade-offs and of Stirling cryocooler literature, it was decided to design for a displacer stroke of 10 to 12 mm and speed of 5 Hz. The suitability of this long stroke and slow speed for the first stage was evaluated by Cryoweiss simulations of a single 120 K stage for 9 combinations of stroke (7.6, 12.7, 25.4 mm) and radial gap (0.02, 0.05, 0.10 mm). Each case had an expansion cylinder diameter (70, 54, or 38 mm, resp.) corresponding to the same swept volume (29 cm^3) as a prospective first stage, a pressure cycle of 2 MPa to 4 MPa, and a nominal 300 series CRES screen regenerator. The Cryoweiss simulations indicated that the 0.10 mm radial gap would be very effective in suppressing shuttle loss without significant pumping loss, and that the 12.7 mm stroke would yield the best performance of 122 W net refrigeration at 120 K from the 29 cm^3 expansion swept volume at 5 Hz.

Subsequent Cryoweiss simulations of a single 120 K stage were performed holding the expansion cylinder diameter constant at 76 mm while varying stroke, radial gap, and speed, ignoring gross refrigeration, to evaluate the losses associated with the larger diameter required for the stepped-diameter multi-stage machine. Again, with a 12.7 mm stroke and 0.10 mm radial gap the shuttle and pumping losses were found to be well managed while the conduction losses were predominant but acceptable.

The Cryoweiss results were confirmed to agree with manual calculations of conduction losses and gross refrigeration. Also, several layout studies were performed to evaluate trade-offs in expansion and compression pistons strokes, drive mechanism, configuration, and balancing schemes to confirm the combination of a 12.7 mm displacer stroke and 19 mm compressor stroke.

Since Cryoweiss cannot simulate multiple stages and is questionable for analysis below 80 K in its assumptions of ideal gas and simplified regenerator losses, it still remained to confirm the appropriate refrigeration capacities and dimensioning of each of the 4 expansion stages.

To select a practical compromise of expansion spaces sizing for the foregoing requirements, trade-offs, and range of possible loads corresponding to series vs parallel stages and 80% to 90% recuperative cooling, refrigeration capacities for several sets of stepped displacer diameters were calculated from the isothermal expansion equation as summarized below.

REFRIGERATION LOAD (watts)

<u>Stage Temp. (K)</u>	<u>Parallel Stages</u>		<u>Series Stages</u>	
	<u>90% Recup.</u>	<u>80% Recup.</u>	<u>90% Recup.</u>	<u>80% Recup.</u>
120	13.1	26.2	55.2	110.4
50	6.4	12.8	17.5	35.0
20	2.4	12.8	4.4	8.8
10	1.0	2.0	1.0	2.0

Isothermal refrigeration generated = $m R T \ln (P_{\max}/P_{\min})$.

For helium expansion from 4 MPa to 2 MPa between diameters d_o and d_i with 1.27 cm stroke at 5 Hz, isothermal refrigeration = $7.18 (d_o^2 - d_i^2) \rho T$, watts.

Helium at 3 MPa and T =	120 K	50 K	20 K	10 K
ρ gm/cm ³ =	0.012	0.025	0.07	0.13

REFRIGERATION CAPACITY (watts)

<u>Stage Temp. (K)</u>	<u>Displacer Dia. (cm)</u>	<u>Isothermal Refrigeration</u>		
		<u>X 1.0</u>	<u>X 0.3</u>	<u>X 0.15</u>
120	7.62	334	100	50
50	5.08	141	42	21
20	3.18	85	26	13
10	1.27	15	4.5	2.2
120	7.62	396	119	59
50	4.45	120	36	18
20	2.54	49	15	7.4
10	1.27	15	4.5	2.2
120	10.16	729	219	109
50	5.72	203	61	30
20	3.18	85	26	13
10	1.27	15	4.5	2.2

The middle set of stepped displacer diameters above was selected to proceed with design detailing based on providing a good match of refrigeration capacities for the possible loads without requiring an impractically large compression piston. The final dimensions arrived at in the prototype cryocooler were, for the compression piston 152 mm diameter and 19.1 mm stroke, and for the expansion piston 76 mm diameter and 14.3 mm stroke, resulting in a 5.34:1 compression/expansion swept volume ratio.

Cryoweiss computer simulations of a single-stage 120 K Stirling cryocooler were also used to design the cooler, which removes the heat rejected in the compression phase of the cycle. The cooler must transfer all of the heat due to the refrigeration load and work input, including mechanical and thermodynamic inefficiencies, to the 300 K external coolant flow without introducing excessive void volume or flow restriction in the internal

helium working fluid. Cryoweiss was used to evaluate the effects of void volume, flow restriction, heat transfer rates and fin efficiency on Stirling system performance in iteratively arriving at an effective cooler design. The lower stages were accounted for by equivalent cooler heat load, helium mass displacement, and system void volume in the single-stage model.

The cooler, which can be seen in Figure 3a, includes an annular gas-to-liquid heat exchanger surrounding the base of the expansion cylinder, and liquid coolant passages around the annular heat exchanger and across the compression space head. The annular heat exchanger consists of 200 densely spaced longitudinal fins protruding radially inward for the helium gas to flow through between the compression space and first stage regenerator, and an external helical channel enclosed by an outer sleeve to form the liquid coolant passage. The internal longitudinal fins and the external helical channel are integrally formed in a single 6061 aluminum cylinder to minimize thermal resistance. The enclosing coolant passage sleeve and adjoining compression space head are also 6061 aluminum for high thermal conductivity.

4.4 Multi-Stage Stirling Computer Model

It is apparent in the preceding discussions that multi-stage Stirling design involves complex interactions among numerous variables. At best, the most sophisticated computer models of single-stage Stirling systems only approximately analyze and predict real machine operation. Prior to the subject project, there were no known computer models which attempted to analyze multi-stage Stirling operation. A major task of the subject Phase II project was derivation of a multi-stage Stirling simulation program with realistic modeling of thermo-fluid losses and other non-idealities. This 'second order' multi-stage Stirling computer model will evolve and be refined interactively with the design and testing of the prototype cryocooler.

First order analysis utilizes theory such as the well-known Schmidt analysis to predict Stirling machine performance. Such theories are highly idealized but have the advantage of closed form solutions for the pressure and energy flow relations. They are useful for assessing the probable effects of changing the principal design parameters of a Stirling system.

Second order analysis attempts to predict the actual machine performance with a practicable level of accuracy. It utilizes a basic analysis of the operating cycle, such as the Schmidt cycle with isothermal processes, or the more complicated cycle with adiabatic compression and expansion processes first proposed by Finkelstein. Predictions derived from these basic cycles are subsequently corrected to allow for the various parasitic losses characteristic of Stirling machines. Second order analyses typically require the use of digital computers and involve time step or cyclic interval procedures to obtain the pressure characteristic with integral procedures for the energy transfers, net work transfers and parasitic losses.

Third order analysis attempts an uncompromising simulation of the energy and fluid flows in the various spaces of a Stirling machine. It employs advanced mathematical procedures involving two or three dimensional finite element or finite difference time step procedures. Solutions are feasible only using high speed digital computers. The analysis requires the provision of a large amount of data, most of which is not well known and consumes substantial computing time and effort.

The Stirling simulation programs used by General Pneumatics were developed at the University of Calgary by Dr. G. Walker, R. Fauvel, and M. Weiss (Bib. 37). They are based on a procedure devised by Prof. J. Smith and his colleagues at the Massachusetts Institute of Technology and utilized by Dr. W. Martini in a second order, isothermal, decoupled corrections simulation technique which has proven effective in giving reasonable results with minimum computing time when compared with third order analysis techniques. The programs are written in Fortran 77 and adapted for use on

microcomputers using MS-DOS 2.0 or higher. They are completely modular to facilitate modification or addition of subroutines, and include extensive graphics of the effects of variables on Stirling machine performance, which are highly useful for design refinement and optimization. The version of the Stirling simulation programs which is directed to cryorefrigerators is called CRYOWEISS.

The basic program requires definition of heat exchanger areas and volumes, compression and expansion space volume variation, mean gas pressure, and coolant and expansion cylinder temperatures. Gas properties such as pressure and temperature dependent parameters for viscosity, conductivity, heat capacity, Prandtl Number, etc., are processed in a subroutine which allows choosing different gases as the working fluid. Heat exchange, fluid, and mechanical losses are handled in a separate subroutine which allows easy implementation of new analysis techniques and data. Several other subroutines correlate design configuration, drive, and dimensioning data into a general form for use in the basic program.

Shortly prior to his death in 1987, Dr. Martini was commissioned by the National Bureau of Standards (now NIST) to devise a second order simulation program for a Stirling cryocooler with 4 expansion stages. At the time of his death the Martini multi-stage Stirling program was incomplete. Subsequently, Dr. Radebaugh of NIST provided the material to Dr. Walker for further development for the subject project. The program was to take advantage of Dr. Walker's work on multi-stage Stirling analysis to date (Bib. 34, 36) and incorporate computerized data for helium real properties also provided by Dr. Radebaugh. When completed, the program was to simulate the performance of the subject four-stage Stirling cryocooler, including the effects of real gas properties, non-ideal regenerators, and thermo-fluid losses.

The completed multi-stage Stirling simulation program is named MULTI. It is menu driven, graphics oriented, uses the DEOGRAF graphics routines developed by DEOCOMP Corp., and is written in FORTRAN 77 for personal computers using MS-DOS 2.0 or higher. The

program simulates a two-piston Stirling cryocooler having 4 stepped expansion spaces which are interconnected through 4 annular gap regenerators or porous matrix regenerators of various menu-selected materials.

Input data to the program includes piston diameters, strokes, and phase angle, regenerators, cooler, and void volumes specifications, operating temperatures, charge pressure, and speed. The program calculates the refrigeration available at the given temperatures for each of the 4 expansion stages, the input power required, and the internal pressure-volume relationships. Tabulated and graphical output includes conduction, flow friction, pumping and shuttle losses, pressure vs time, pressure vs the swept volumes, power input vs speed for different constant mean pressures, refrigeration capacity vs speed at different constant mean pressures for each of the 4 expansion spaces, and the effect of piston phase angle on performance for given speed, pressure, and temperatures. An example printout is included as Appendix A.

The program employs a second order hybrid isothermal analysis which takes into account finite material heat capacities but assumes perfect heat transfer between the materials and the working gas. It also assumes that for each incremental time step the working gas pressure is equal throughout the system. Flow pressure losses are calculated separately for each time step, summed over the cycle, and added to the required power input. Similarly, net refrigeration available at each of the 4 stages is determined by subtracting parasitic losses from gross refrigeration calculated from pressure-volume relationships for each stage.

The program can operate with real (helium) or ideal gas properties. However, it requires about 40 times longer with real gas properties than with ideal gas. Since the difference in results is minor for temperatures above 20 K, a provision is incorporated to allow use of real gas properties below 20 K and ideal gas above 20 K to increase program speed.

In debugging trial runs, the program was found to have an occasional instability in the fourth stage for specified temperatures below 12 K. The instability, exhibited as rising temperature, is thought to be related to the real phenomenon of regenerator ineffectiveness due to diminishing regenerator heat capacity below 12 K compared with helium. This is comparable to excess heat dissipation indicated for regenerator ineffectiveness for similar conditions by the REGEN programs.

As of the end of Phase II, the MULTI program was operational (as exemplified in Appendix A) but still lacked a subroutine for calculating flow pressure drops through porous matrix regenerators (such was in place for annular gap regenerators), and validation and refinement by correlation with multi-stage cryocooler test data.

4.5 Regenerators

A regenerator cyclically absorbs heat from and releases heat back to the working fluid. In the ideal Stirling refrigeration cycle, the working fluid takes on heat at constant volume as it passes through a regenerator from a cold expansion space to a warmer compression space. Heat is rejected from the system by isothermal compression in the compression space. The working fluid then passes back through the regenerator for constant volume regenerative cooling. Heat is stored in the regenerator for transport out in the next cycle. Finally, refrigeration occurs by isothermal expansion in the expansion space where heat is absorbed by the working fluid.

In a Stirling machine the flow surges first one way then the other so that little or none of the working fluid passes completely through the regenerator matrix. This, combined with the axial temperature gradient, complicates the energy flow so the incremental details are not well understood and theories of regenerator operation in Stirling machines are highly idealized. It is common, for example, to assume a linear axial temperature gradient and to ignore the local temperature variations in both matrix and gas that must occur.

More thorough analyses of regenerator performance require computer simulations such as with the REGEN programs as described in Section 4.3.

Two factors critical to a Stirling cryocooler's power efficiency and ability to reach low temperature are the dead volume and the thermo-fluid performance of the regenerator. Dead volume is volume in the working space, e.g. in the heat exchangers, which does not vary cyclically and therefore reduces compression ratio while causing power losses due to heat flows resulting from compression and expansion of the gas in the void. Favorable thermo-fluid characteristics are low fluid friction and thermal conductivity in the flow (axial) direction, and high radial conductivity, surface area, and heat capacity to promote heat transfer with minimum temperature difference between the matrix and the working fluid.

Providing effective regenerator heat capacity is a fundamental problem in achieving temperatures below 20 K with regenerative cycle cryocoolers (e.g. Stirling, Gifford-McMahan, pulse tube, etc.). Ideally, the regenerator should have high heat capacity and heat transport capabilities such that heat exchange with the helium working fluid at a high rate does not cause significant temperature fluctuation in the regenerator. Also, the regenerator should introduce minimal axial heat conduction, flow restriction, void (compressible) volume, and clogging susceptibility in the helium flow path.

Heat capacity is a serious problem in very low temperature regenerators because the specific heat and thermal conductivity of solids decrease with temperature while density remains constant, whereas the specific heat and density of helium increase with decreasing temperature. This makes it very difficult to effectively couple enough regenerator heat capacity to the helium working fluid. The specific heat capacity of materials falls off steeply with decreasing temperature below 100 K. This is due to the inherent decrease, with temperature, in lattice vibration energy, which is the primary form of thermal energy, and to a lesser degree in electron energy. Thus, as atomic freedom is diminished by decreasing temperature, so is a material's capacity to store thermal

energy. As depicted in Figure 7, a few materials undergo magnetic moment transitions in internal energy over narrow temperature changes below 20 K, which has the effect of a spike in heat capacity. Because such transitions occur over only a few degrees in temperature change, they are of limited value in providing a small supplemental heat capacity and are not very effective during start-up from ambient temperature.

Making matters worse, helium at only 1 MPa pressure has a higher specific heat capacity than virtually all other materials below 12 K. For size and weight practicality, cryocoolers typically have helium charge pressures of 1 to 2 MPa. Thus, a large amount of regenerator material is required to provide more heat capacity than the helium working fluid itself. Adding regenerator material creates problems with flow restriction, void volume, axial conduction losses, and time required to transfer heat into and out of the regenerator matrix. The last factor necessitates a low flow rate which, in Stirling machines, results in slow operating speed and high drive mechanism loads for a given power level (torque x rad/sec).

Regenerator ineffectiveness results from deficient heat transfer between the matrix and the working fluid due to insufficient matrix heat capacity or heat transport rate, and heat dissipation due to compression/expansion of working fluid in the regenerator void volume. Regenerator ineffectiveness directly subtracts from the refrigeration produced in a cryocooler, thereby necessitating a larger machine and greater power input for a given amount of refrigeration. The requirement for a larger machine compounds the reduction in power efficiency by proportionately increasing the void volume and heat transfer losses.

The criticality of regenerator ineffectiveness in cryocoolers is illustrated by noting that, with a heat sink temperature of 300 K, the ratio of heat cycled in a perfect regenerator per unit of refrigeration produced at various temperatures is: 14 at 77 K, 70 at 20 K, and 140 at 10 K. Thus, for each watt of refrigeration at 10 K, a 0.5% regenerator inefficiency causes a $0.5\% \times 140 = 0.7$ watt refrigeration loss requiring increased size and power input by a factor of more* than $1/(1 - 0.7) = 3.3$ (*due to the compounding effect of increasing size).

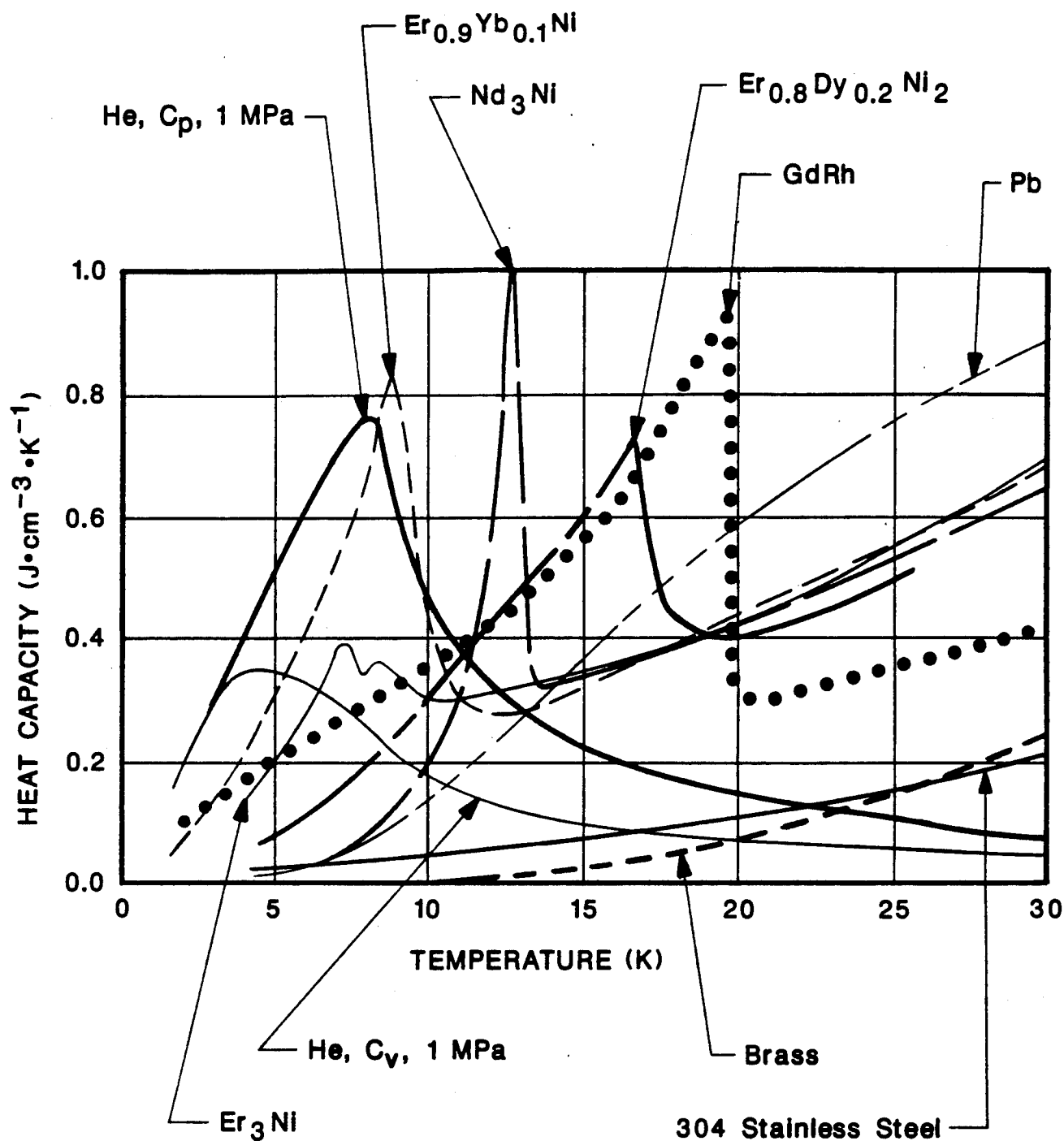


FIGURE 7. VOLUMETRIC HEAT CAPACITIES OF VARIOUS MATERIALS

To translate this into terms of input power required, the minimum theoretical (Carnot) input power required per watt of refrigeration at 10 K, with a 300 K heat sink, is $(300 - 10)/10 = 29$ watts/watt. Real cryocoolers have typically achieved less than 1 to 2% of Carnot efficiency at 10 K, requiring 1500 to 3000 watts/watt, largely due to regenerator inefficiency. A regenerator inefficiency of only $1/140 \approx 0.7\%$ would result in zero power efficiency, i.e. no refrigeration producible at 10 K. An improvement of only 0.1% in regenerator efficiency might well double power efficiency, reducing input power required by 750 to 1500 watts/watt.

In addition to the size and weight impacts associated with power efficiency, regenerator ineffectiveness limits operating speed with inversely proportionate effect on system size and weight. Currently, 10 K cryocoolers are limited to operating speeds in the range of 0.5 to 5 Hz, and consequently weigh several hundred kg per watt of refrigeration, because of the very poor specific heat capacity and transport rate of conventional regenerators. In contrast, 80 K cryocoolers operate at speeds of 30 to 60 Hz and weigh on the order of a kg per watt of refrigeration. Increases in the specific heat capacity or transport rate of regenerators for 10 K cryocoolers would allow proportionate increases in operating speed, which would allow more than proportionate reduction in machine size and weight, since parasitic losses also decrease with machine size.

Since refrigeration is produced in proportion to the rate of doing work, operation at higher speed and power efficiency corresponds with much lower drive forces and bearing loads. Higher operating speed is also essential to employing flexure suspension, linear resonant drive systems, which require very short strokes of less than 1 mm (for flexure life) and resonant frequency in the range of 30 to 60 Hz (for weight and power efficiency). Such systems have been found to be key to extending the operating life of 80 K cryocoolers from a few 1000's of hours to several 10,000's of hours.

Conventional regenerators have contained stacked fine wire mesh, coiled foil, porous sintered powder, or, in the coldest stages, snugly packed lead/antimony microspheres.

Various combinations of rare earth compounds, such as those in Figure 7, are being researched for very cold regenerators but offer marginal benefits and are very difficult to produce in suitable forms.

Energy Science Laboratories, Inc. (ESLI) of San Diego, California was contracted for the research and development of the regenerator matrices for the subject prototype multi-stage cryocooler. ESLI has pioneered the development of a class of novel composite materials for use in thermal energy storage applications. These thermal composite materials consist of layers of high conductivity materials (metal or crystalline graphite fibers) which conduct heat into high heat capacity matrix materials. The layered structure allows a very large anisotropy in thermal conductivity, which suppresses axial conduction losses. Thermal composite regenerators offer thermal flux, penetration, and specific heat capacity far surpassing conventional materials.

A measure of regenerator thermal performance is the product of the thermal conductivity (K) and the volumetric heat capacity (C). Table 1 illustrates how compositing leads to a high KC product. A 50-50 composite is illustrated in Table 1, but other composite proportions may be more suitable for a given application. Table 2 lists the thermal characteristics of example regenerator materials and shows how composites can provide thermal penetration and power-to-weight characteristics surpassing conventional regenerator materials such as lead and copper.

ESLI researched various materials to determine possible candidates for the high-K and high-C components at the temperatures of interest. These materials included high purity copper and aluminum foils and carbon fibers for conductivity, and polyimide film, iron-doped spinel ceramic, and cordierite ceramic honeycomb for thermal capacitance. Composites tested included carbon-carbon, graphite fiber in glass, and carbon fiber in YLA RS-3 polycyanate, a resin tested by General Dynamics to withstand thermal shock from room to cryogenic temperature. Cryogenic-suitable adhesives evaluated included various epoxies, bismaleimide, Durimid 120 polyamide, and FEP Teflon. ESLI also

Table 1. Compositing for high KC product

Material	Thermal Conductivity, K	Specific Heat, C	KC
high-K	100	1	100
high-C	1	100	100
50-50 composite	50	50	2500

Table 2. Figures of merit for selected regenerator materials (T = 100 K)

Material	Thermal Conductivity, K (W/k-m)	Specific Heat, C (J/kg-k)	Density, D (kg/m ³)	KDC (x 10 ⁻⁶) ¹	KDC ² (x 10 ⁻⁹)	K _{radial} /K _{axial}
Lead	39.6	120	11400	54.2	6.50	1
Organic	0.2	600	870	0.104	0.063	1
Copper	483	250	9800	1075	269	1
50% Cu/Org.	242	425	4885	502	312	1208
Graphite	2500	146	2200	805	118	10
50% Gra/Org.	1250	373	1550	723	270	6250

$K_{\text{radial}}/K_{\text{axial}}$ - measures anisotropy in thermal conductivity

KDC - measures thermal penetration or flux

KDC² - measures power-to-weight ratio

investigated a scheme of mixing rare earth powders in adhesive to form high thermal capacity layers between metal foils and thereby avoid the problem of rare earth materials being very brittle and difficult to melt or shape. Careful attention was given to selecting materials which would insure contaminant free operation as well as to the thermal, mass, corrosion, and flow properties. Several prospective regenerator designs, along with their advantages and disadvantages, are described in Table 3.

TABLE 3. PROSPECTIVE REGENERATORS

Description	Advantages	Disadvantages
Baseline regenerator, stacked metal screens or Brunswick feltmetal	Standard structure with proven performance	Relatively high pressure drop
Graphite-epoxy fins with anisotropic conductivity, thermal composite, 50-70% graphite fiber, remainder resin matrix	Strong thermal penetration into matrix with extremely high anisotropic conductivity, $K_{rad}/K_{axl} = 100$	Requires cutting of hundreds of either slots or plates
Perforated plastic film in parallel plate geometry, Hoeschst-Celanase Vectra liquid crystal polymer film, Allied Aclar film or Dupont Kapton film	Potentially better heat transfer to pressure drop ratios with lower conduction losses than in parallel plates	Fabrication technique to be developed
Polymer tubular arrays or extruded thin wall plastic honeycomb	Potentially better heat transfer to pressure drop ratios with lower conduction losses than parallel plates	Fabricating hundreds of fine tubes
Carbon fibers in a porous phenolic matrix	High conduction anisotropy	Can make crude prototype, but controlling final properties is difficult. Pressure drop unknown

Regenerator design thermo-fluid dynamics trade-offs were evaluated by extensive computer analyses at ESLI and GP WRC. The basic performance parameters included heat capacity and transfer rate, conducted losses, flow resistance, and void volume. The

modeling programs used to evaluate the regenerators were REGEN and CRYOWEISS, modified as needed to account for the various regenerator designs' non-idealities. Concurrently with the computer analyses, ESLI was evaluating the practicality and developing fabrication techniques for the regenerator designs.

Starting with the conventional stacked metal screen regenerators, commercially available screens were examined using the CRYOWEISS Stirling simulation codes. Both market and tensile grade meshes were examined. The market grade mesh has a tighter weave, hence a higher fill factor. The mesh sizes examined varied from a maximum of 90, i.e. 90 holes per inch in either direction, to a minimum of 400 for market grade and 230 for tensile grade mesh.

For each of the 8 tensile and 15 market grade meshes, a series of 25 simulations was done in close coordination with cryocooler design parameters derived at GP WRC.

An interesting result was observed from these computer simulations. The optimum performance was not very sensitive to mesh size. The market grade 200 mesh defined the best net refrigeration for a given gross power input. Variation among meshes was due mainly to the change in machine pressure ratio resulting from the change in regenerator void volume.

Coarse meshes whose wire size was far from optimum, as for example the M90 mesh (market grade, size 90), showed a substantial increase in machine efficiency as the regenerator was lengthened at constant volume. This implied that the balance between flow loss and conduction loss was not optimum, as expected for a very coarse mesh with low flow loss. The overall performance also increased if the total volume was increased somewhat while the regenerator was lengthened. This meant that the regenerator was undersized for this particular coarse mesh, and improved as its volume was increased. For the M400 mesh, the trends were generally opposite, with flow loss being too high and a slightly lower volume and shorter regenerator length giving increased efficiency. Super-

imposed on these trends was the expected effect of regenerator void volume on overall machine power and refrigeration. If regenerator void volume was decreased, the machine pressure ratio was increased, and both net refrigeration and gross power requirements were increased.

The net result of these analyses is that the baseline designs chosen for the upper 2 stages of the prototype cryocooler employ stacked M200 mesh screens of 316 CRES, which appears to be near the mesh upper limit and a good compromise of efficiency vs net refrigeration. The conventional regenerators chosen for the lower 2 stages contain 0.2 mm diameter lead/antimony microspheres packed to a near theoretical fill factor of 62%. A composite regenerator consisting of electrostatically flocked radially oriented carbon fibers in an annular gap between G-10 fiberglass/epoxy tubes was also fabricated for the fourth stage. Composite regenerators based on nested tapered epoxy shells were also designed for the third and fourth stages but fabrication attempts were not successful as of the end of the Phase II project.

In some applications, notably the upper stages involving moderate temperatures and slow speed, thermal composites may not offer sufficient advantage to justify their use over simpler stacked screen or planar duct regenerators. In further development it is planned to consult with ESLI in continued testing of thermal composite regenerators in the prototype multi-stage cryocooler. Use of the prototype cryocooler as a test bed for various types of advanced regenerators leading to higher efficiency, smaller, faster operating speed machines allowing use of high reliability non-wearing drive mechanisms and seals is a continuing development objective.

4.6 Drive Mechanism, Piston Guides and Seals

To reach temperatures approaching 10 K with current regenerator technology requires very slow operating speed. Drive forces required for a given power level vary inversely with operating speed and stroke. Thus a 10 K Stirling cryocooler involves slow operating

speed (e.g. under 10 Hz) and correspondingly high drive forces. (A Gifford-McMahon cryocooler avoids this dilemma by valving the pressure cycle which allows a displacer/regenerator to reciprocate at very slow speed, e.g. under 1 Hz, while a continuously rotating compressor operates at high speed, but at the cost of much lower thermodynamic efficiency than a Stirling machine.) To employ non-wearing bearings, piston seals and guides requires a linear motor drive, to avoid side forces, and, particularly for flexures, short strokes which necessitate a high speed-force product for a given work (displacement) rate. In a reciprocating linear motor drive the kinetic energy must be absorbed and returned at the end of each stroke by springs at a resonant operating frequency or impractically large driving force and power will be required. A linear motor drive for resonant operation under 10 Hz, especially with short strokes, would entail prohibitively large masses and drive forces. Therefore, in order to reach 10 K and to allow testing over a variable slow operating speed, the subject Stirling cryocooler employs a type of crank mechanism with lubricated bearings driven through speed reduction pulleys by an ac induction motor with a variable frequency controller. As such, the subject cryocooler is a developmental test bed for researching multi-stage Stirling cryocooler analysis, design, and regenerators advancements, and is not a flight prototype.

Various forms of drive mechanisms were evaluated for best suitability to accommodate the loads with the fewest bearings, minimum wear, and longest life. The mechanisms evaluated were conventional crank and connecting rods, rolling Scotch yoke, Rhombic drive, and Ross linkage. The conventional crank and the Scotch yoke were found to impose excessive side forces on the piston seals and guides. This is tolerable in machines where the piston rings can be lubricated with a hydrodynamic film of oil separating them from the cylinder wall. In Stirling cryocoolers, residual oil on the cylinder walls would accumulate in and clog the regenerator matrix and would solidify in the cold spaces.

The Rhombic and Ross mechanisms were specifically developed for Stirling machines. Both minimize side forces, but the Rhombic drive involves more bearings and complexity. The Ross linkage was therefore preferred.

The Ross linkage was invented by Andy Ross of Columbus, Ohio, with whom General Pneumatics maintains a licensing and consulting agreement. As diagrammed in Figure 2, the crank 'OA' rotates about the crankshaft axis 'O'. A rigid yoke 'ACE' is attached to the crankpin at 'A' and to the swinglink at 'B', having a fulcrum at 'D'. As the crankpin 'A' rotates, the swinglink bearing 'B' describes a circular arc while the extremities 'C' and 'E' describe very narrow 'figure eights'. Thus points 'C' and 'E' depart only slightly from a straight line motion along the axes of the cylinders. The resulting piston motion is very closely sinusoidal with a 90 degree phase difference necessary for optimum Stirling performance. The sinusoidal motion has the benefit that higher frequency components of dynamic forces at multiples of the running speed are minimized and are much smaller than those from other reciprocating drive mechanisms. The Ross linkage has the advantages of:

- o Gives the pistons optimum phasing, sinusoidal motion, and straight line travel.
- o Minimizes piston side forces, permitting use of oil-free piston seals, while minimizing seal wear to promote long operating life.
- o Requires relatively small size and weight for a given swept volume.
- o Facilitates a large bore/small stroke ratio for low piston seal rubbing speeds and short heat exchangers (regenerators and cooler) with minimal fluid pressure losses.
- o Allows closely spaced parallel cylinders which are easily connected with compact heat exchangers and minimum dead volume to promote high thermodynamic efficiency.

The motions of the pistons and drive linkages were verified by a computer kinematics simulation of the design. The lateral motion of the expansion piston connecting rod bearing is 0.02 mm, which is accommodated by minute flexing in the rod and radial clearance in the piston bore. The lateral motion of the compression piston connecting rod bearing is 0.16 mm, which is accommodated by a negligible 0.037 degree rocking motion of the piston.

A dynamic forces analysis of the pistons and drive mechanism was also performed using the Machinery Kinematics and Dynamics (MKAD) computer program. The program allowed accurate modeling of the kinematics and mass properties of the system. Output from the program included components positions, velocities, accelerations, forces, and reactions as a function of time. It was determined that the system would generate a peak unbalance force of less than 44 N at 5 Hz in the axis parallel to piston motion. The unbalance force is reacted by the crankshaft, its bearings, and the block structure. For development hardware testing in a laboratory this unbalance force is small and does not pose a problem. A dynamic balancing mechanism consisting of 2 pairs of counter-rotating wheels, as shown in Figure 8, was designed. By proper phasing of balancing masses on the 4 wheels all inertial unbalance forces and moments can be canceled. But to limit cost and complexity, such a balancing mechanism was not included in the development hardware.

An analysis was also performed of the combined pressure-induced and inertial loads and torques for sizing the structural members and bearings. The calculated peak bearing load is 15 klb, which is shared by a pair of crank lobe bearings and by the crankshaft end support bearings. The peak stress, including stress concentration factors, is 70 kpsi due primarily to bending stress in the shaft adjacent to the crank lobe. The crankshaft is VASCOMAX 300 CVM (cobalt vacuum melt) AMS 6514B maraging steel heat treated to R_c54 with the crank lobe bearing journal nitrided to R_c58-62 . The yoke and piston rods are 7075-T651 aluminum, the swinglink is 304 CRES, its fulcrum shaft is AISI 4340 steel hardened to R_c43-46 , and the crankcase and cylinder head plate are 6061-T651 aluminum.

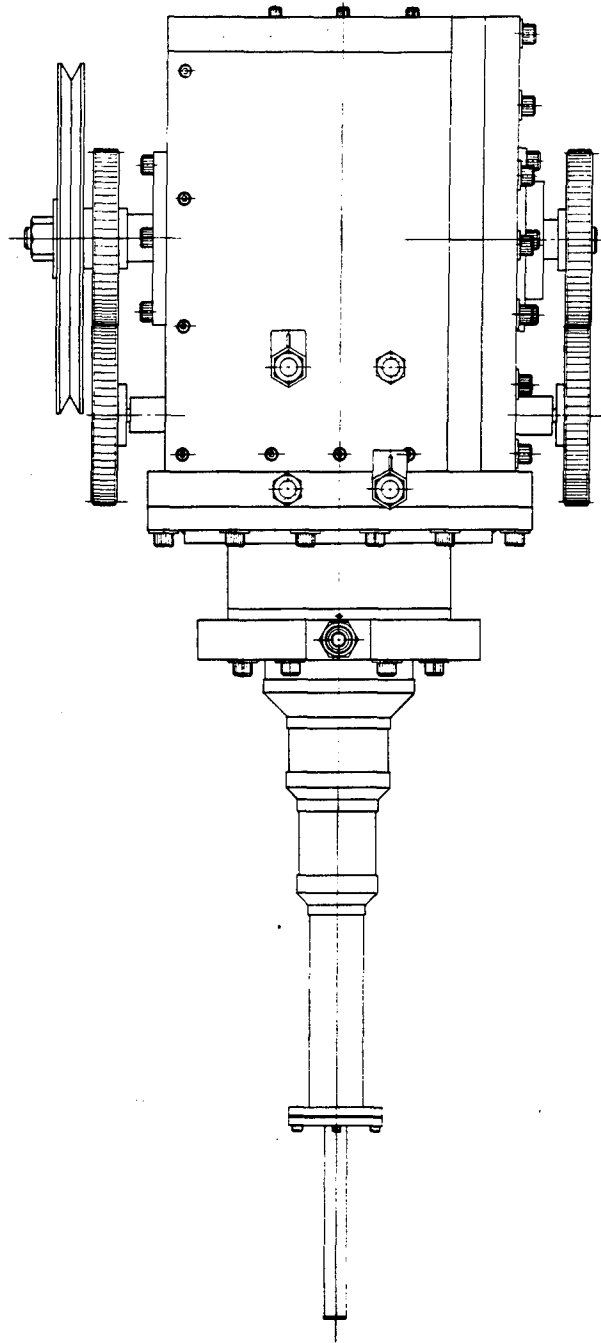


**FIGURE 8. COUNTER-ROTATING DYNAMIC BALANCE
WHEELS ARRANGEMENT**

The drive mechanism is housed in a helium-pressurized crankcase, as shown in Figures 3 a and b. One end of the crankshaft terminates in a bearing enclosed in a crankcase wall. The other end of the crankshaft passes through a bearing and a helium shaft seal in the opposite wall and couples to the drive motor (not shown). The crankshaft end support bearings are spherical roller bearings which can carry high radial loads, limit axial travel, and tolerate misalignments. The crank lobe bearings consist of a pair of cylindrical roller bearings, for high radial load capacity, bracketed by a pair of deep-groove ball bearings to limit axial motion of the yoke relative to the shaft. The ball bearing inner races are clearance fit on the shaft to insure that they are not subjected to high radial loads. Spherical roller bearings are also used to support the ends of the swinglink fulcrum shaft at the crankcase walls. All of the above rolling-element bearings are grease-pack lubricated and sealed with lip seals.

The swinglink and the piston rods connections to the yoke are Garlock DU bushings, which accommodate the small oscillations at these points. These bearings consist of a cylindrical steel casing, a porous bronze layer impregnated with a PTFE (polytetrafluoroethylene) and lead mixture, and a PTFE-lead overlay. The shaft journals which ride in these bushings are polished 304 CRES. Although the DU bearings are self-lubricated, friction is minimized by oil wicking through capillary holes in the journals from felt reservoirs within the shafts.

A number of lubricants were considered for the drive mechanism, including various lithium complex mineral oil greases, silicone greases, and 2 synthetic fluorocarbon greases: Dupont Krytox GPL-206 and Castrol Braycote 601. Power Up NNL 690, a high film strength, boundary lubricant enhanced, synthetic hydrocarbon oil was chosen for baseline testing in the DU journal bearings, and a proprietary thixotropic grease based on NNL 690 was selected for the grease-packed roller and ball bearings.

The straight line motion of the Ross mechanism facilitates the incorporation of metal bellows seals behind the pistons, as shown in Figure 3a, to prevent migration of

contaminants such as lubricant vapors from the crankcase into the cryocooler working spaces. These bellows seals are made of welded AMS 350 steel by the Belfab Division of Pacific Scientific in Daytona Beach, Florida. The crankcase is pressurized with helium to the cryocooler cycle minimum (charge) pressure to offset the differential pressure loads on the drive mechanism and the bellows. The pressure in the bellows spaces is subject to small fluctuations above the charge pressure due to cyclic volume variation and leakage past the pistons. Helium is returned to the working space by the piston lip seals when the pressure cycle falls below the bellows space pressure. The system charge pressure is maintained from a pressure-regulated compressed helium reservoir through check valves which prevent contaminated flow from the crankcase to the working space and limit the pressure differential across the bellows should the crankcase lose pressure.

The piston seals, one located near the face of the compression piston and the other near the base of the expansion piston, are pressure-loaded lip seals which exert increasing sealing force against the cylinder wall as pressure in the working space increases, and relax as the pressure differential across them decreases. This reduces running friction and wear, and limits pressure buildup in the bellows spaces behind the seals by allowing helium to return to the working space during the low pressure parts of the cycle. Each piston also has a relatively wide guide band which extends behind the piston lip seal. The guide bands and the lip seals are made of Dixon Industries Rulon® LD, a glass-fiber-reinforced polytetrafluoroethylene (PTFE Teflon) which has demonstrated low friction and wear in similar applications and wear testing (Bib. 16, 28, 31, 40). The expansion piston also has 2 spring-loaded, lapped-split seal rings on each of the first 3 displacer stages (6 rings total) as can be seen in Figure 3a. These rings are made of unreinforced PTFE Teflon. Each ring rides in a groove in the displacer and is lightly preloaded against the cylinder wall by a wavy band spring in the groove. The distinction between the displacer seal rings and the piston lip seals is that the piston seals seal tightly against the working space pressure cycle, whereas the displacer seals force the helium to flow through the regenerators without opposing a significant pressure differential. The straight line

motion of the Ross drive mechanism and nominal clearance of the piston guide bands in the cylinders results in minimal side forces and rubbing pressures on the guides and seals.

5.0 FABRICATION, ASSEMBLY, AND TESTING

5.1 Compressor and J-T Cryostat

As described in Section 4.2, the detail design of the three-stage compressor was completed, but fabrication was not, during Phase II. The J-T cryostat was fabricated, as shown in Figure 6, and was leak, pressure, and flow tested, but was not integrated with the multi-stage Stirling cryocooler as of the end of Phase II.

5.2 Regenerators

Because they are intimately tied together both thermodynamically and dimensionally, the detail design and fabrication of the regenerators and the 4 stage expansion cylinder assembly proceeded in close coordination between ESLI and GP WRC. Regenerator structural integrity, heat capacity, flow area, length, pressure drop, and conduction losses trade-offs had to be matched with displacer requirements for diameter, stroke, length, heat transfer and helium flow paths at each stage. Detail dimensioning, materials, joints, seals, assembly provisions, and whether the regenerators should integrally provide the outer pressure containment wall and/or the inner displacer cylinder wall were resolved in continuing collaboration. It was decided that the regenerators would be cylindrical cartridges sized to precisely fit in annular spaces between the pressure housing and the displacer cylinder at each stage.

As described in Section 4.5, ESLI evaluated and tested a number of regenerator designs and materials, and successfully fabricated wire mesh regenerators for the upper 2 stages, lead/antimony microsphere regenerators for the lower 2 stages, and an electroflocked carbon fiber alternative regenerator for the fourth stage.

The stacked screen regenerators exemplify ingenious fabrication technique and tooling which allowed machining of the screens as a clamped stack without the potential problem of flushing out potting. The regenerators each consist of several hundred layers of 200 strands per inch 316 CRES screen mesh that have been clamped together and machined to form a precision annular cylinder. The screens are each rotated 5 degrees relative to the next to maximize gas-to-mesh heat transfer, and are held together by a thin sleeve of melt-bonded FEP Teflon. The mesh stack for the first stage regenerator, shown in Figure 9, is 85 mm o.d., 77 mm i.d., and 51 mm long, with 136 g mass at a 31% fill factor. The second stage regenerator mesh stack is 53 mm o.d., 45 mm i.d., and 51 mm long, with 80 g mass at a 31% fill factor.

For each regenerator, stacks of screen squares were first clamped between tooling plates in a jig for boring, as shown in Figure 9a. Squares were used to aid in rotating each screen by 5 degrees. After boring, the stacks were reclamped onto precision mandrels for turning of the outside diameter, followed by spray, ultrasonic, and vapor cleaning with trichloroethane. Each stack was then wrapped in FEP Teflon shrink tubing, Kapton, and TFE Teflon, and heated in an oven to melt bond the FEP Teflon. The TFE Teflon contained the melt and the Kapton prevented mixing of the FEP and TFE. The TFE and Kapton layers were then machined away in finishing the outer diameter. Final cleaning consisted of 30 minutes in a 10% sulfuric acid bath, 15 minutes in a 20% nitric acid bath, 3 baths of boiling distilled water, oven and vacuum drying.

The third and fourth stage regenerators each consist of 0.2 mm diameter microspheres of 95% lead and 5% antimony contained in the annulus between 0.38 mm wall G-10 fiberglass/epoxy tubes. The third stage regenerator is 33 mm o.d., 26 mm i.d., 102 mm long, and contains 135 g of microspheres at a 63.7% fill factor. The fourth stage regenerator is 19 mm o.d., 13 mm i.d., 102 mm long, and contains 56.8 g of microspheres at a 62.3% fill factor. Settling of the microspheres was induced by prolonged vibration and spinning.

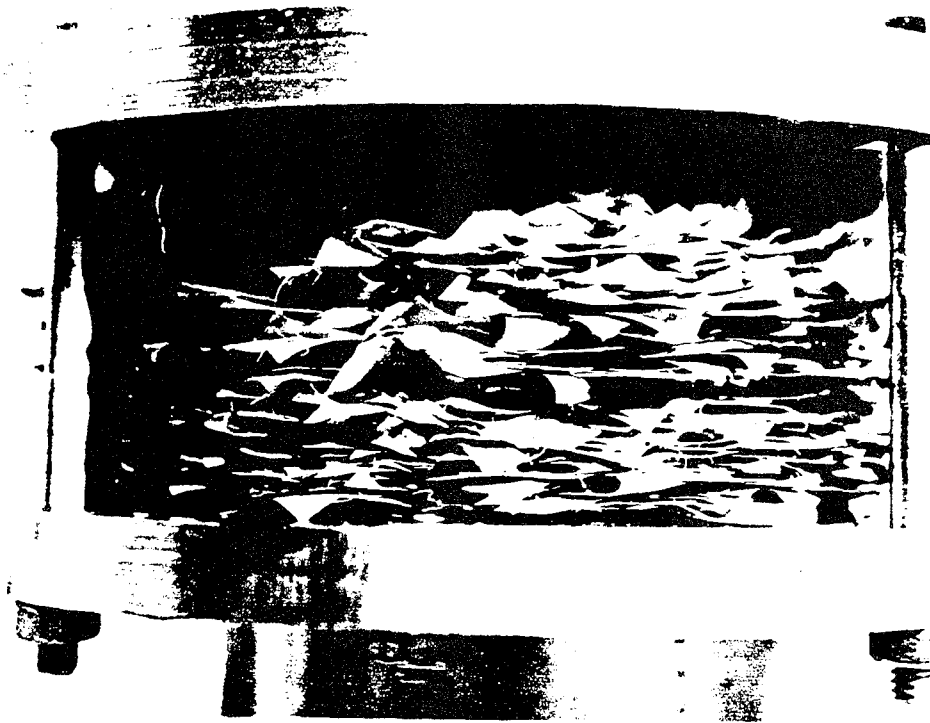


FIGURE 9a. REGENERATOR MESH STACK IN BORING FIXTURE

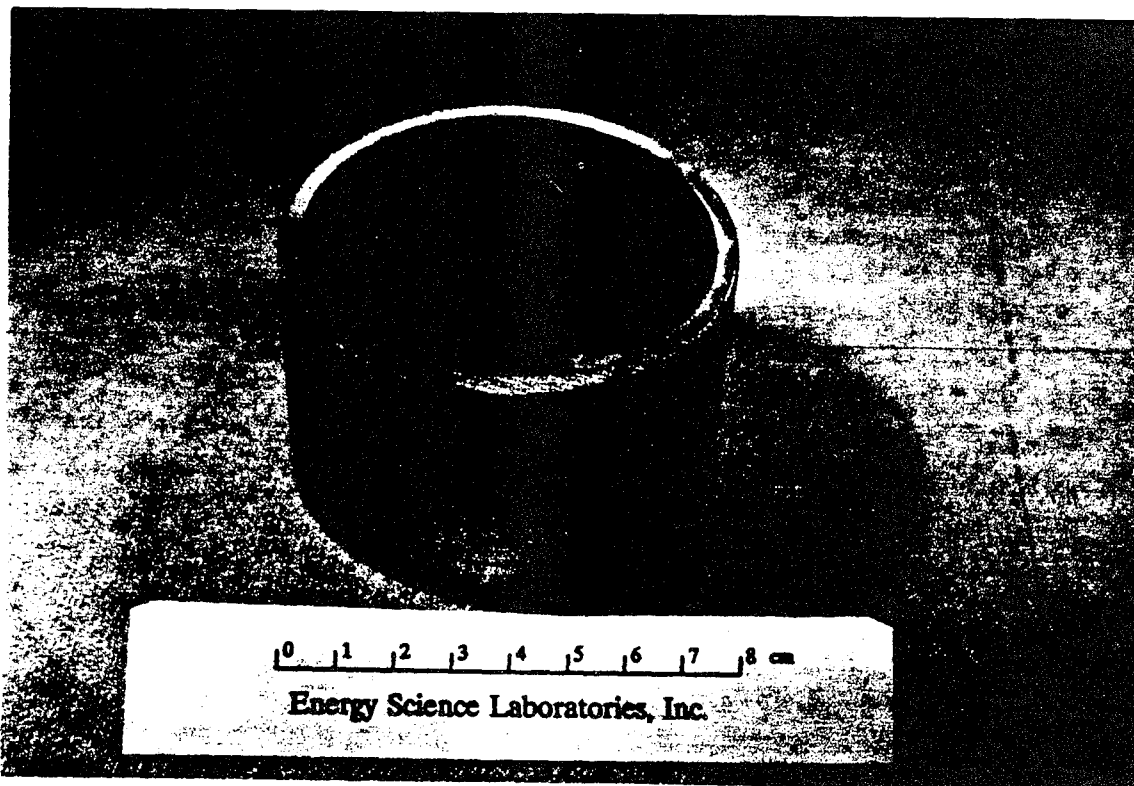


FIGURE 9b. COMPLETED FIRST STAGE REGENERATOR MESH STACK

The microspheres are restrained at the ends by 316 CRES header rings which are epoxied in the annular gaps. The header rings have drilled helium flow holes covered by 2 layers of 200 mesh 316 CRES screen rotated 45 degrees and continuous-welded to the header. The 200 mesh screen has 0.050 mm diameter wires and 0.076 mm across holes. Containment of the microspheres was initially tested by suspending the spheres in the screen over white filter paper in an ultrasonic bath for 2 hours with no visible debris generation. The completed regenerators were similarly tested for microsphere containment and debris generation by vibration at various frequencies for 48 hours or more.

The flocked carbon fiber regenerator is the same size as the lead/antimony microsphere regenerator for the fourth stage. It consists of a dense flocking of radially oriented carbon whiskers which extend across a 1.6 mm annular gap between thin-walled G-10 fiberglass/epoxy tubes. The whiskers are electrostatically oriented and anchored in a 0.6 mm layer of lead-powder-filled Stycast 1266 epoxy inside the outer tube. Header rings of G-10 with helium flow holes are epoxied in the ends of the regenerator. Thin-walled G-10 tubes are used in simple annular gap regenerators because they provide a good ratio of heat capacity to conduction loss. This flocked carbon fiber regenerator should provide better performance because of the high radial conductance of the carbon fibers into the added heat capacity of the lead-filled epoxy.

Regenerator testing at ESLI included repeated (10 or more) thermal shocks by plunging into liquid nitrogen followed by heating with a hot air gun, prolonged vibration to check for debris generation, pressure drop and single blow thermal tests. As of the end of Phase II development, the wire mesh and the packed microsphere regenerators were successfully tested in the multi-stage cryocooler. The flocked-fiber regenerator and other regenerator designs not completed during Phase II will be comparatively tested in continuing development of the multi-stage cryocooler.

5.3 Cryocooler Prototype

The assembled crankcase and major coldhead components of the prototype cryocooler are shown in Figure 10. The drive mechanism components and assembly, which were described in Section 4.6, are shown in Figure 11.

For fabrication expedience and economy, the crankcase is assembled from 6061-T651 aluminum plates. Although boltheads are visible around the side in Figure 10, the only plate that is removable is the cover plate (front in Figure 10, removed in Figure 11b). The other 5 plates of the cubical crankcase are continuous-bead TIG welded around their inside edges. Because of the cubical shape, relatively thick walls are required to withstand the pressurization. Further development will lead to a more weight efficient cylindrical crankcase.

Referring to Figure 3 in Section 4.1, the compression piston (the top of which can be seen in Figure 11B) and the expansion piston (attached to the bottom of the 4 stage displacer in Figure 10) are machined from 6061-T6 aluminum. Their respective connecting rods each consist of bolted together upper and lower segments which are fabricated from 7075-T6 aluminum. The compression cylinder liner is a thermal-shrink-fit 6061-T6 aluminum sleeve, the bore of which is treated with a PTFE-impregnated hard anodize called Nituff® (Nimet Industries, Inc. of South Bend, Indiana) and honed to a 0.2 to 0.3 micron finish. The expansion piston runs in a thin-wall 304 CRES sleeve which provides the inner wall of the working gas passage through the cooler, as described in Section 4.6. This expansion cylinder sleeve is also honed to a 0.2 to 0.3 micron finish. The compression and expansion pistons both incorporate lip seal rings and guide bands made of Rulon LD, as described in Section 4.6.

The 4 stage displacer, which attaches to the top of the expansion piston, is fabricated from AMOCO Torlon® 7230, a polyamide-imide copolymer with 3% PTFE added for lubricity. The displacer was turned as a single rigid piece from 3 pieces of Torlon which

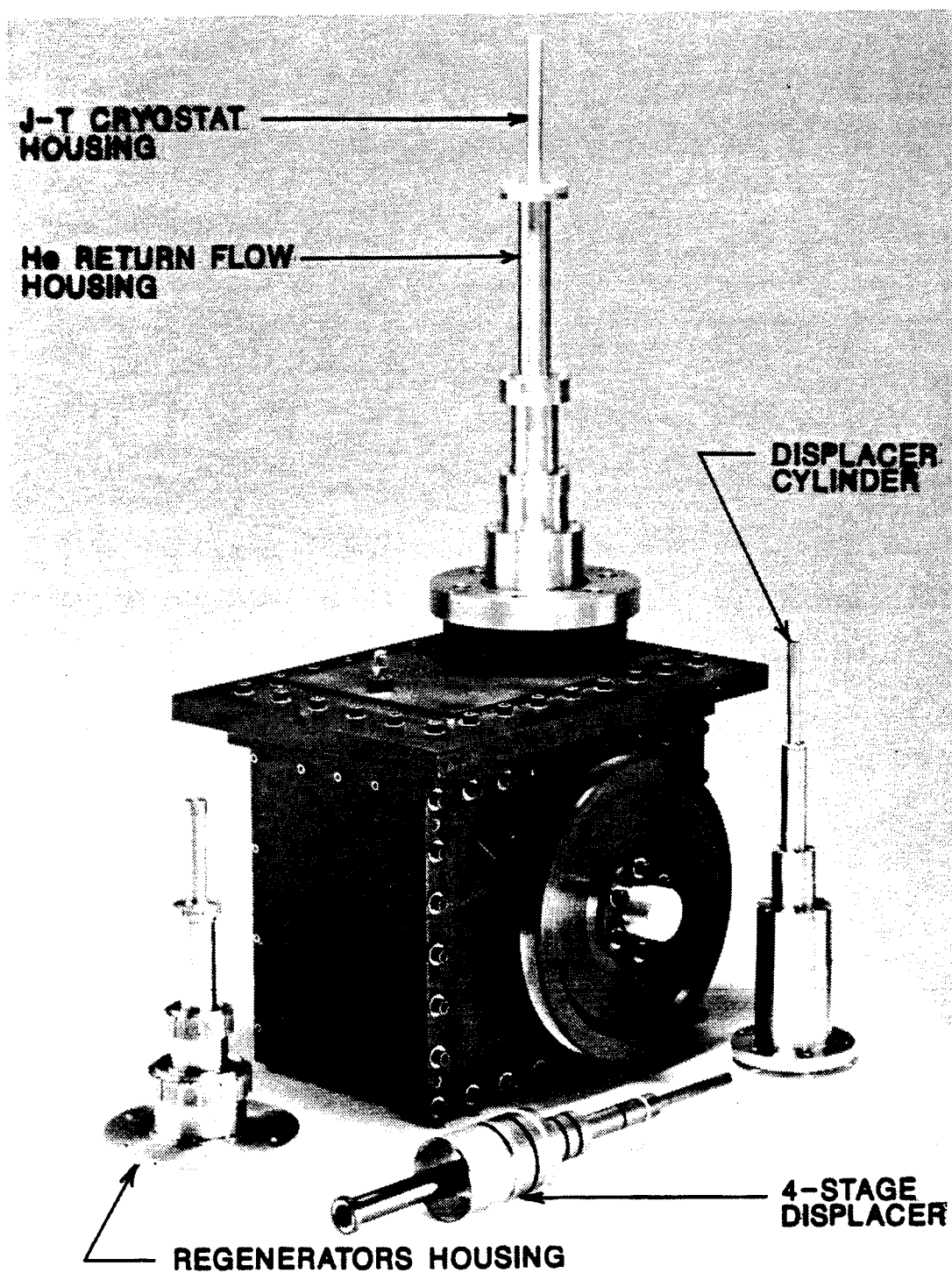


FIGURE 10. PROTOTYPE ASSEMBLY AND MAJOR COLDHEAD COMPONENTS

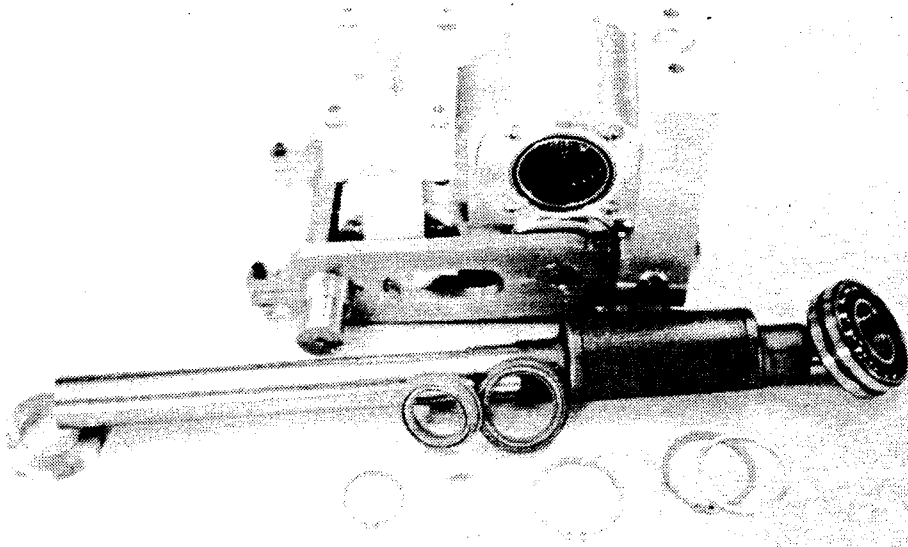


FIGURE 11a. DRIVE MECHANISM YOKE, PISTON RODS, SWINGLINK, AND CRANKSHAFT

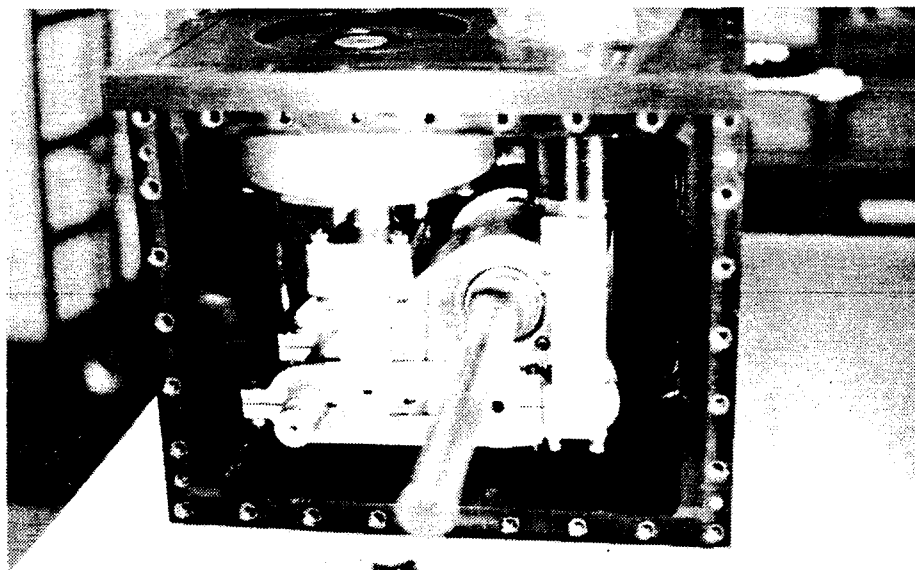


FIGURE 11b. DRIVE MECHANISM AND BELLOWS ASSEMBLED INTO CRANKCASE

were glued together with Torlon 4000F-45 powder in N-methyl-2-pyrrolidone because of the limited availability of suitable stock and to allow hollowing of the third stage, as well as the first and second stages, to limit thermal conduction. Torlon 7230 was chosen for its combination of cryogenic strength, wear resistance, and low thermal conductivity and expansion coefficient. Tests were performed at liquid nitrogen temperature (77 K) to measure the thermal contraction rate of the Torlon 7230 and check the impact and shock strength of the Torlon-Torlon bond.

The 4 stage displacer cylinder and the regenerators housing, shown in Figure 10, each consist of a stack of 4 tightly piloted 316L CRES sections. The displacer cylinder bores are honed to a 0.2 to 0.3 micron finish. Precision cylindrical alignment of the bores is achieved by integrally machined shoulders and pilot bores. The lengths of the Torlon displacer steps were final machined to match the measured depths in the displacer cylinder stack. The 4 annular regenerators (not shown in Figure 10) fit over the outside diameters of the respective displacer cylinder sections.

The displacer cylinder sections and the regenerators are held together axially by the regenerators housing, which is part of the pressure containment housing. The 4 regenerator housing sections are clamped together by bolts through flanges which are brazed to the ends of the sections. The bolts thread into split rings of 303 CRES above (as seen in Figure 3) each pair of clamped flanges. These joints are sealed against helium leakage by copper C-rings in grooves between the flanges. The flanges were originally all of C10100 OFHC copper to conduct the external heat loads into each stage. However, pressure testing revealed that the lower (as seen in Figure 3) flanges at the first and second stages had inadequate stiffness and yield strength, and they were replaced with 303 CRES flanges. This had little effect on heat load coupling because the upper flange in each pair has the interstage helium flow passages and remained as copper.

The low pressure helium return flow housing and attached J-T cryostat housing, shown in Figure 10, are made up of thin-walled 316 CRES tubular sections bolted together

through brazed-on flanges. This housing serves to channel cold incoming boil-off flow from a liquid helium storage dewar, or return flow from the J-T cryostat, to recuperatively cool the finned tube feed line to the J-T cryostat, and is needed only when the J-T stage is integrated with the system.

5.3 Assembly and Test

Assembly and testing began with low pressure leak testing of the crankcase and the coldhead as separate subassemblies. Various leaks, primarily in the weld and braze joints, were found and corrected. For these and subsequent subassembly pressure tests, the cylinder/cooler head was mated either to the crankcase, with a blanking plate substituting for the coldhead, or to the coldhead, with a blanking plate substituting for the crankcase. The crankshaft through-bore was also closed off with a blanking plate. The drive mechanism, pistons, and bellows were not installed.

The subassemblies were then subjected to high pressure hydrostatic testing to measure structural deflections. The crankcase side plates exhibited excessive elastic bulging at 2 MPa, due to the bolted/welded joints being more flexible than predicted. This would have affected crankshaft and swinglink bearing alignments, and was corrected by addition of a parallel-bars girdle clamp which was preloaded by shims against the side plates such as to maintain bearing alignments to pressures above 2 MPa.

Because the coldhead/cooler could be subjected to peak cyclic pressures of up to 4 MPa, that subassembly was hydrostatically tested to 5 MPa. As described in Section 5.2, the lower copper flanges at the first and second coldhead stages diaphragmmed excessively and were replaced with 303 CRES flanges to provide adequate clamping stiffness and insure against leaks or fatigue failure. It was also found that the cylinder/cooler head plate bulged too much in the center, imposing excessive flexing in the aluminum welds of the coolant jacket across the top of the plate (underneath as seen in Figure 3a) and around the base of the expansion cylinder. This would be corrected

in a redesign by adding a head-to-crankcase bolt through the center of the head. The same effect was accomplished by adding an external bridge brace across the head, which applied a restraining force to the center of the plate through a spacer installed through the coolant jacket cover plate.

After successful completion of the static pressure tests, the coldhead (with baseline stacked 316 CRES screen and lead/antimony microsphere regenerators), cylinder/cooler head, and crankcase were assembled and the pistons, bellows, and drive mechanism were installed for running alignments checks. The assembled cryocooler was installed in its test stand, as shown in Figure 12a but without the coldwell dewar. The drive mechanism was operated by hand and to increasing speed with the drive motor while listening for problems with a mechanic's stethoscope. The drive mechanism was then disassembled for inspection and reinstalled to proceed with operational tests.

The cryocooler was subjected to a series of prolonged evacuations and purges, initially with nitrogen then helium, while warmed with heat lamps to flush air and moisture from the working spaces prior to charging with helium. Temperature sensors and flexible foil/Kapton tape heaters were installed on the 4 coldhead stages as shown in Figure 12b. The temperature sensors were Scientific Instruments Si410B silicon diodes and 9350-1 four channel readout. The diodes were calibrated by Scientific Instruments at 4.2 K and 77.4 K. To limit stray heat conduction to the cold stages, each heater had only 2 leads. The resistances of the heater elements and of the complete circuits were precisely measured at room temperature for later comparison with circuit resistance measured at operating temperature in order to subtract lead resistance for calculating heat loads based on heater current.

The test coldwell dewar, diagrammed in Figure 13, was installed over the coldhead, as seen in Figure 12a, and the cryocooler working space, bellows space, and crankcase were each connected through check valves to the pressure-regulated compressed helium supply. The crankcase and bellows space pressures were monitored with dial pressure

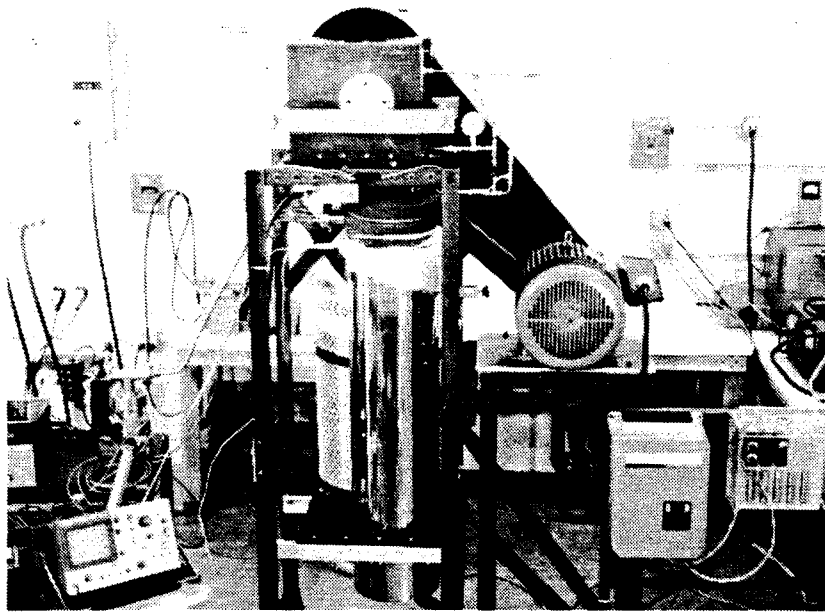


FIGURE 12a. PROTOTYPE SYSTEM IN TEST STAND

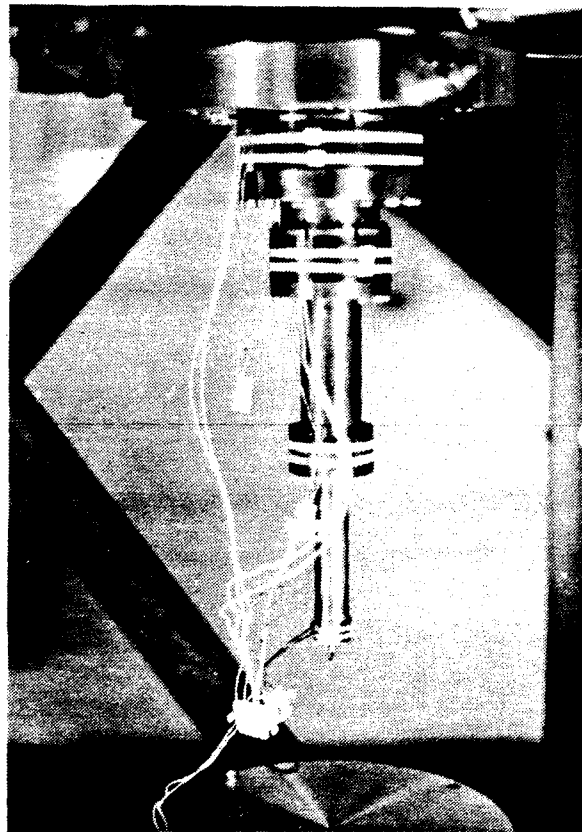
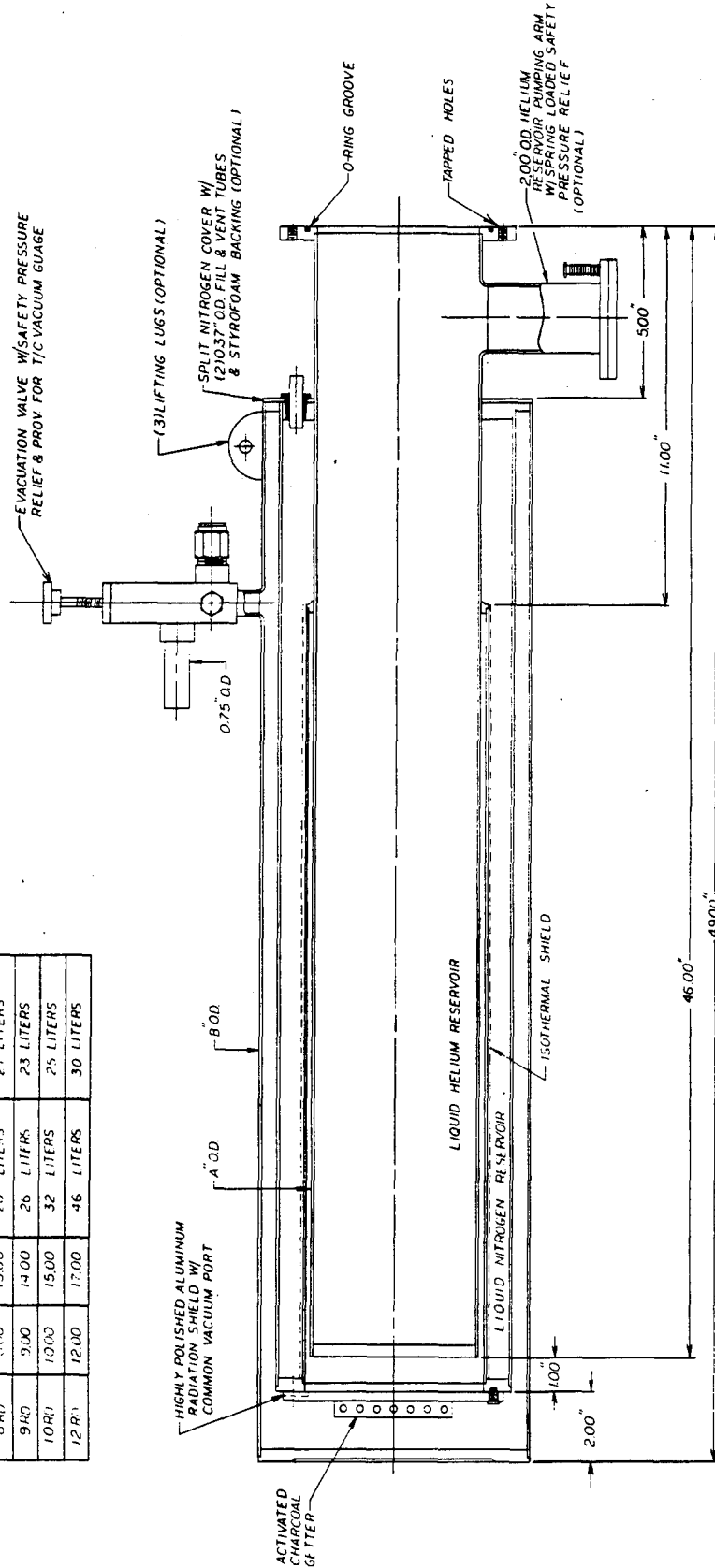


FIGURE 12b. COLDHEAD WITH TEST HEATERS AND TEMPERATURE SENSORS

MODEL	A	B	RECOMMENDED HELIUM CAPACITY	RECOMMENDED NITROGEN CAPACITY
5RD	5.00	8.00	8 LITERS	10 LITERS
6RD	6.00	10.00	11 LITERS	12 LITERS
7RD	7.00	11.00	16 LITERS	14 LITERS
8RD	8.00	13.00	20 LITERS	21 LITERS
9RD	9.00	14.00	26 LITERS	23 LITERS
10RD	10.00	15.00	32 LITERS	25 LITERS
12RD	12.00	17.00	46 LITERS	30 LITERS



RESEARCH COMPANY 215 Spencer Street, Boston, MA 02118	
PROJECT NO. 533 OBF	
LIQUID HELIUM RESEARCH DEWAR	
DATE	BY
10/1/77	R. PERRY
DESIGNED BY	NTS
CHECKED BY	JRC
APPROVED BY	MASTER

FIGURE 13. SYSTEM TEST DEWAR

gauges and the working space pressure cycle was read out by a dynamic pressure sensor displayed on an oscilloscope and a strip chart recorder. In operational testing, the working pressure cycle proved to be a smooth sinusoid with a ratio of 2:1 over the charge pressure, as designed, and the bellows space pressure fluctuated less than 0.1 MPa above the charge pressure.

An approximate test system diagram is shown as Figure 5 in the preliminary test plan in Appendix B.

In initial performance testing, the coldwell was vacuum pumped to below 1 millitorr and the dewar intermediate jacket was filled with liquid nitrogen. Operating at 4.92 Hz with 0.52 MPa (75 psig) charge pressure, the cryocooler achieved a cooldown to the following temperatures within 2.5 hours: 132 K, 93 K, 50 K, and 22 K at the first, second, third, and fourth stages, respectively (to be abbreviated, for example, 132/93/50/22 K, in the following discussions). However, continued operation at various speeds and charge pressures failed to produce a lower fourth stage temperature.

The following refinements were then made. The temperature sensors on the third and fourth stages were replaced with like sensors but which had phosphor/bronze leads to reduce sensor error due to conducted heat. The heater leads were redressed to better thermally anchor them to upper stages to intercept stray heat loads. A closed-end cylindrical shield of 3 layers of aluminized mylar multi-layer insulation was installed to extend down from the first stage and enclose the coldhead. The vacuum in the dewar vacuum jacket was verified by pumping it to below 1 millitorr.

The cryocooler then achieved a cooldown from room temperature to 130/75/44/11 K within 1.5 hours operating at 4.77 Hz and 0.48 MPa (70 psig) charge pressure. In subsequent tests without applied heat loads, the cryocooler achieved typical temperatures of 140/80/45/10 K within 2 hours operating at speeds of 3.3 to 4.2 Hz and charge pressures of 0.34 to 0.52 MPa (50 to 75 psig).

Further testing was conducted to preliminarily check the cryocooler's responses to combinations of speed from 3.1 to 5.3 Hz, charge pressure from 0.17 to 0.86 MPa (25 to 125 psig), and applied heat loads. The responses of each stage to heat loads applied at that stage are summarized* in Figures 14 through 17. The steady-stage responses of all 4 stage temperatures to heat loads applied to a particular stage are summarized* as follows for various combination of speed and charge pressures:

At 4.2 Hz, 0.48 MPa (70 psig) charge:

1 watt to fourth stage; 138/80/42/18 K
2 watts to third stage; 138/79/47/11 K
5 watts to third stage; 138/80/63/12 K

At 4.2 Hz, 0.55 MPa (80 psig) charge:

1 watt to fourth stage; 124/82/42/18 K
5 watts to third stage; 123/82/68/14 K
5 watts to second stage; 133/96/46/11 K
20 watts to first stage; 155/104/51/12 K

At 4.75 Hz, 0.59 MPa (85 psig) charge:

1 watt to fourth stage; 116/76/38/17 K
2 watts to third stage; 116/76/44/11 K
5 watts to third stage; 116/76/52/12 K

At 4.75 Hz, 0.69 MPa (100 psig) charge:

1 watt to fourth stage; 109/68/38/15 K
2 watts to third stage; 108/67/40/10 K
5 watts to third stage; 109/68/49/12 K

*The raw test data was taken over small time increments to observe transients and allow stabilizing, and includes additional operating speeds, charge pressures, and heat loads.

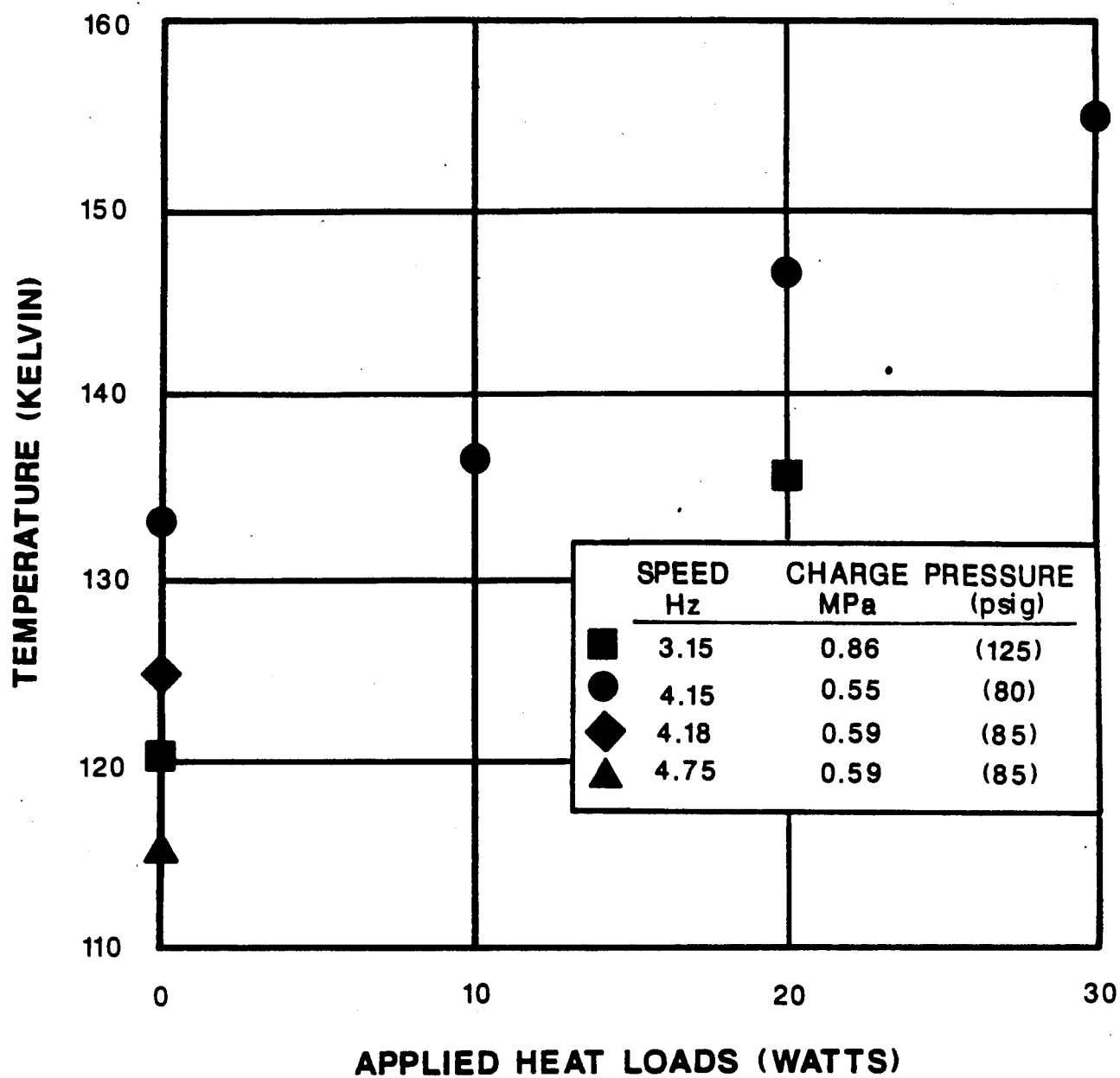


FIGURE 14. FIRST STAGE HEAT LOAD TESTS

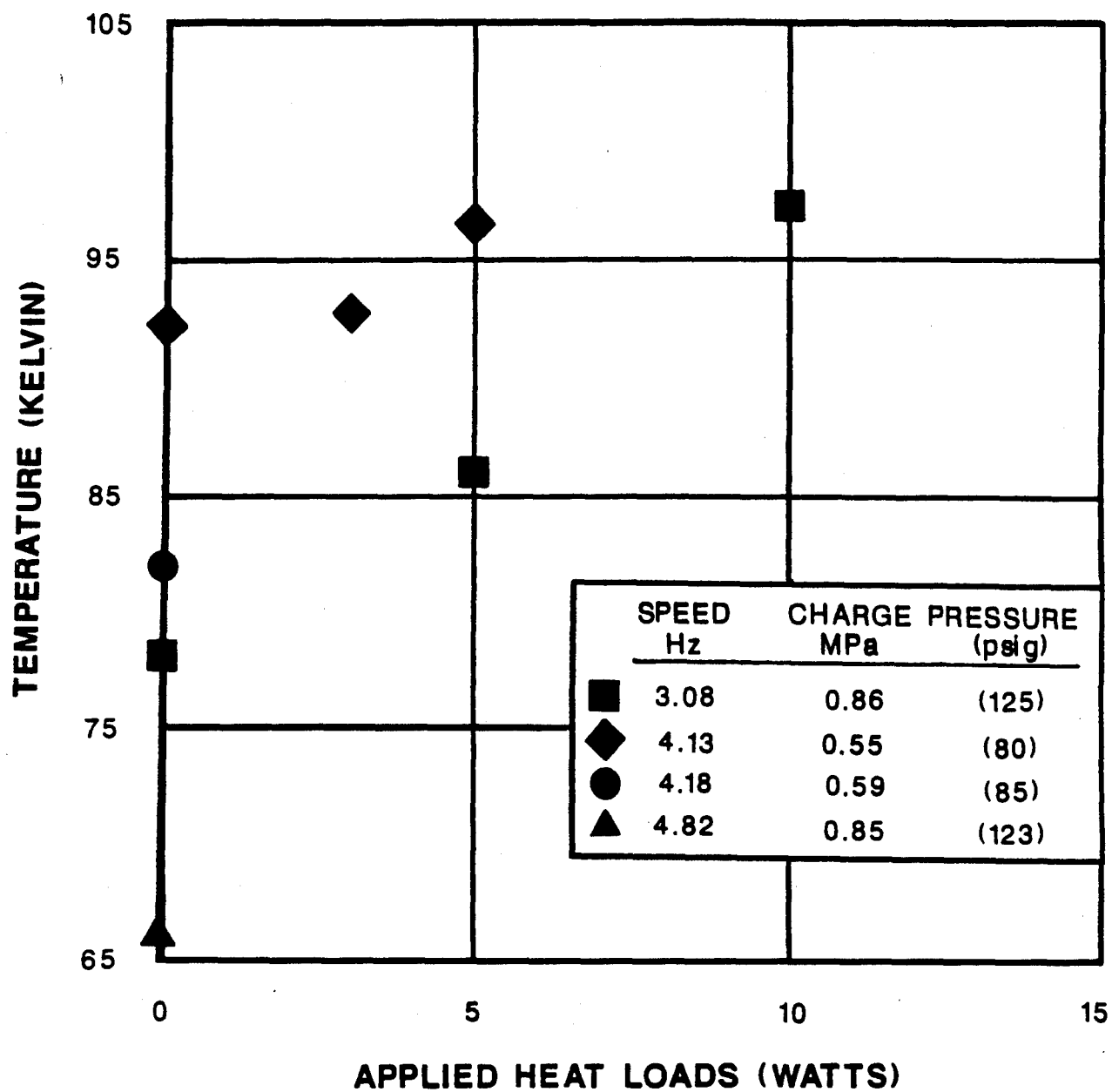


FIGURE 15. SECOND STAGE HEAT LOAD TESTS

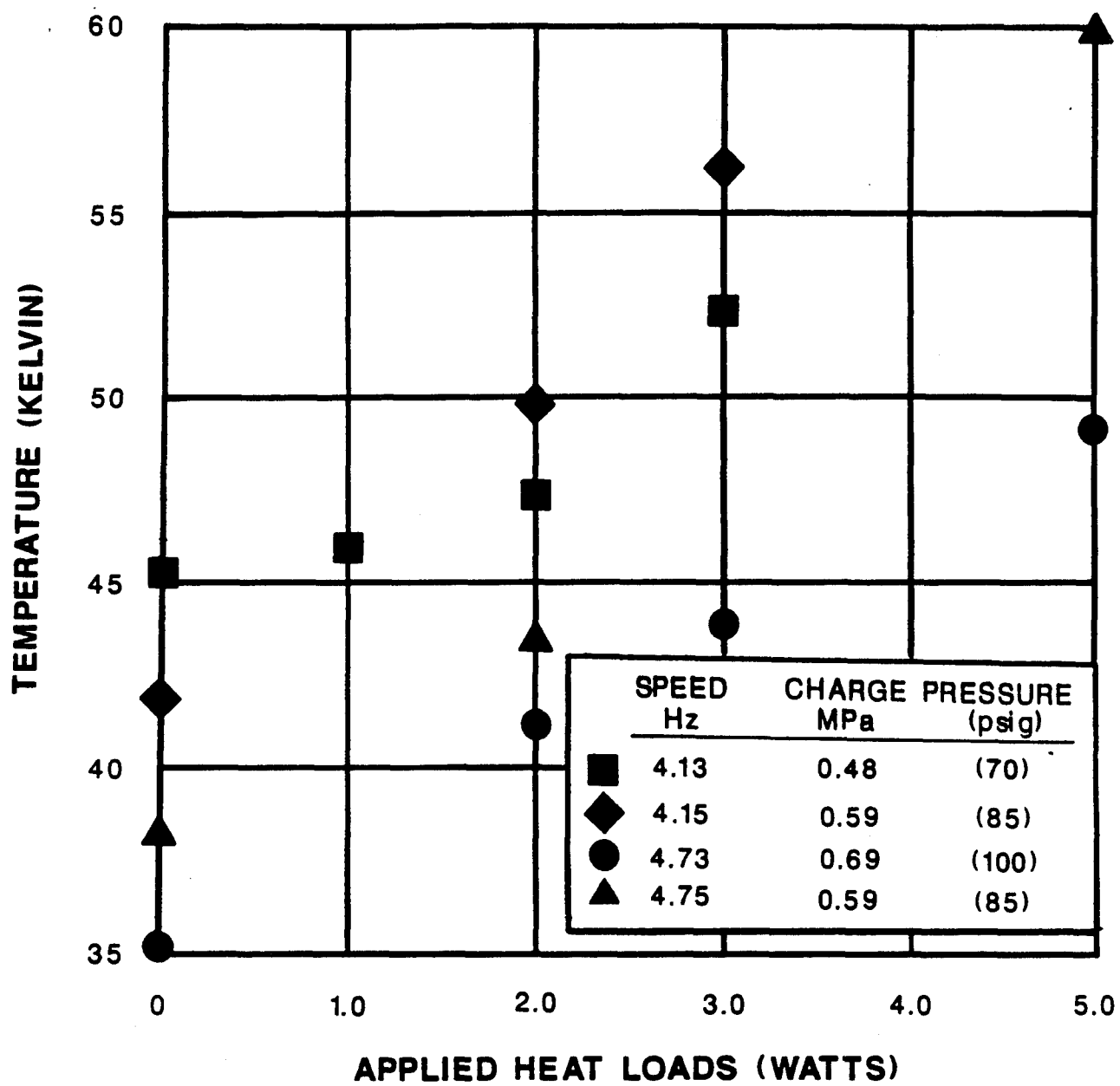


FIGURE 16. THIRD STAGE HEAT LOAD TESTS

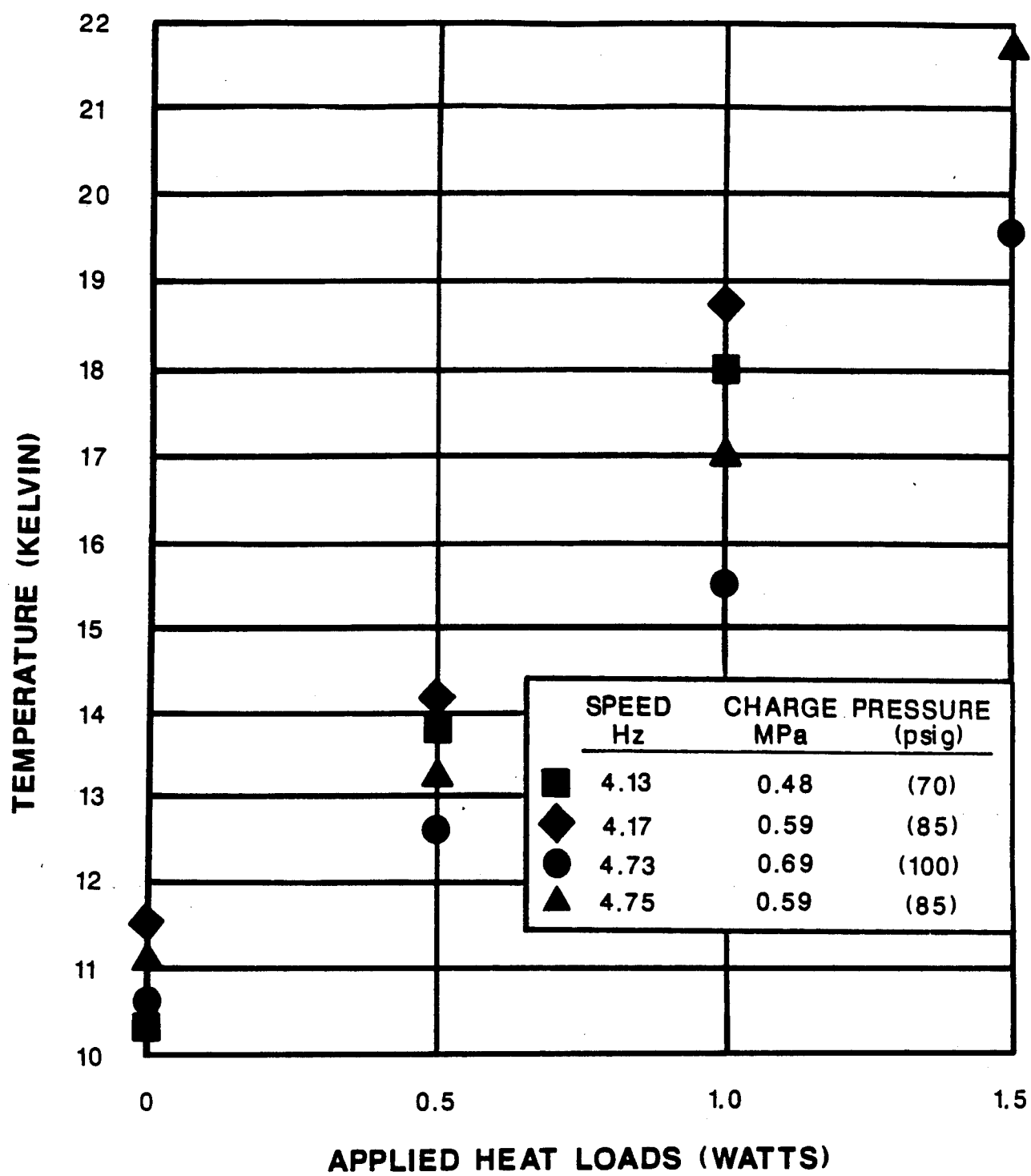


FIGURE 17. FOURTH STAGE HEAT LOAD TESTS

Phase II concluded with these basic performance tests. As can be seen, the stage temperatures came remarkably close to those predicted, considering the limited analytical tools and data available for multi-stage Stirling cryocooler design. Overall, cryocooler performance degraded with speeds above 5 Hz or charge pressures above 0.69 MPa (100 psig), which may be limited by regenerator(s) effectiveness as expected. Further testing is needed to determine more optimum combinations of speed, charge pressure, regenerator alternatives, heat load combinations, and for correlation with and refinement of the multi-stage Stirling computer model.

6.0 CONCLUSION AND CONTINUED DEVELOPMENT

The broad objective of this research is to advance the development of small-scale cryocoolers for producing temperatures down to and below 10 K with a 300 K heat sink. Toward that end, this report has surveyed the candidate types of cryocoolers, identified why the Stirling cycle offers the best theoretic potential, and described the successful analysis, design, fabrication, and initial testing of a 10 K multi-stage Stirling test-bed cryocooler.

The fundamental development problem is that current Stirling and other regenerative cycle cryocoolers are inefficient and limited to very slow operating speed in reaching 10 K. Other types of cryocoolers, although capable of higher operating speeds, are even less efficient. The Carnot ideal shows that the theoretic minimum power required to lift heat from 10 K to 300 K is 29 watts per watt. Real cryocoolers typically achieve less than 1 to 2% of Carnot efficiency, requiring 1500 to 3000 watts per watt. Such power requirements at slow operating speed necessitate large driving forces. Furthermore, the slow speed and large forces impede the use of high reliability provisions such as non-rubbing bearings, seals, and linear motor drives.

Reducing the drive forces requires increasing the operating speed and/or efficiency, which are contingent on improving Stirling design optimization and regenerators

effectiveness. The subject Phase II prototype cryocooler can now serve as a versatile test bed for advancing multi-stage Stirling analysis, design, and regenerators technology, leading to higher efficiency, faster operating speed, smaller machines employing high reliability non-wearing drive mechanisms and seals.

Much has been learned and will continue to be learned from the test-bed-cryocooler built in this Phase II project. Continued development objectives will include:

- o Identify parasitics and ways to control them.
- o Vary operating speed, charge pressure, cycle pressure ratio, and heat loads to study trade-offs affecting temperatures, power efficiency, and drive loads.
- o Test regenerator variations in comparison with the baseline stacked screen and lead/antimony microspheres regenerators to develop higher effectiveness.
- o Integrate the J-T cryostat with the 10 K cryocooler test bed to demonstrate the liquefaction of helium.
- o Evaluate piston seals, guides, bellows, and bearings performance, and other failure modes.
- o Refine the baseline design analyses and the multi-stage Stirling computer model by correlation with test data.
- o Improve the regenerators modeling in the multi-stage computer model, possibly by incorporating REGEN programs.
- o Apply the refined analyses and computer model to define additional testing.

- o Derive how to optimize multi-stage Stirling cryocooler pressure, speed, displacements, regenerators, and configuration to reduce drive power and loads.
- o Identify ways to reduce weight, minimize vibration, and design for hermetic sealing including the drive motor.
- o Determine methods to improve reliability and life, such as by employing linear motors, flexures, and non-rubbing seals.

BIBLIOGRAPHY OF RELATED WORK

- 1 Arp, V., Radebaugh, R., Interactive Program for Microcomputers to Calculate the Optimum Regenerator Geometry for Cryocoolers (REGEN and REGEN2), AFWAL-TR-87-3040, Aug 1987
- 2 Barron. R., Cryogenic Systems, 2nd Ed., Oxford University Press, Oxford, U.K., 1985
- 3 Bradshaw, T. W., "First Results on a Prototype Two Stage Miniature Stirling Cycle Cooler for Spaceflight Applications", Fourth International Cryocoolers Conf., Easton, MD, Sept 1986
- 4 Breon, S. R., "Liquid Helium Servicing from the Space Station", NASA/GSFC, Cryogenics, Vol. 28, No. 2, 1988
- 5 Castles, S. H., "Current Developments in NASA Cryogenic Cooler Technology", Advances in Cryogenic Engineering, Vol. 33, Plenum Press, New York, NY, 1988
- 6 Chan, C. K., et al, "Performance of Three-Stage Pulse Tube Cooler", Fourth Interagency Meeting on Cryocoolers, Plymouth, MA, 1990
- 7 Chan, C. K., "Survey of Cooling Techniques", JPL Invention Report NPO-17457/6964, July 1989
- 8 DiPirro, M. J., "Superfluid Helium On-Orbit Transfer Flight Experiment: performance estimates", Cryogenics, Vol. 28, No. 2, 1988
- 9 Doige, A. G., and Walker, G., "Dynamics of the Ross-Stirling Engine", Third International Stirling Engine Conference, Rome, Italy, June 1986
- 10 Fieldhouse, I. B., Porter, R. W., "Cryogenic Cooling of Infrared Electronics", GACIAC SOAR-86-02, May 1986
- 11 Gasser, M. (Ed.), Refrigeration for Cryogenic Sensors, NASA Conference Publication 2287, 1983
- 12 Green, G., et al, "Low Temperature Ribbon Regenerator", Second Interagency Meeting on Cryocoolers, Easton, MD, Sept 1986
- 13 Hands, B. A., Cryogenic Engineering, Academic Press, San Diego, CA, 1986
- 14 Jones, J., "Sorption Cryogenic Refrigeration - Status and Future", Advances in Cryogenic Engineering, Vol. 33, Plenum Press, New York, NY, 1988

- 15 Keung, C. S., Lindale, E., "Effect of Leakage Through Clearance Seals on the Performance of a 10 K Stirling-Cycle Refrigerator", Third Cryocooler Conf., Boulder, CO, Sept 1984
- 16 Knox, L., et al, "Design of a Flight Qualified Long-Life Cryocooler", Third Cryocooler Conf., Boulder, CO, Sept 1984
- 17 Ledford, O., "Cryogenics for Space Systems", Advanced Technology International, Los Angeles, CA, Nov 1986
- 18 Marsden, D., "System Design Requirements for Infra-Red Detector Cryocoolers", Fourth International Cryocooler Conf., Easton, MD, Sept 1986
- 19 McFarlane, R., et al, "Long Life Stirling Cryocooler for Space Applications", Fifth International Cryocooler Conf., Monterey, CA, Aug 1988
- 20 Orłowska, A. H., and Davey, G., "Measurements of Losses in a Stirling Cycle Cooler", Cryogenics, Vol. 27, 1987
- 21 Radebaugh, R., "A Review of Pulse-Tube Refrigeration", Advances in Cryogenic Engineering, Vol. 35, 1990
- 22 Radebaugh, R., "Development of a Thermoacoustically Driven Orifice Pulse Tube Refrigerator", Fourth Interagency Meeting on Cryocoolers, Plymouth, MA, 1990
- 23 Radebaugh, R., et al, "Optimization of a Pulse-Tube Refrigerator for a Fixed Compressor Swept Volume", Fifth Intl. Cryocooler Conf., Monterey, CA 1988
- 24 Radebaugh, R., "Pulse Tube Refrigeration - A New Type of Cryocooler", Eighteenth Intl. Conf. on Low Temperature Physics, Kyoto, Japan, 1987
- 25 Radebaugh, R., Herrmann, S., "Refrigeration Efficiency of Pulse-Tube Refrigerators", Fourth Intl. Cryocooler Conf., Easton, MD, 1986
- 26 Radebaugh, R., "Ineffectiveness of Powder Regenerators in the 10 K Temperature Range", Second Interagency Meeting on Cryocoolers, Easton, MD, Sept 1986
- 27 Radebaugh, R., Louie, B., "A Simple, First Step to the Optimization of Regenerator Geometry", Third Cryocooler Conf., Boulder, CO, Sept 1984
- 28 Sherman, N. I., "Dynamic Seal Development for a Five-Year Vuilleumier Cryocooler", Second Interagency Meeting on Cryocoolers, Easton, MD, Sept 1986

- 29 Smith, J., et al, "Survey of the State of the Art of Miniature Cryocoolers for Superconducting Devices", Mass. Institute of Tech., Cambridge, MA, 1984
- 30 Storch, P. J. and Radebaugh, R., "Development and Experimental Test of an Analytical Model of the Orifice Pulse Tube Refrigerator", Advances in Cryogenic Engineering, Vol. 33, 1988
- 31 Swanson, J., et al, Cryogenic Cooler Seals Investigation, AFWAL-TR-85-3026, Air Force Wright Aeronautical Lab., June 1985
- 32 Tward, E., et al, 1990, "Pulse Tube Refrigerator Performance", Advances in Cryogenic Engineering, Vol. 35, 1990
- 33 Wade, L., et al, "Test Performance of an Efficient 130 K Sorption Refrigerator", 1991 Space Cryogenics Workshop, NASA LeRC, Cleveland, OH, June 1991
- 34 Walker, G., Urieli, I., "An Ideal Adiabatic Analysis of a Stirling Cryocooler with Multiple Expansion Stages", Low Temperature Engineering and Cryogenics Conf., Southampton, U.K., July 1990
- 35 Walker, G., Miniature Refrigerators for Cryogenic Sensors and Cold Electronics, Oxford University Press, Oxford, U.K., 1989
- 36 Walker, G., "Cycle Analysis for Stirling Refrigerator with Multiple Expansion Stages", University of Calgary, 1988
- 37 Walker, G., et al, "Microcomputer Simulation of Stirling Cryocoolers", Twelfth International Cryogenic Engineering Conference, Southampton, U.K., July 1988
- 38 Walker, G., Cryocoolers, Vol. 1 and 2, Plenum Press, New York, NY, 1983
- 39 Walker, G., Stirling Engines, Oxford University Press, Oxford, U.K., 1980
- 40 Vourgourakis, E. J., "Development of the Five-Year Vuilleumier Cryocooler", Second Interagency Meeting on Cryocoolers, Easton, MD, Sept 1986
- 41 Zimmerman, J. E., Sullivan, D. B., A Study of Design Principles for Refrigerators for Low Power Cryoelectronic Devices, National Bureau of Standards, TN-1049, January, 1982

APPENDIX A

**Example Printout from
Multiple Expansion Stirling Cryocooler Simulator
Computer Program**

MULTIPLE EXPANSION STIRLING CRYOCOOLER SIMULATOR PC VERSION 1.0

(CRYOCOOLER TYPE: TWO PISTON WITH SEPARATED CYLINDERS)

RUN FOR: colin

DATE: 90/11/08

ENGINE NAME: gpi6

----- SPECIFIED INPUT VALUES -----

PROGRAM CONTROL PARAMETERS

1. Number of time steps per cycle: 24
2. Gas property option (1=ideal,2=real): 1

OPERATING CONDITIONS

1. Gas charge pressure at assumed initial temp. with
compressor piston at bottom dead center [MPa]: 1.00
2. Frequency of operation [Hz]: 5.00
3. Metal temperature at ambient portion of
cooler [K]: 300.00
4. Metal temp. at 1st expansion space [K]: 230.00
5. Metal temp. at 2st expansion space [K]: 160.00
6. Metal temp. at 3st expansion space [K]: 90.00
7. Metal temp. at 4st expansion space [K]: 60.00
8. Cooler load at end of cold finger [mW]: 1000.0

MECHANICAL DRIVE DIMENSION

1. Radius of compressor crank [cm]: 0.50
2. Radius of expander crank [cm]: 0.50
3. Length of connecting rod to expander [cm]: 3.00
4. Length of connecting rod to compressor
piston [cm]: 3.00
5. Phase angle [degrees]: 80.00
6. Diameter of compressor piston [cm]: 12.50
7. End clearance of compressor piston [cm]: 0.01
8. Diameter of cooler [cm]: 1.00
9. Length of cooler [cm]: 1.00
A. End clearance at both ends of expander
travel [cm]: 0.01

FOUR STAGES OF EXPANDER DIMENSIONS

	1st	2nd	3rd	4th
1. Stage number	1	1	1	1
2. Design option (1):	1	1	1	1
3. ID pressure cylinder [cm]:	7.50	5.35	3.30	1.70
4. W.Th. pressure cylinder [cm]:	0.05	0.05	0.05	0.05
5. Length pressure cylinder[cm]:	7.50	10.00	12.00	15.00
6. Pressure cylinder material(2):	1	1	1	1
7. Cylinder-displcer Gap[cm]:	0.05	0.05	0.05	0.05
8. Expander wall thickness[cm]:	0.05	0.05	0.05	0.05
9. Expander wall material,(2)	2	2	2	2
A. Regenerator packing material(2):	4	4	4	4
B. Packng type(1=sp.2=fib):	1	1	1	1
C. Diameter packing[MICRONS]:	0.05	0.05	0.05	0.05
D. Porosity, fraction:	0.40	0.40	0.40	0.40

(1) Option code: 1 = Solid expander, annular regenerator
 2 = Packed expander-regenerator and seals
 3 = Packed expander-regenerator and annular gap regenerator

(2) Material code: 1=s.s., 2=G-10, 3=nylon, 4=lead, 5=brass
 6=nickle, 7=Gd,Rh, 8=Gd,Er,Rh.

NGLE DEG]	PRESS [MPa]	COMP. VOL. [cc]	EXPANSION SPACE VOLUMES [cc]				EXPANSION SPACE TEMPERATURES [K]			
			(1)	(2)	(3)	(4)	(1)	(2)	(3)	(4)
0.0	1.00	123.95	14.36	9.20	4.17	1.45	230.00	160.00	90.00	60.00
15.0	1.06	122.20	11.45	7.34	3.32	1.15	230.00	160.00	90.01	60.02
30.0	1.14	117.01	8.47	5.43	2.46	0.85	230.01	160.01	90.02	60.04
45.0	1.26	108.54	5.66	3.63	1.64	0.57	230.01	160.02	90.03	60.07
60.0	1.42	97.12	3.25	2.08	0.94	0.33	230.01	160.02	90.05	60.11
75.0	1.63	83.27	1.45	0.93	0.42	0.15	230.02	160.03	90.07	60.15
90.0	1.89	67.74	0.42	0.27	0.12	0.04	230.02	160.04	90.10	60.20
105.0	2.18	51.51	0.28	0.18	0.08	0.03	230.02	160.05	90.12	60.26
120.0	2.49	35.76	1.01	0.65	0.29	0.10	230.03	160.06	90.15	60.32
135.0	2.72	21.76	2.57	1.65	0.75	0.26	230.03	160.07	90.17	60.37
150.0	2.80	10.73	4.80	3.08	1.39	0.48	230.04	160.07	90.18	60.39
165.0	2.70	3.66	7.51	4.81	2.18	0.76	230.03	160.07	90.17	60.36
180.0	2.45	1.23	10.45	6.70	3.03	1.05	230.03	160.05	90.14	60.30
195.0	2.14	3.66	13.41	8.59	3.89	1.35	230.01	160.03	90.09	60.21
210.0	1.84	10.73	16.18	10.37	4.70	1.63	230.00	160.01	90.05	60.11
225.0	1.59	21.76	18.59	11.91	5.40	1.87	229.99	159.99	90.00	60.03
240.0	1.39	35.76	20.51	13.14	5.96	2.07	229.98	159.97	89.97	59.96
255.0	1.23	51.51	21.87	14.01	6.35	2.20	229.97	159.96	89.94	59.90
270.0	1.12	67.74	22.61	14.49	6.57	2.28	229.97	159.95	89.92	59.86
285.0	1.04	83.27	22.72	14.56	6.60	2.29	229.96	159.94	89.90	59.83
300.0	0.99	97.12	22.19	14.22	6.44	2.24	229.96	159.94	89.89	59.81
315.0	0.96	108.54	21.03	13.47	6.11	2.12	229.96	159.94	89.89	59.80
330.0	0.95	117.01	19.29	12.36	5.60	1.94	229.96	159.94	89.89	59.80
345.0	0.96	122.20	17.03	10.91	4.94	1.72	229.96	159.94	89.89	59.80
360.0	1.00	123.95	14.36	9.20	4.17	1.45	229.96	159.94	89.89	59.82

CYCLE NO. 1 EXPANSION SPACE TEMPERATURES 230.0 159.9 89.9 59.8

----- CALCULATED OUTPUT AFTER 1 CYCLE -----

MECHANICAL POWER INPUT (Summation Method)	Watts
P-V power:	214.241
Cooler flow loss:	0.304
Regenerator flow loss(1st STAGE):	0.418
(2nd STAGE):	0.195
(3rd STAGE):	0.045
(4th STAGE):	0.004
TOTAL POWER INPUT:	215.209

TOTAL POWER INPUT (Mechanical Drive Method)	Watts
Compressor drive:	441.007
Expander drive:	226.782
Cooler flow loss:	0.304
TOTAL POWER INPUT:	668.093

ITEMIZED HEATS FOR CYCLE[W], (+ve is heating; -ve is cooling)

(ZONE)	Compression Space		Expansion Space			
	and Cooler	(1st)	(2nd)	(3rd)	(4th)	
Heat Transfer from gas:	439.8	-113.3	-70.5	-31.5	-10.9	
Cylinder Wall Conduction(in):	0.0	1.5	0.7	0.3	0.0	
Cylinder Wall Conduction(out):	-1.5	-0.7	-0.3	0.0	0.0	
Expander Wall Conduction(in):	0.0	0.1	0.0	0.0	0.0	
Expander Wall Conduction(out):	-0.1	0.0	0.0	0.0	0.0	
Matrix Conduction(in):	0.0	0.0	0.0	0.0	0.0	
Matrix Conduction(out):	0.0	0.0	0.0	0.0	0.0	
Shuttle loss (in):	0.0	0.7	0.3	0.1	0.0	
Shuttle loss (out):	-0.7	-0.3	-0.1	0.0	0.0	
Pumping loss (in):	0.0	0.0	0.0	0.0	0.0	
Pumping loss (out):	0.0	0.0	0.0	0.0	0.0	
Flow Friction:	0.5	0.3	0.1	0.0	0.0	
Load:	0.0	0.0	0.0	0.0	1.0	
Net Heat (Sum):	438.0	-111.8	-69.8	-31.1	-9.9	
Net Heat (DeltT):	438.0	-111.8	-69.8	-31.1	-9.9	

TEMPERATURES [K]

	Compression Space		Expansion Space			
	and Cooler	(1st)	(2nd)	(3rd)	(4th)	
Start Cycle:	300.00	230.00	160.00	90.00	60.00	
End Cycle:	300.00	229.96	159.94	89.89	59.82	
Maximum:	300.00	230.04	160.07	90.18	60.39	
Minimum:	300.00	229.96	159.94	89.89	59.80	
(Max - Min):	0.00	0.08	0.14	0.30	0.59	

VOLUME AND PRESSURE VARIATION

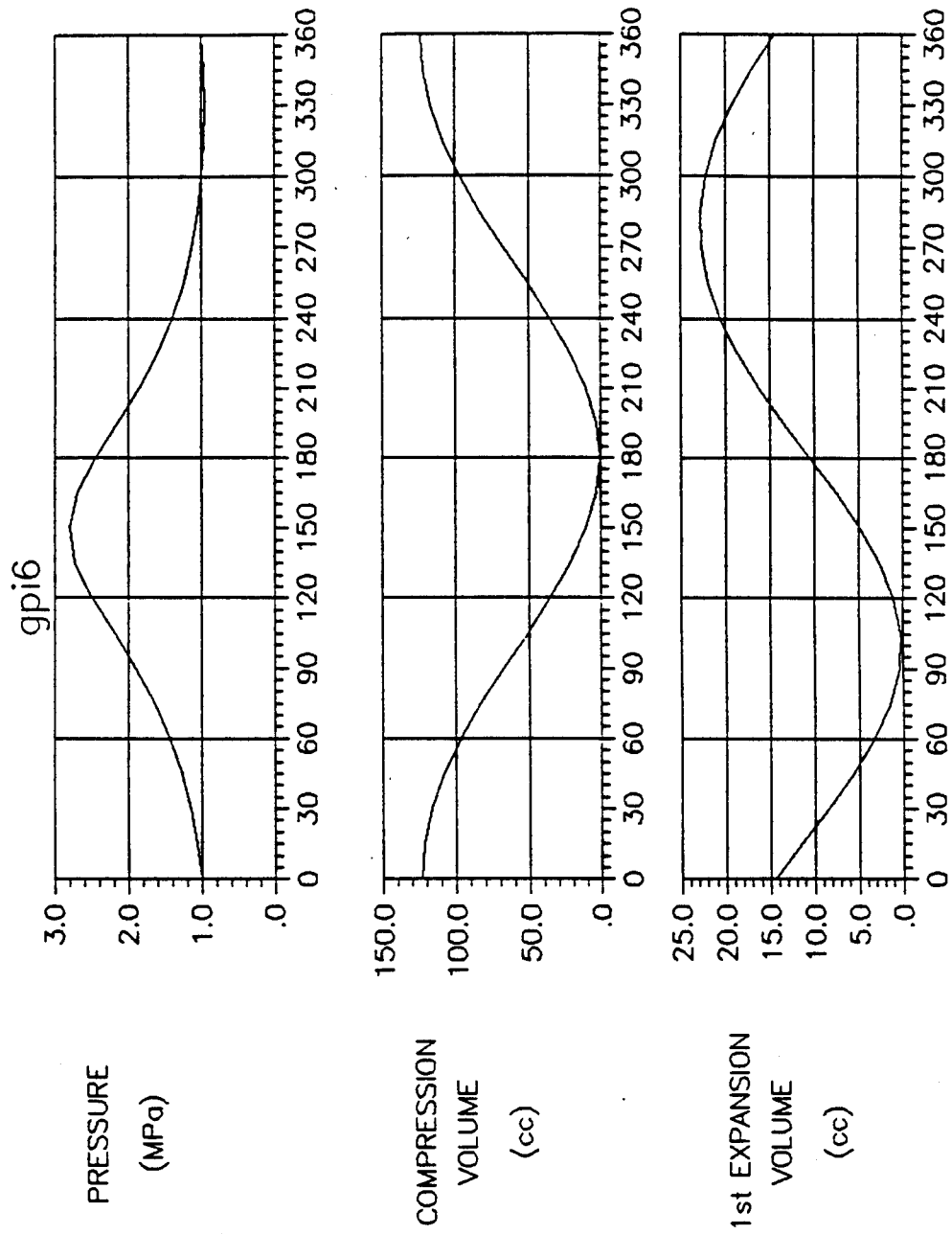


FIGURE 1

CRANK ANGLE (degrees)

NBSGRAPH ver. 1.0

VOLUME AND PRESSURE VARIATION

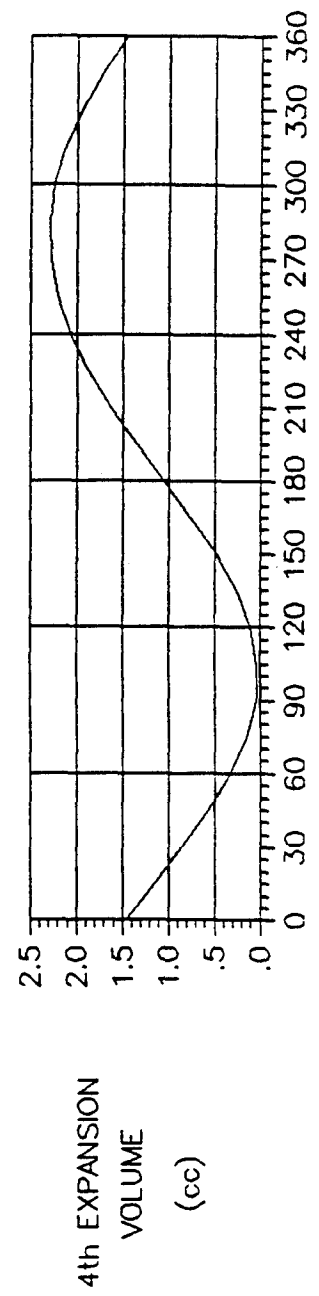
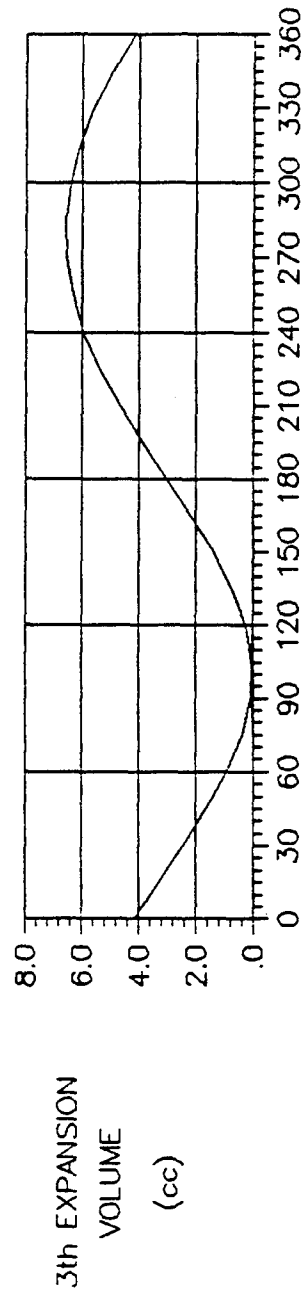
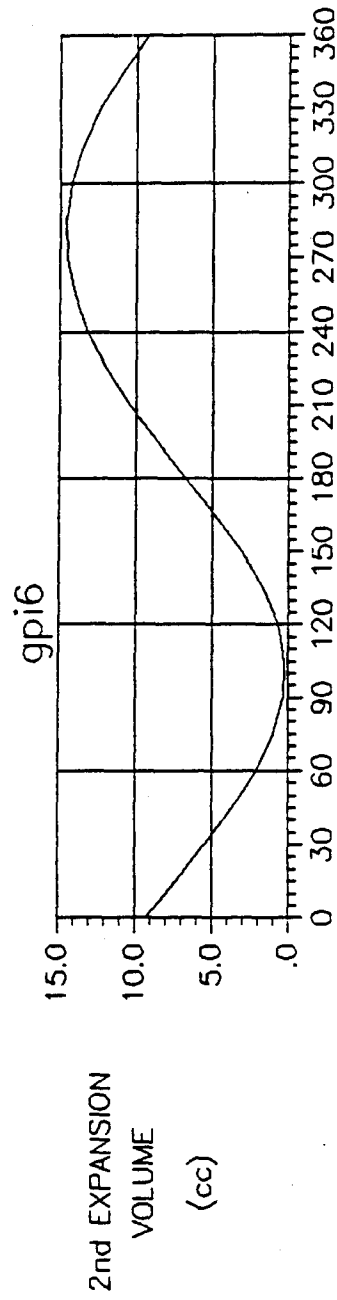


FIGURE 2

CRANK ANGLE (degrees)

NESGRAPH ver. 1.0

P - V DIAGRAM

gpi6

Mean pressure: 1.000 MPa

Speed: 300. rpm

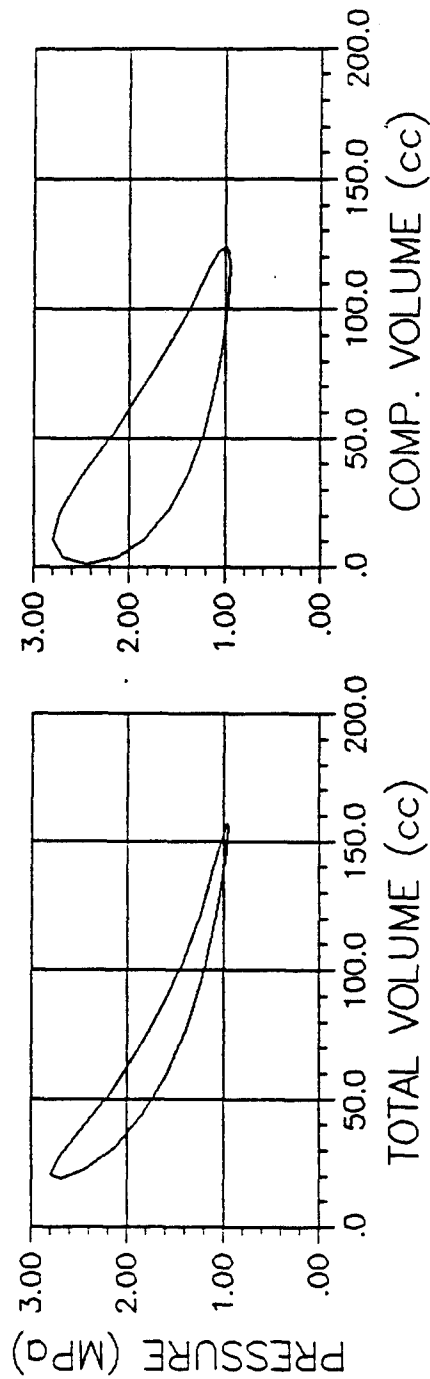


FIGURE 3

NBSGRAPH1 ver. 1.0

P - V DIAGRAM

gpi6

Mean pressure: 1.000 MPa

Speed: 300. rpm

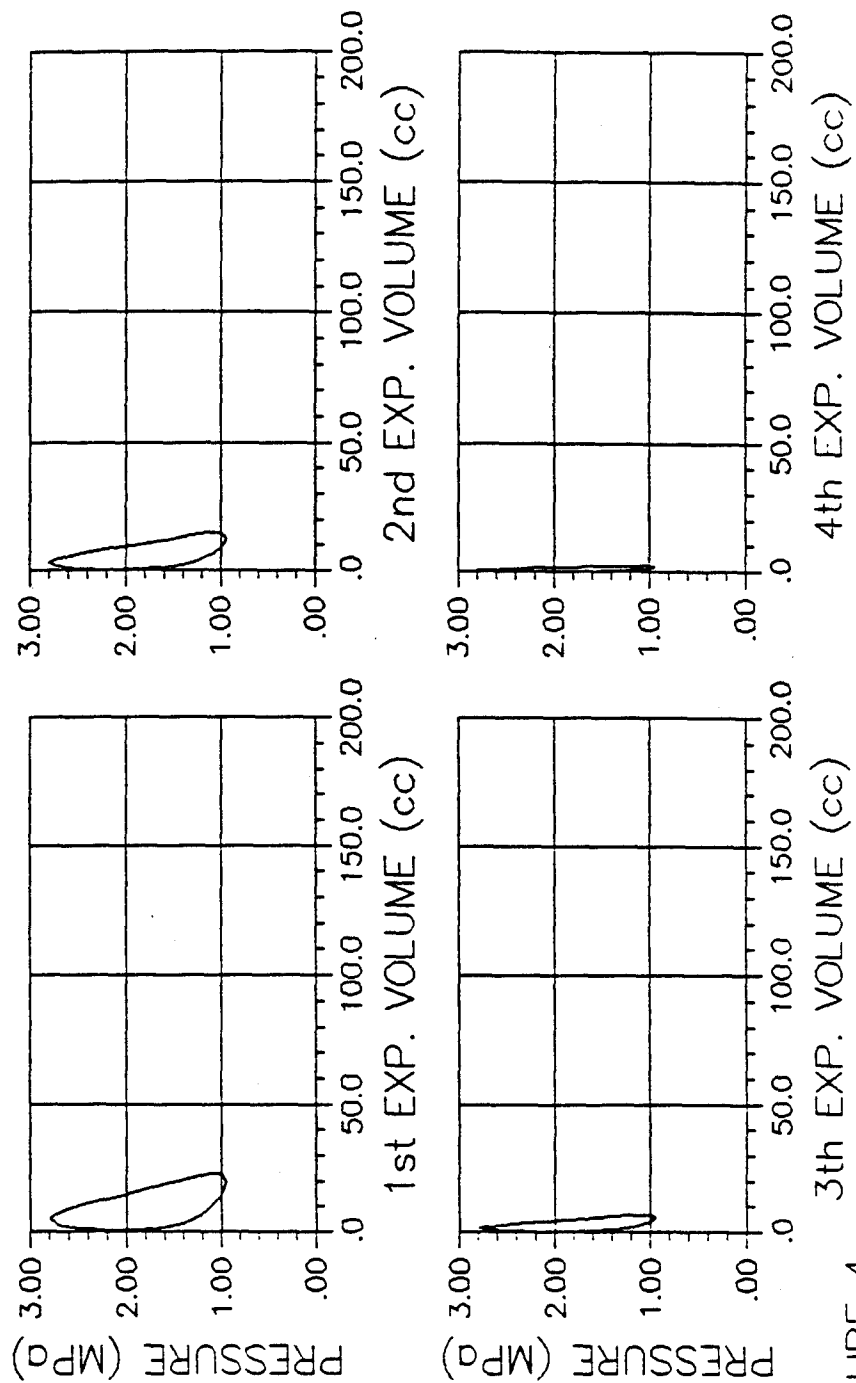


FIGURE 4

NEISGRAPH ver. 1.0

P - V DIAGRAM

gpi6

Mean pressure: 1.000 MPa

Speed: 300. rpm

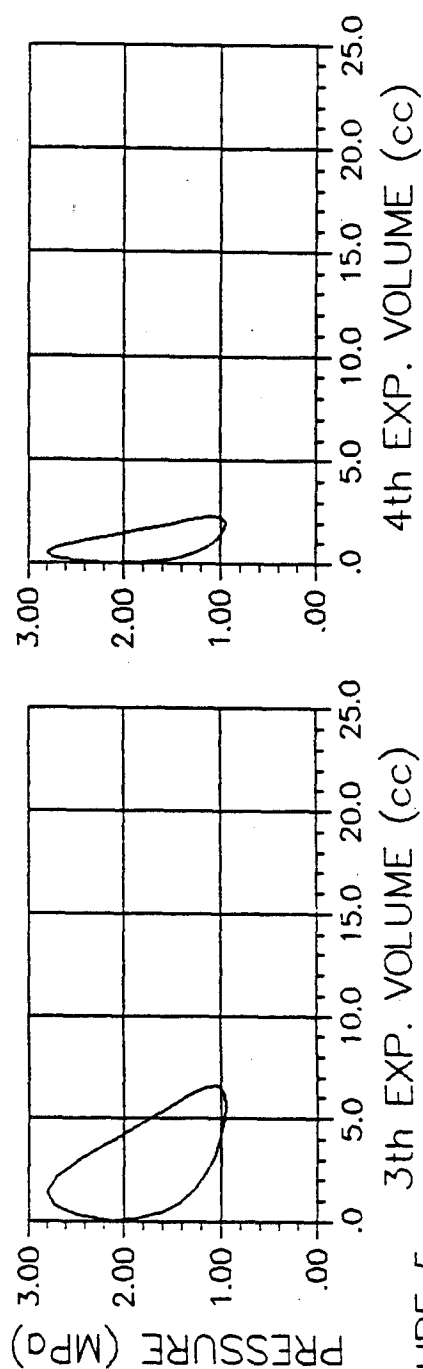
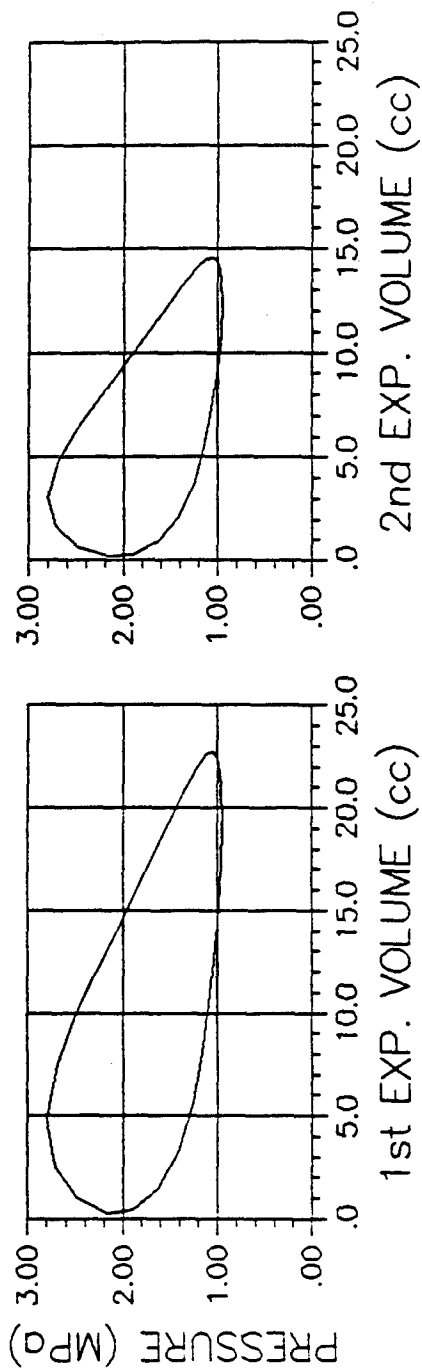


FIGURE 5

NESSGRAPH ver. 1.0

RATIONALIZED P - V DIAGRAM

gpi6

Temp. Ratio: 1.3043 Phase angle: 80.00 degrees

Mean pressure: 1.000 MPa Speed: 300.0 rpm

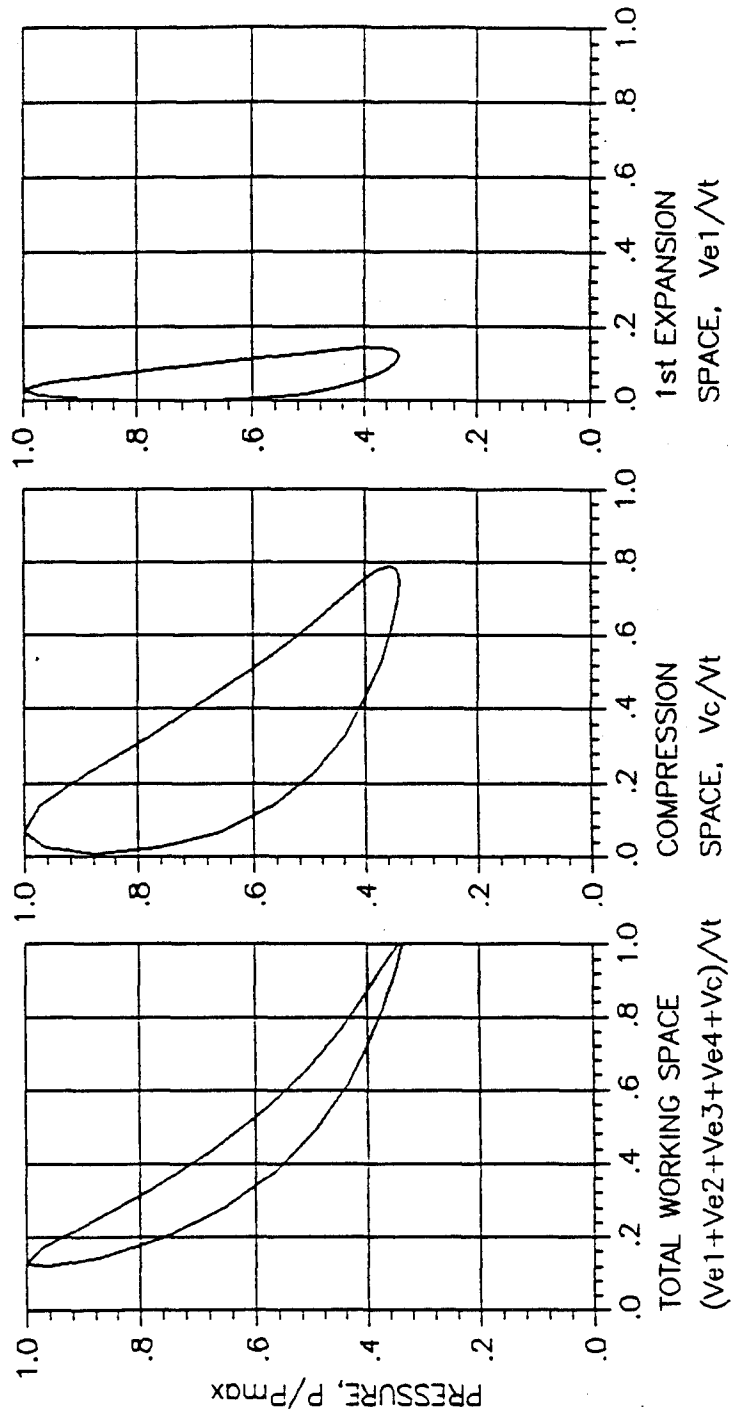


FIGURE 6

NBSGRAPH ver. 1.0

RATIONALIZED P - V DIAGRAM

gpi6

Temp. Ratio: 1.3043	Phase angle: 80.00 degrees
Mean pressure: 1.000 MPa	Speed: 300.0 rpm

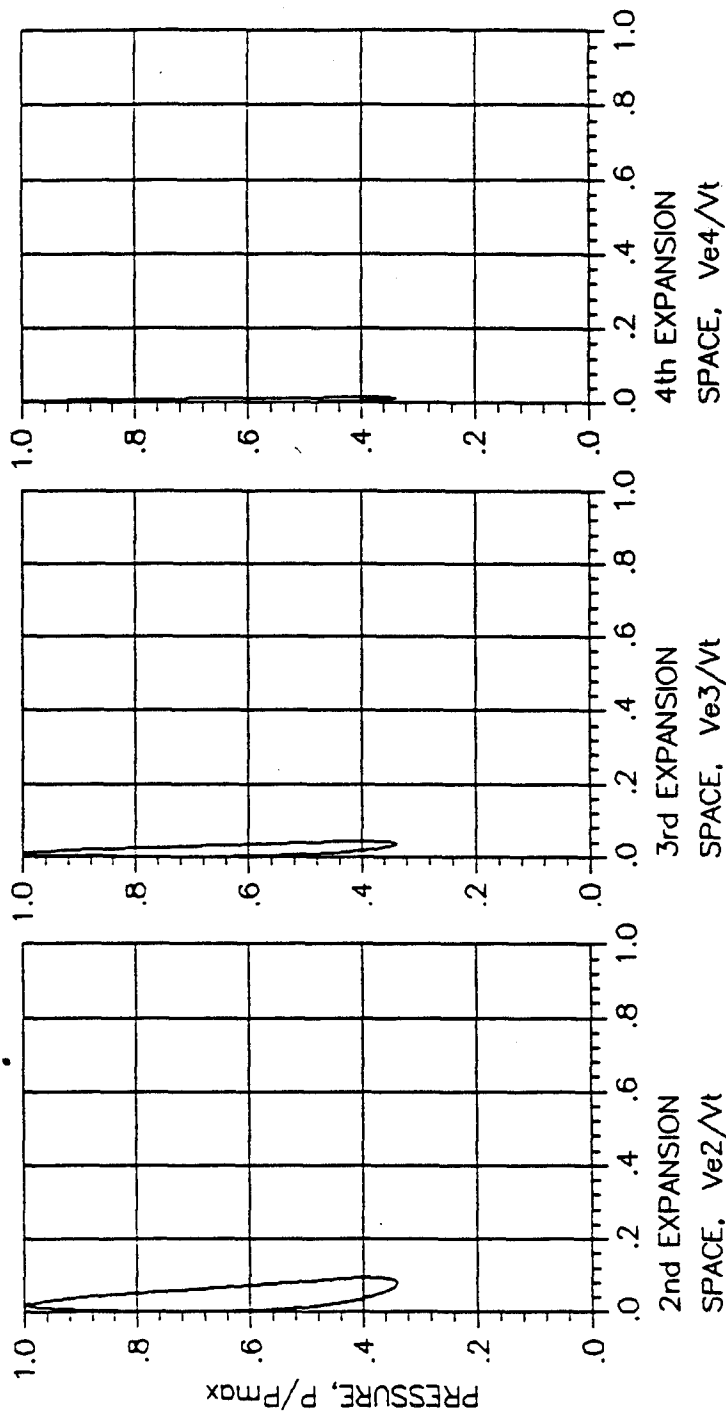


FIGURE 7

NBSGRAPH ver 1.0

RATIONALIZED P - V DIAGRAM

gpi6

Temp. Ratio: 1.3043	Phase angle: 80.00 degrees
Mean pressure: 1.000 MPa	Speed: 300.0 rpm

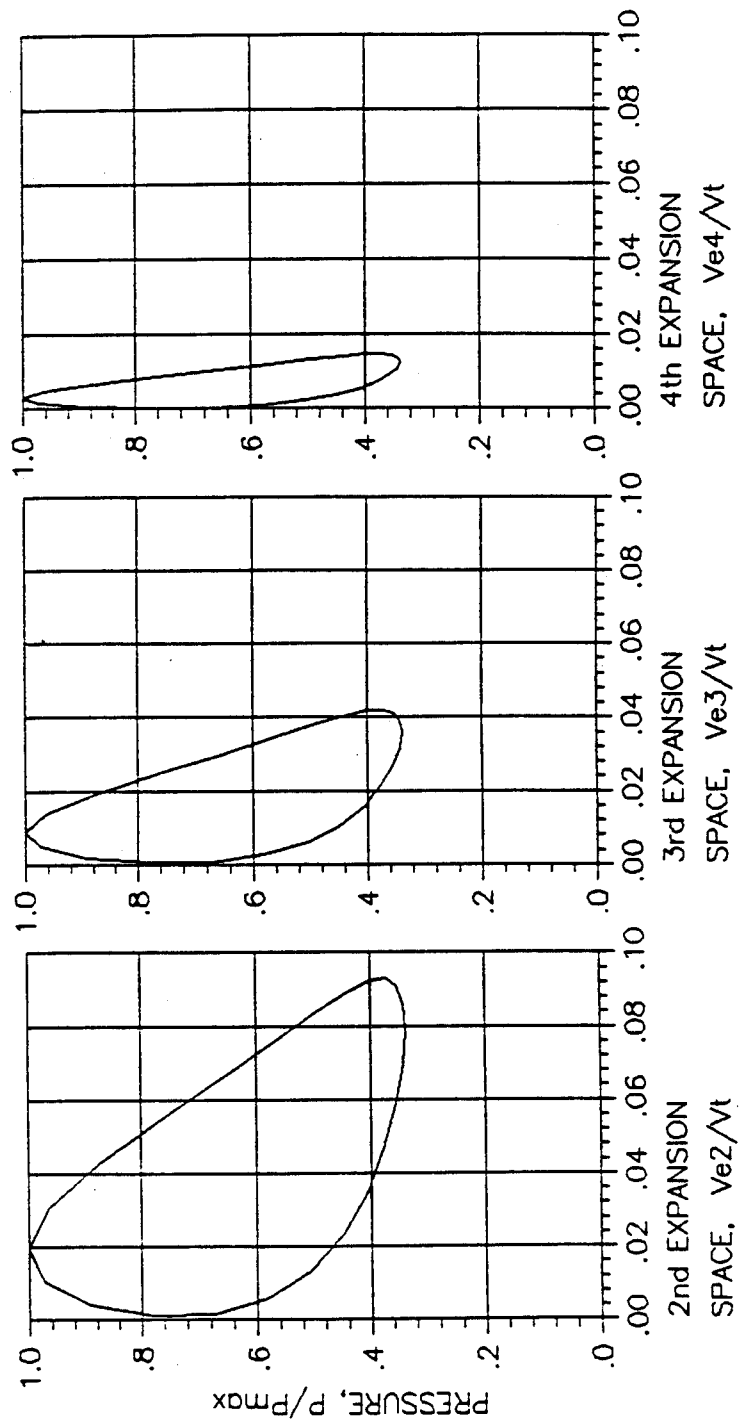


FIGURE 8

NBSGRAPH ver. 1.0

GAS FLOW DISTRIBUTION

gpi6

Mean pressure: 1.000 MPa	—	Compression Space
Speed: 300. rpm	-----	Expansion Space

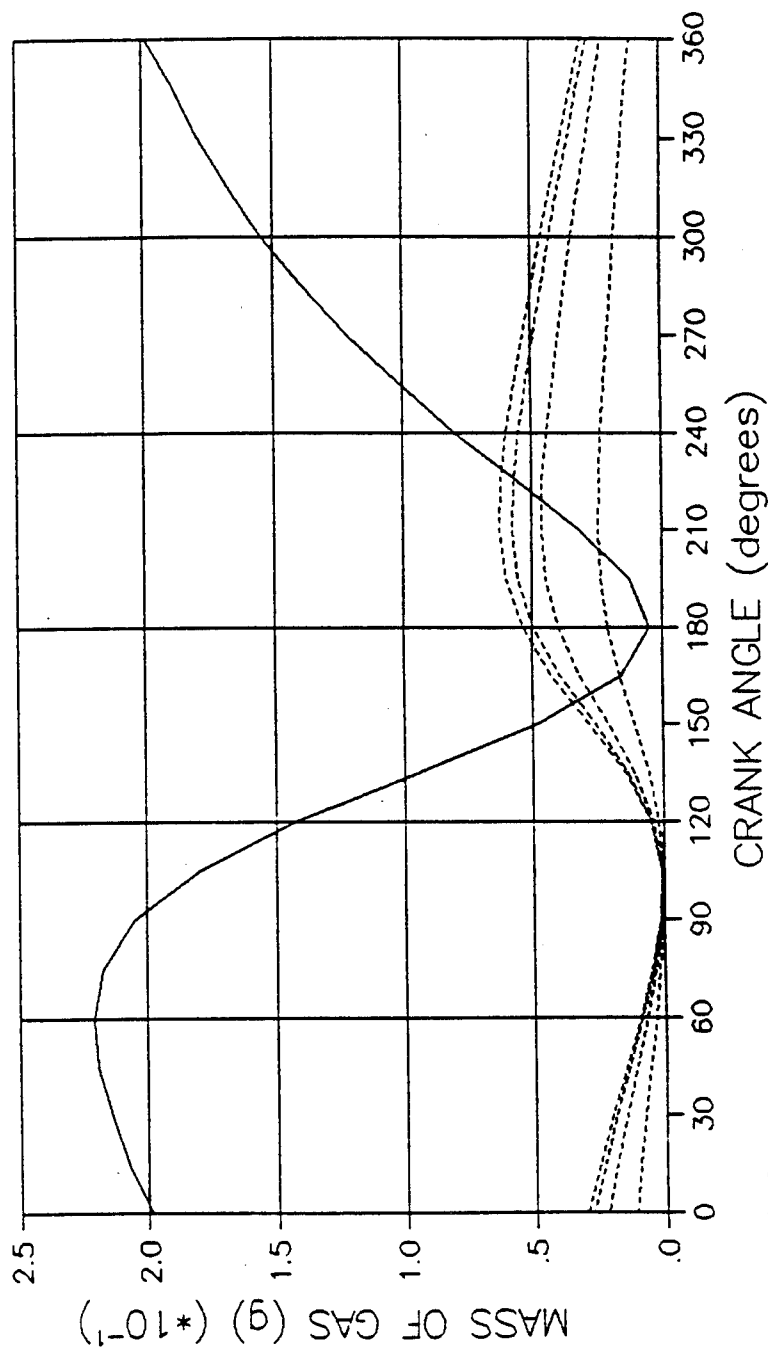


FIGURE 9

NBSGRAPH ver. 1.0

POWER MAP

Exp. Wall Temp.:	230.0 K
Cooling Water Temp.:	300.0 K
Phase angle:	80.0 degrees
	○ 1.000 MPa
	□ 2.000 MPa
	△ 3.000 MPa
	◇ 4.000 MPa
	★ 5.000 MPa

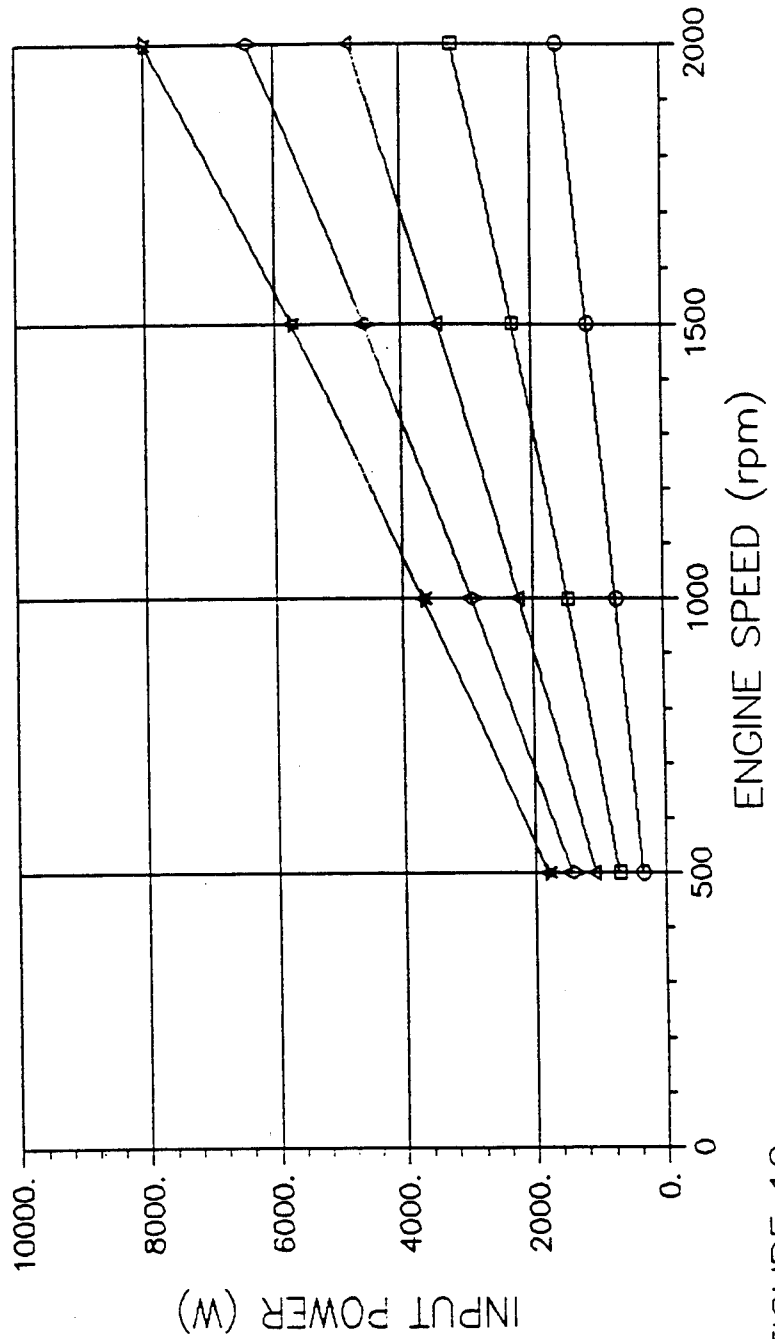


FIGURE 10

HEAT MAP (1ST EXPANSION)

Exp. Wall Temp.: 230.0 K	○ 1.000 MPa
Cooling Water Temp.: 300.0 K	□ 2.000 MPa
Phase angle: 80.0 degrees	△ 3.000 MPa
	◇ 4.000 MPa
	★ 5.000 MPa

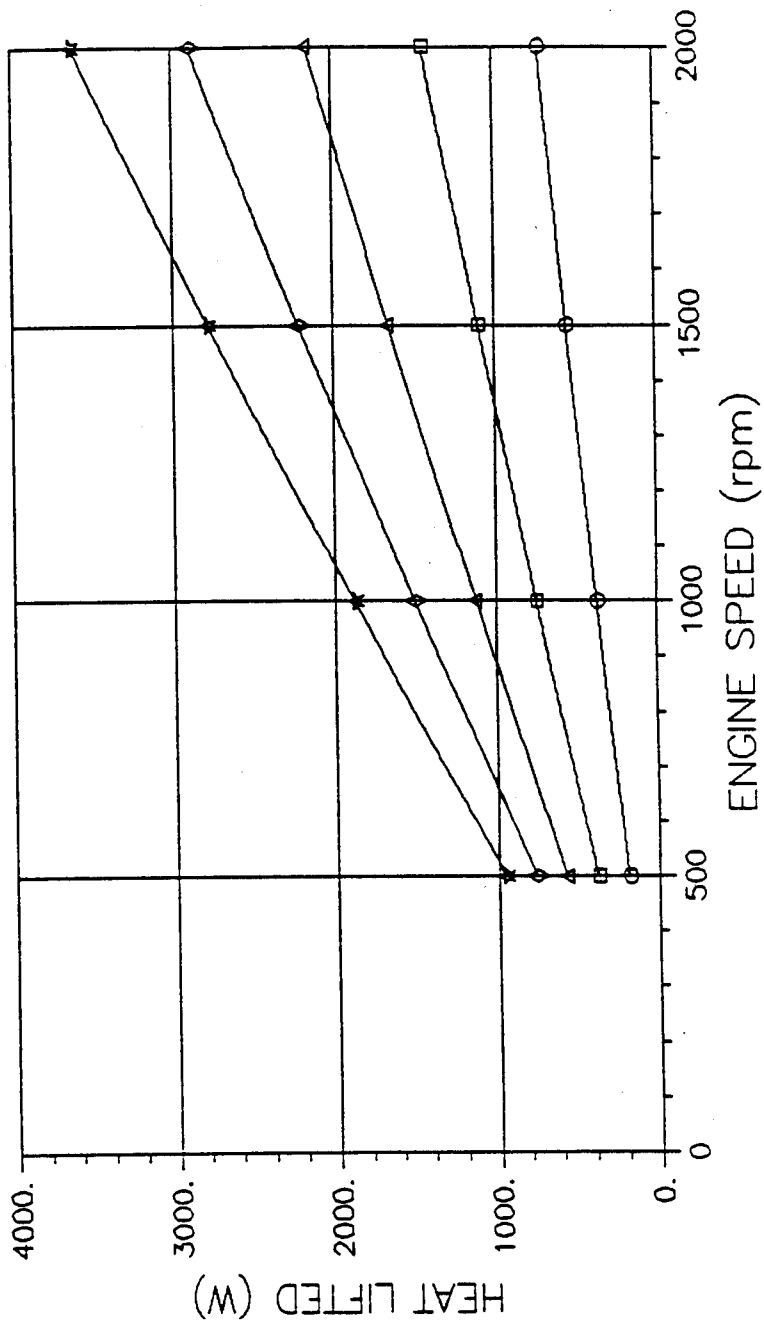


FIGURE 11

HEAT MAP (2ND EXPANSION)

Exp. Wall Temp.:	160.0 K	○	1.000 MPa
Cooling Water Temp.:	300.0 K	□	2.000 MPa
Phase angle:	80.0 degrees	△	3.000 MPa
		◇	4.000 MPa
		★	5.000 MPa

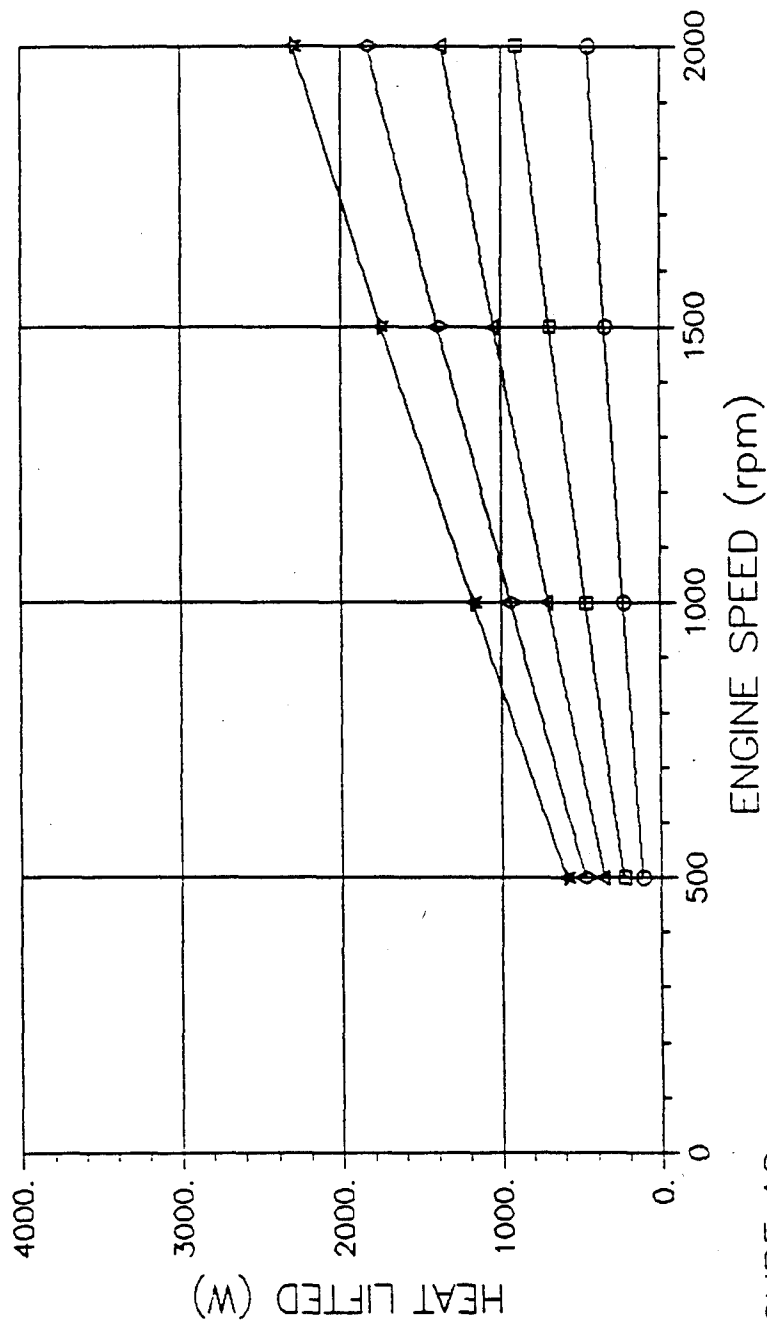


FIGURE 12

NBSGRAPH ver. 1.0

HEAT MAP (3RD EXPANSION)

Exp. Wall Temp.:	90.0 K	○	1.000 MPa
Cooling Water Temp.:	300.0 K	□	2.000 MPa
Phase angle:	80.0 degrees	△	3.000 MPa
		◇	4.000 MPa
		★	5.000 MPa

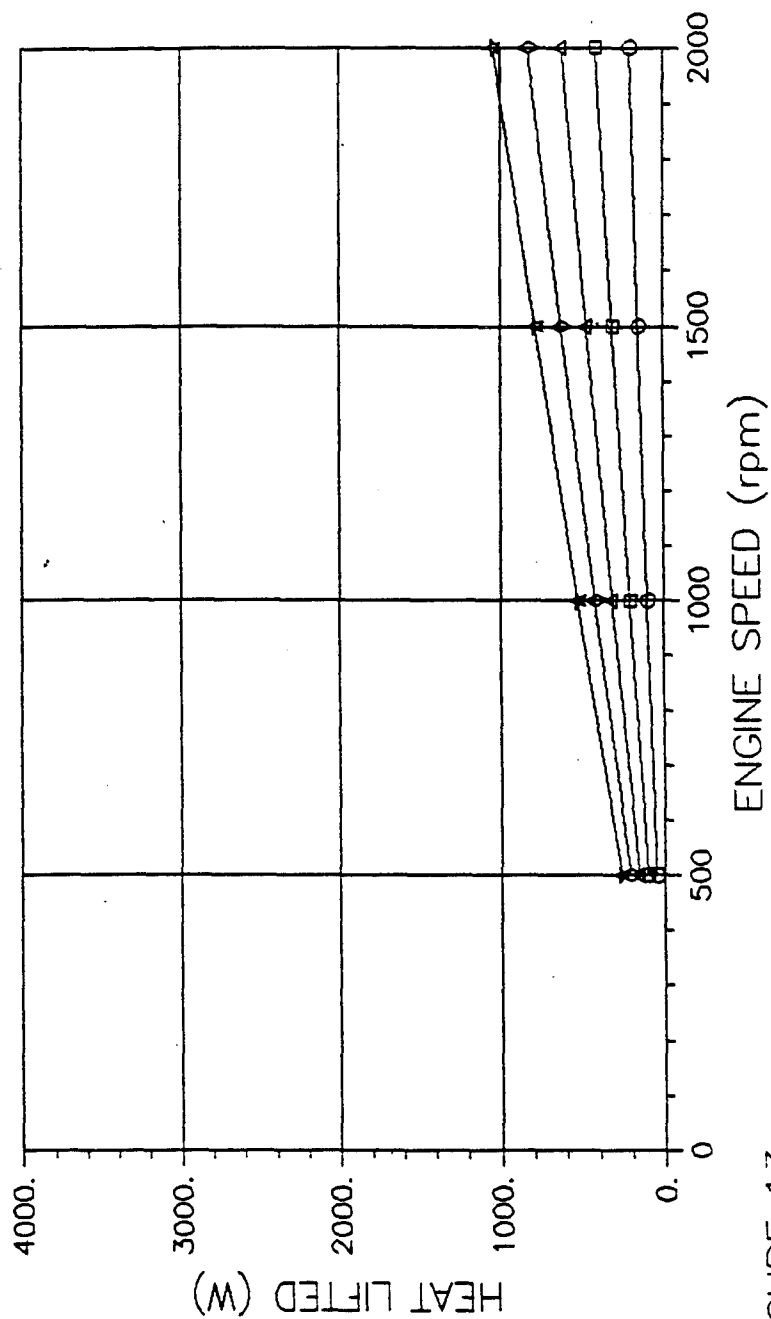
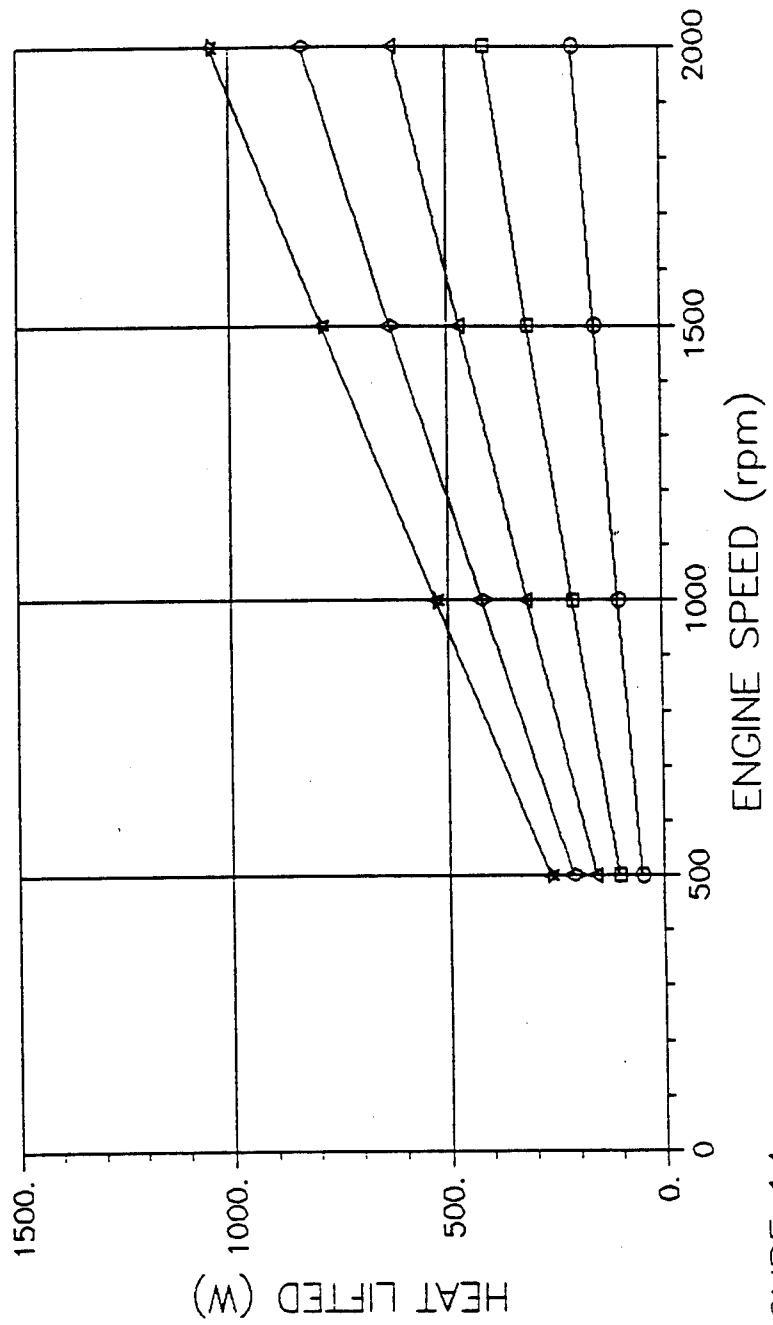


FIGURE 13

NEBGRAPH ver. 1.0

HEAT MAP (3RD EXPANSION)

Exp. Wall Temp.: 90.0 K	○	1.000 MPa
Cooling Water Temp.: 300.0 K	□	2.000 MPa
Phase angle: 80.0 degrees	△	3.000 MPa
	◇	4.000 MPa
	★	5.000 MPa



NBSGRAPH ver. 1.0

FIGURE 14

HEAT MAP (4TH EXPANSION)

Exp. Wall Temp.:	60.0 K	○	1.000 MPa
Cooling Water Temp.:	300.0 K	□	2.000 MPa
Phase angle:	80.0 degrees	△	3.000 MPa
		◇	4.000 MPa
		★	5.000 MPa

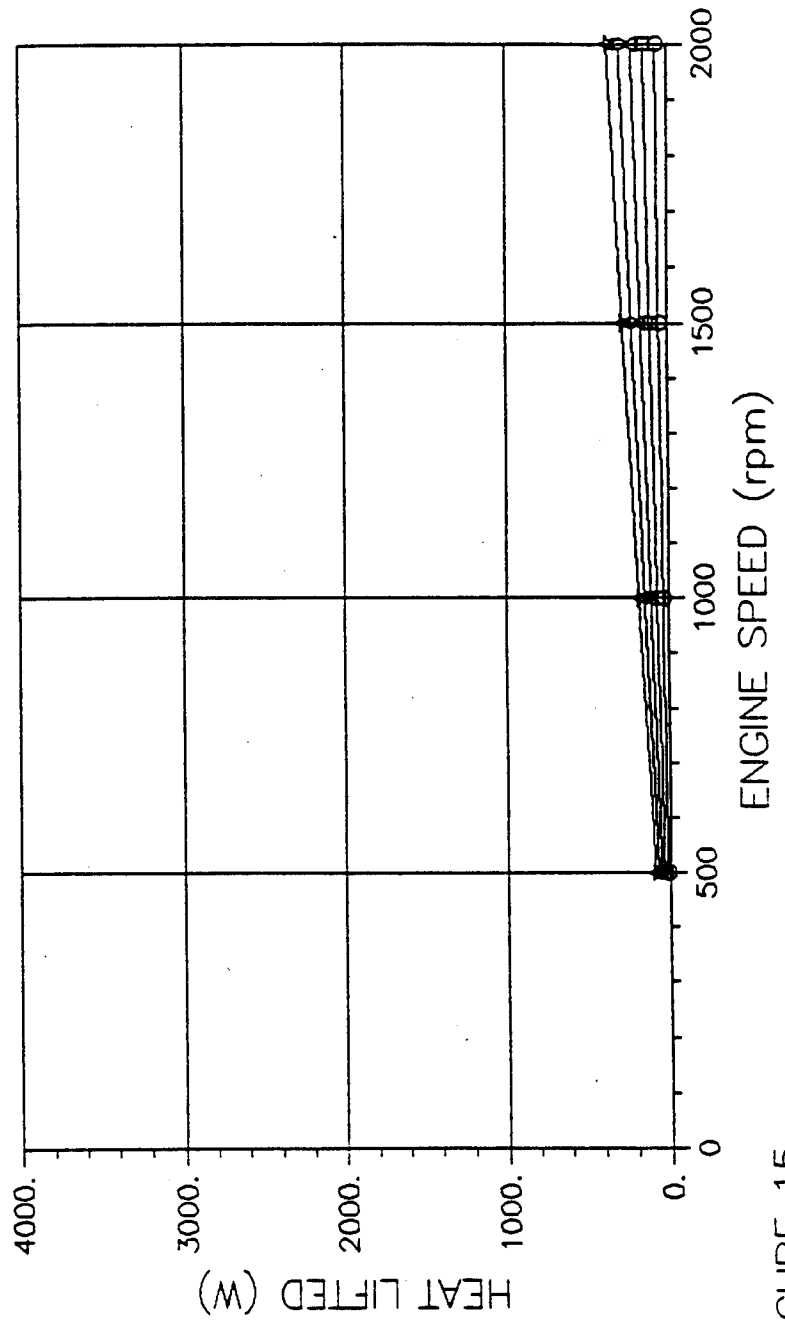


FIGURE 15

HEAT MAP (4TH EXPANSION)

Exp. Wall Temp.: 60.0 K	○ 1.000 MPa
Cooling Water Temp.: 300.0 K	□ 2.000 MPa
Phase angle: 80.0 degrees	△ 3.000 MPa
	◇ 4.000 MPa
	★ 5.000 MPa

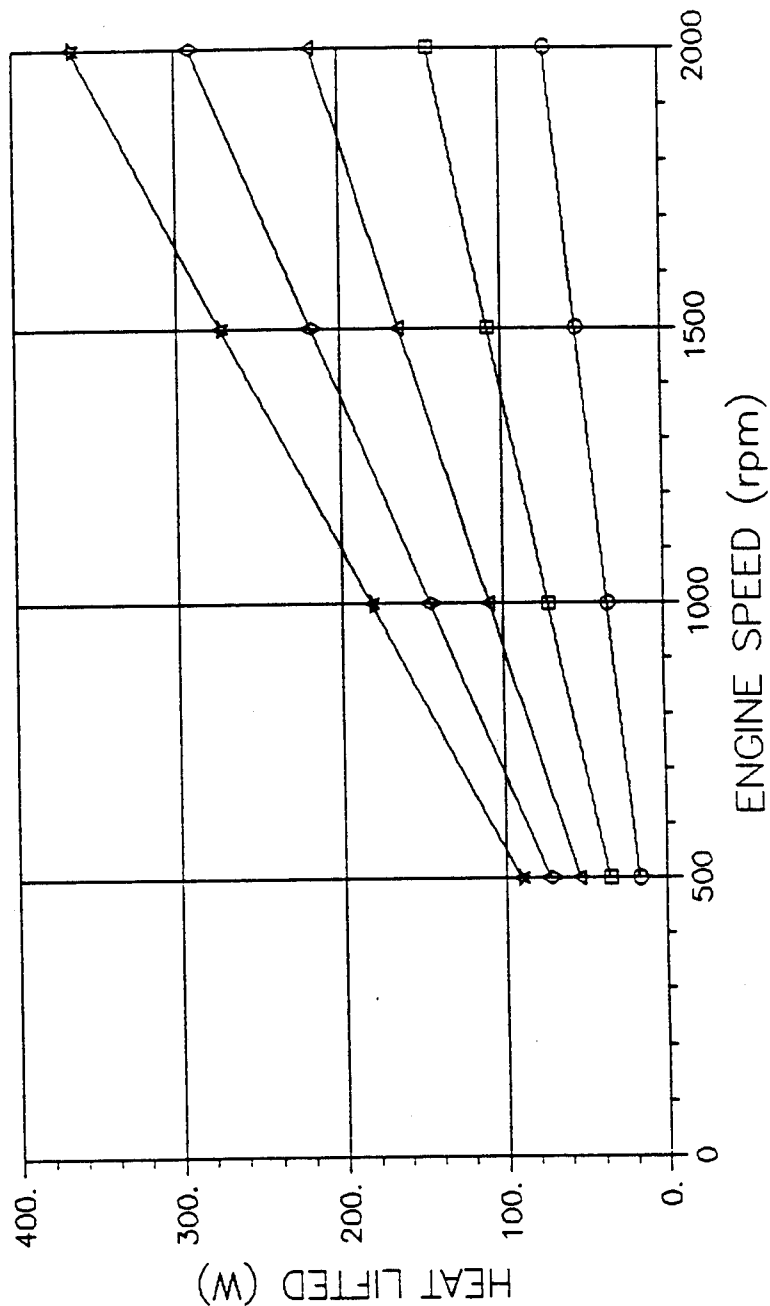


FIGURE 16 NESGRAPH ver. 1.0

C.O.P. MAP (1ST EXPANSION)

Exp. Wall Temp.:	230.0 K	○	1.000 MPa
Cooling Water Temp.:	300.0 K	□	2.000 MPa
Phase angle:	80.0 degrees	△	3.000 MPa
		◇	4.000 MPa
		★	5.000 MPa

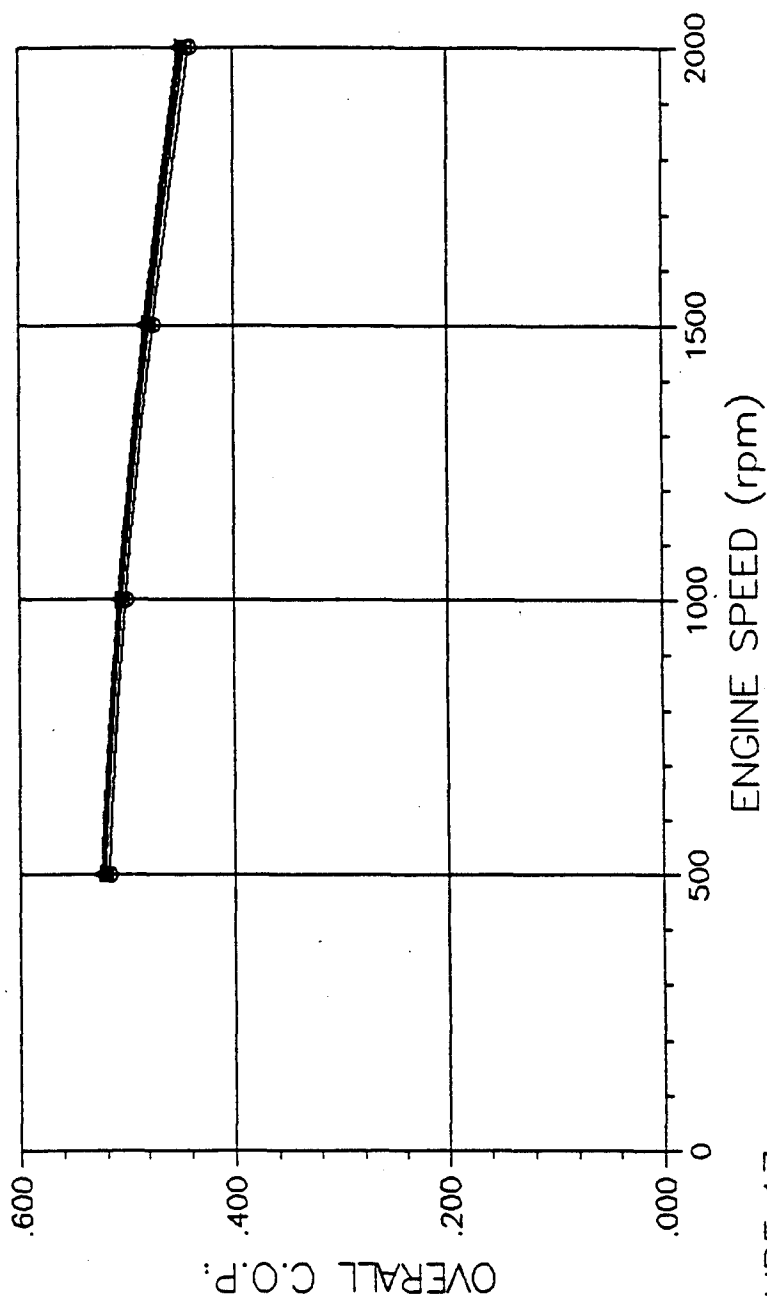


FIGURE 17

NBSGRAPH ver. 1.0

C.O.P. MAP (2ND EXPANSION)

Exp. Wall Temp.:	160.0 K	○	1.000 MPa
Cooling Water Temp.:	300.0 K	□	2.000 MPa
Phase angle:	80.0 degrees	△	3.000 MPa
		◇	4.000 MPa
		★	5.000 MPa

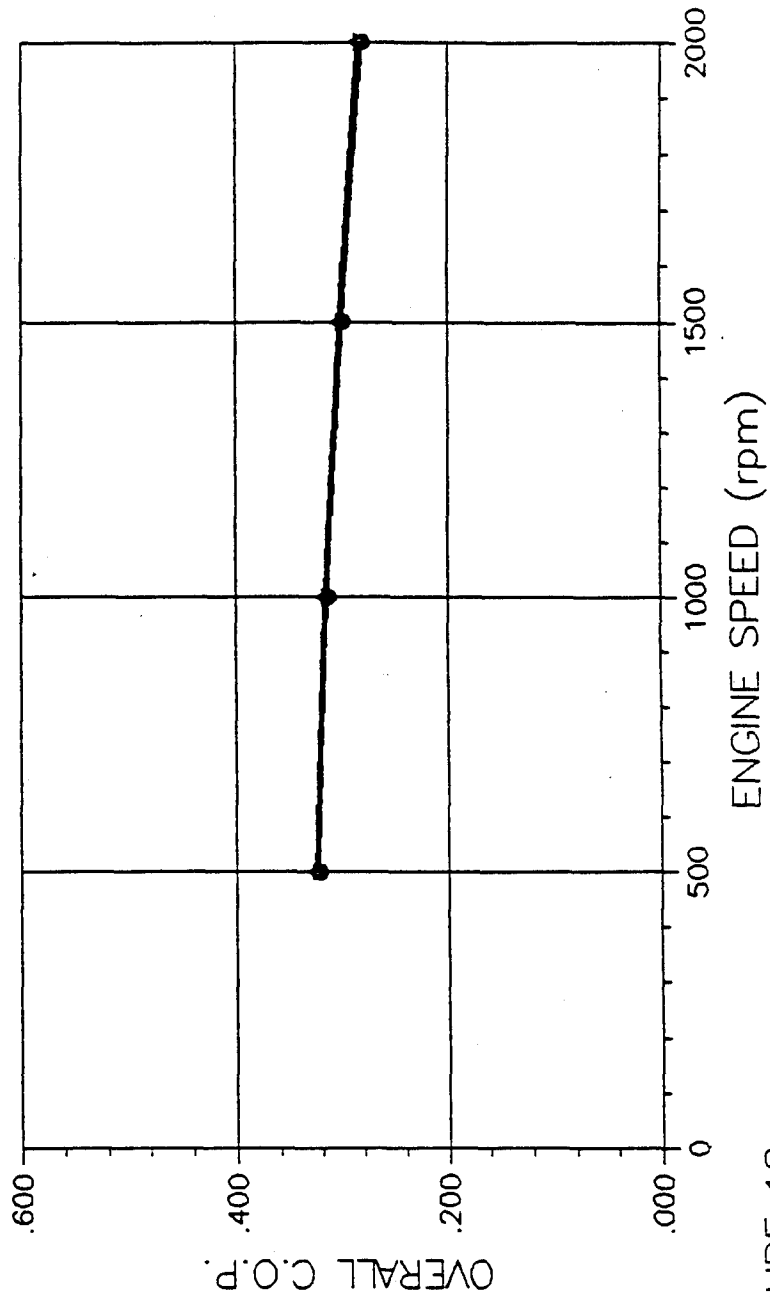


FIGURE 18

NBSGRAPH ver. 1.0

C.O.P. MAP (3RD EXPANSION)

Exp. Wall Temp.:	90.0 K	○	1.000 MPa
Cooling Water Temp.:	300.0 K	□	2.000 MPa
Phase angle:	80.0 degrees	△	3.000 MPa
		◇	4.000 MPa
		★	5.000 MPa

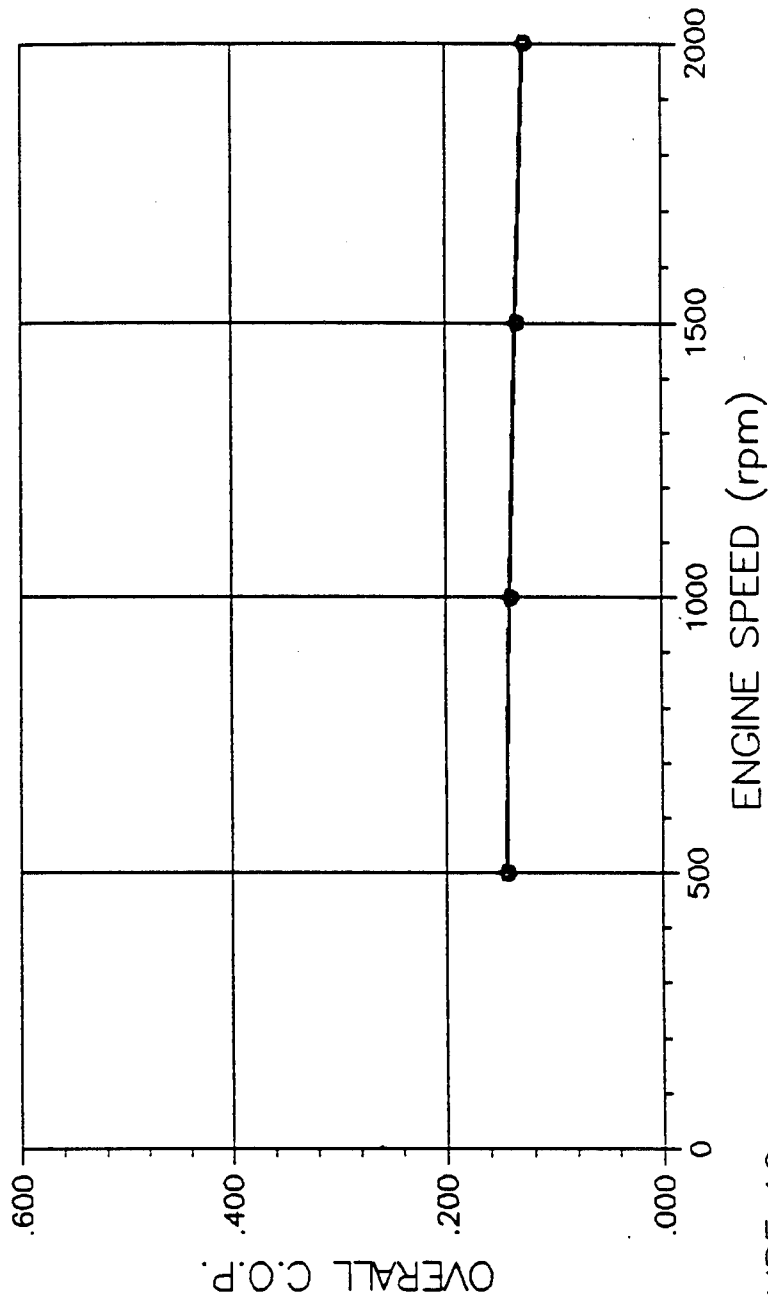


FIGURE 19

NBSGRAPH ver. 1.0

C.O.P. MAP (3RD EXPANSION)

Exp. Wall Temp.:	90.0 K	○	1.000 MPa
Cooling Water Temp.:	300.0 K	□	2.000 MPa
Phase angle:	80.0 degrees	△	3.000 MPa
		◇	4.000 MPa
		★	5.000 MPa

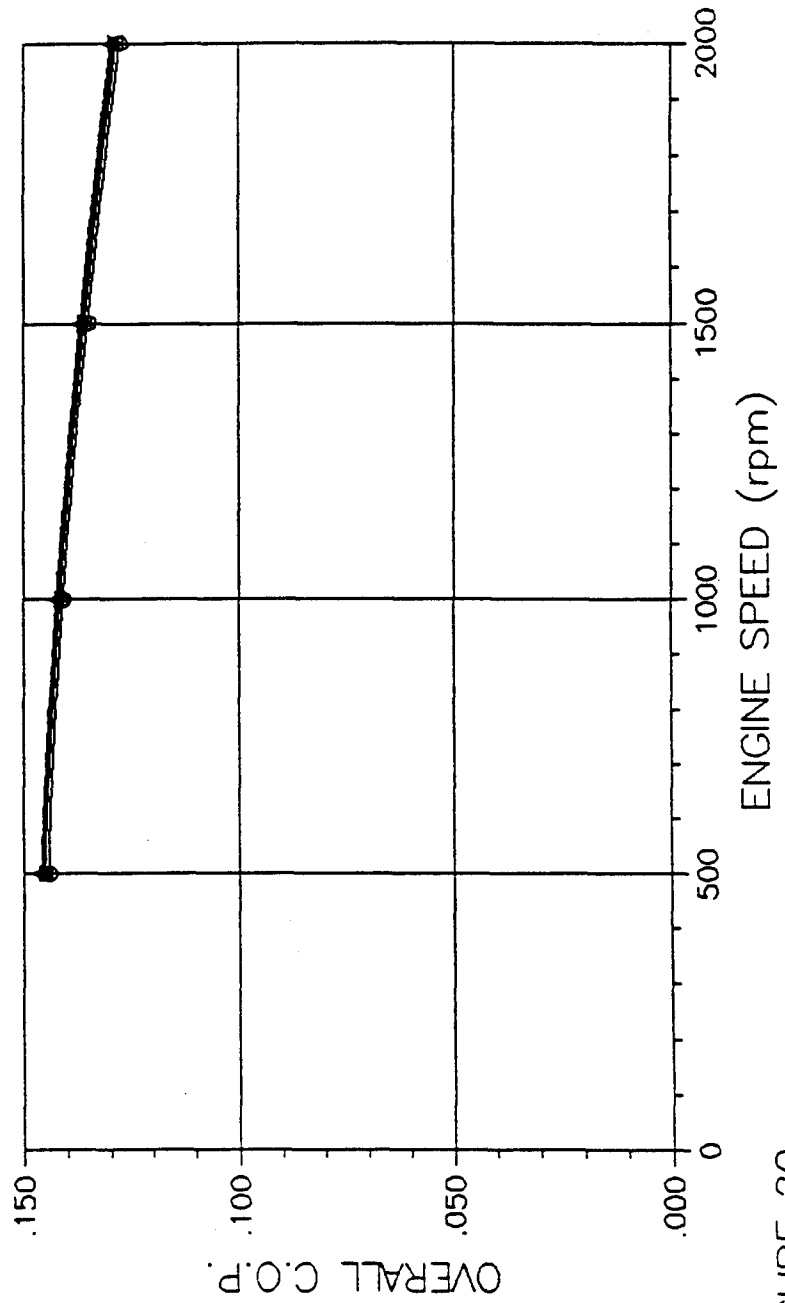


FIGURE 20

C.O.P. MAP (4TH EXPANSION)

Exp. Wall Temp.:	60.0 K	○	1.000 MPa
Cooling Water Temp.:	300.0 K	□	2.000 MPa
Phase angle:	80.0 degrees	△	3.000 MPa
		◇	4.000 MPa
		★	5.000 MPa

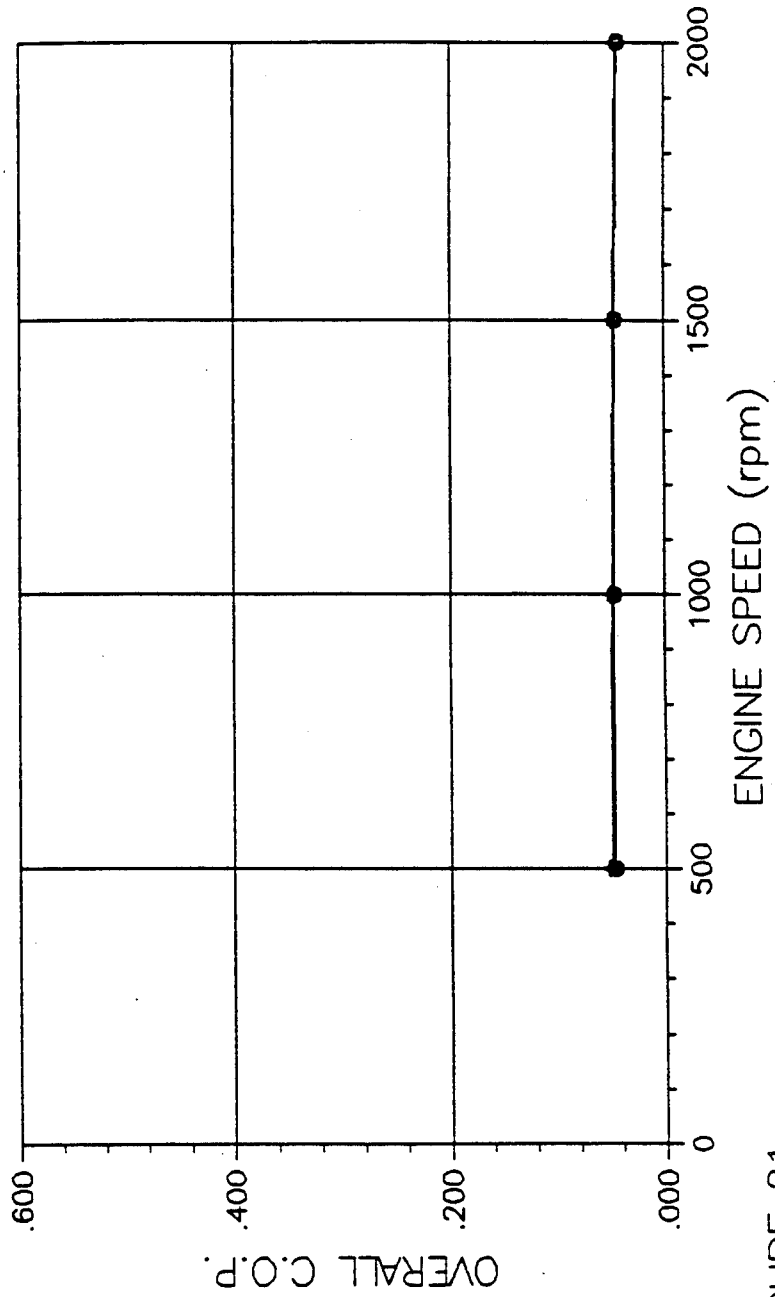


FIGURE 21

NBSGRAPH ver. 1.0

C.O.P. MAP (4TH EXPANSION)

Exp. Wall Temp.:	60.0 K	○	1.000 MPa
Cooling Water Temp.:	300.0 K	□	2.000 MPa
Phase angle:	80.0 degrees	△	3.000 MPa
		◇	4.000 MPa
		★	5.000 MPa

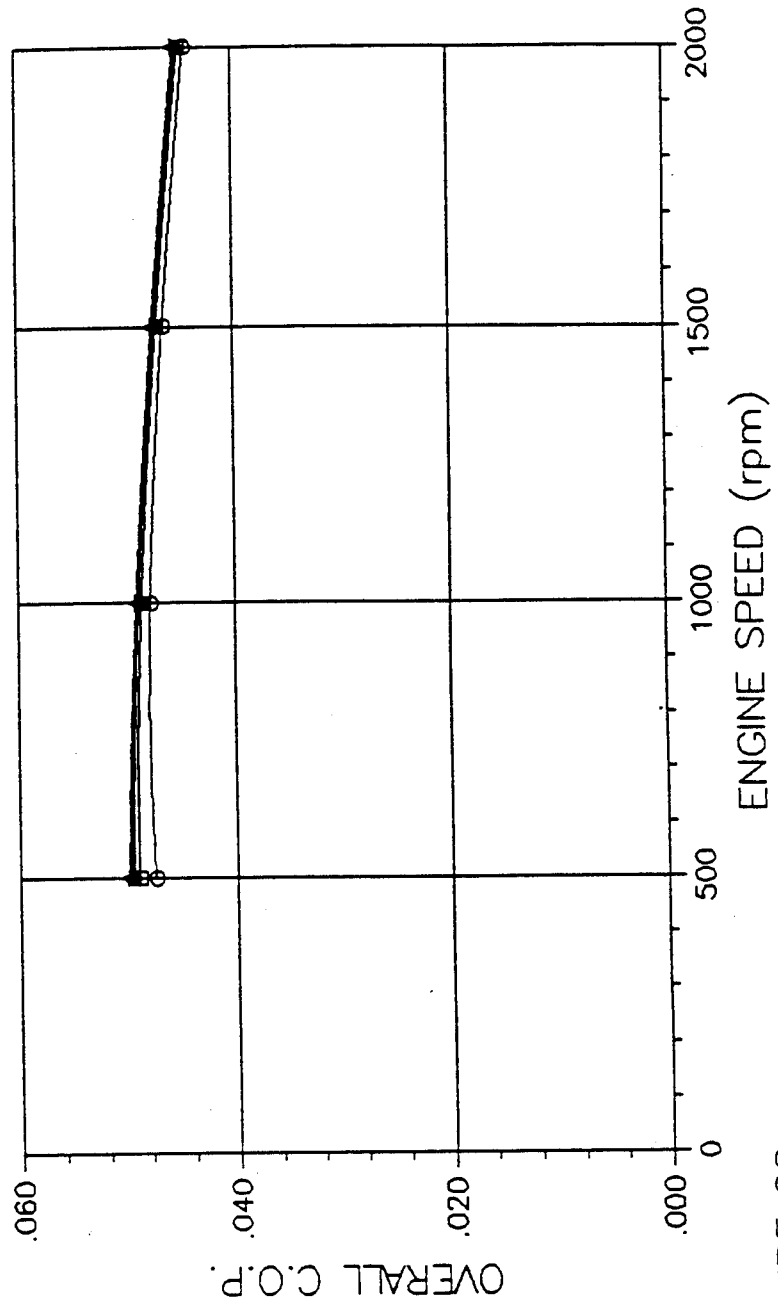


FIGURE 22

NESGRAPH ver. 1.0

EFFECT OF PHASE ANGLE ON COOLER PERFORMANCE

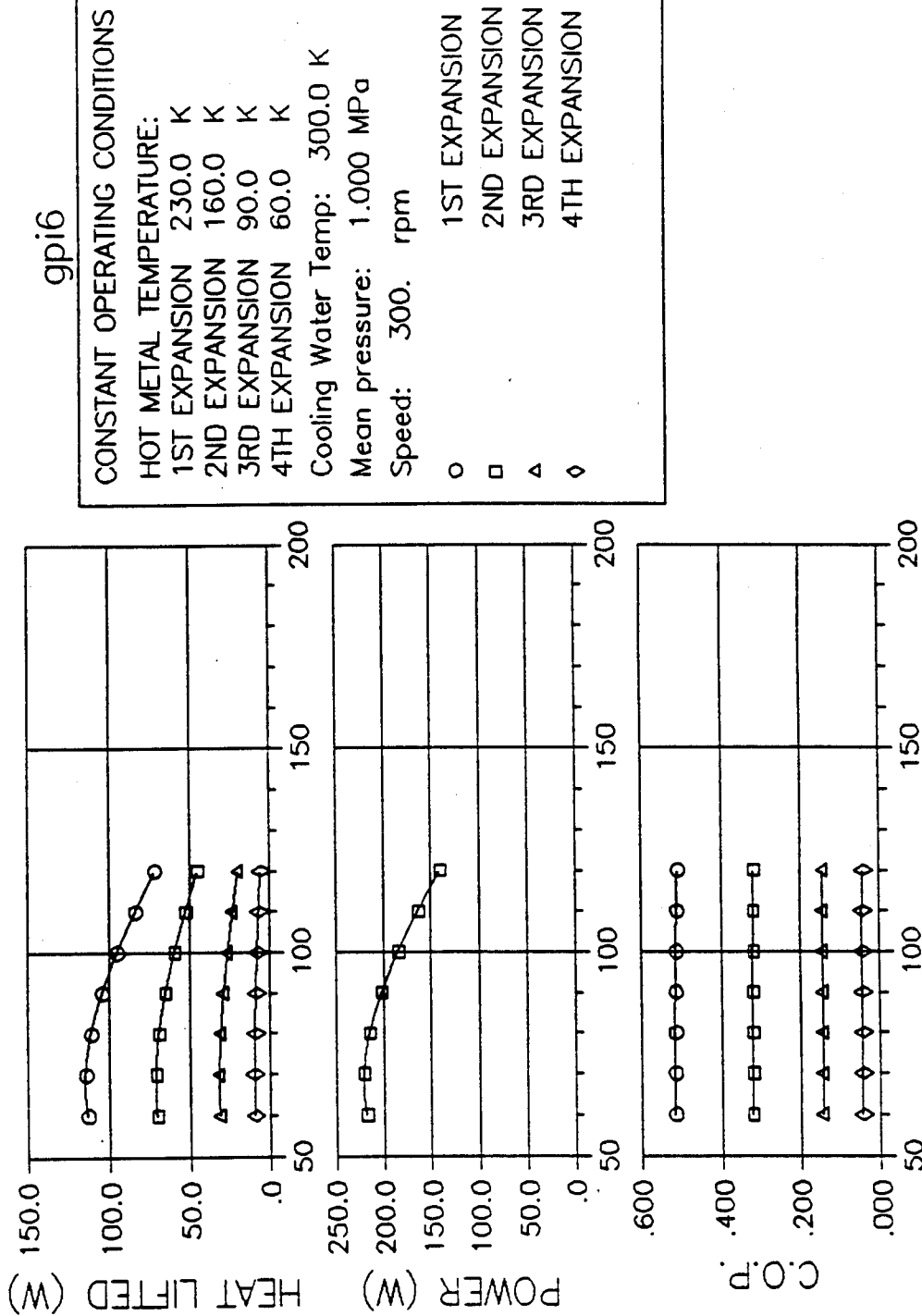


FIGURE 23 PHASE ANGLE (degrees)

APPENDIX B

Preliminary Test Plan

TEST PLAN

for

Strategic Defense Initiative Organization
Small Business Innovation Research
Phase II Development

of

Low Capacity Reliquefier for Storage of
Cryogenic Fluids

Contract F04611-89-C-0055 (January 15, 1990)

CDRL Item Number 1004

Security Classification: Unclassified

Distribution authorized to U. S. government agencies and their contractors; critical technology, August, 1988. Other requests for this document shall be referred to AFAL/TSTR, Edwards AFB, CA 93523-5000.

WARNING - This document contains technical data whose export is restricted by the Arms Export Control Act (Title 22, U.S.C., Sec. 2751 et seq.) or Executive Order 12470. Violation of these export laws is subject to severe criminal penalties.

DESTRUCTION NOTICE - Destroy by any method that will prevent disclosure of the contents or reconstruction of the document.

Prepared for:

AFFTC (AFSC)
Directorate of Contracting
Edwards Air Force Base, California

Prepared by:

General Pneumatics Corporation
Western Research Center
Scottsdale, AZ 85260

Principal Investigator: Woody Ellison

September 1990

TABLE OF CONTENTS

Title Page	1
Table of Contents.	2
1.0 INTRODUCTION	3
1.1 Phase II Development Objective.	3
1.2 System Description.	3
1.3 Test Plan Scope	3
1.4 Government Furnished Equipment.	5
1.5 Applicable Specifications	5
2.0 TEST OBJECTIVES.	5
2.1 Key Developments.	5
2.2 Organization of Testing	7
2.3 Computer Model Correlation.	7
3.0 TEST METHODS	9
3.1 Regenerators.	9
3.2 J-T Cryostat.	9
3.3 Three-Stage Compressor Subassembly.	10
3.4 Stirling Zimmerman Subassembly.	10
3.5 Combined Stirling/Zimmerman and J-T Subassembly	11
3.6 System Integration.	12
3.0 TEST EQUIPMENTS.	13

FIGURES

Figure 1. HELIUM RELIQUEFIER SYSTEM	4
Figure 2. TEST PLAN FLOW DIAGRAM.	8

1.0 INTRODUCTION

1.1 Phase II Development Objective

The objective of the subject Small Business Innovation Research Phase II project is to fabricate and test a proof-of-principles prototype cryorefrigerator to recondense vapor boil-off from a liquid helium storage dewar at a rate of 10 liters of liquid per day with an ambient temperature of approximately 300 K.

1.2 System Description

A conceptual layout of the helium liquefier system is shown in Figure 1. The liquefier is an advanced synthesis of a multi-stage Stirling cryocooler, an integral 3-stage helium compressor, and a Joule-Thomson (J-T) cryostat. Key developments are as follows.

The Stirling cryocooler employs a stepped Zimmerman displacer to generate four successive stages of refrigeration at temperatures of 120 K, 50 K, 20 K, and 10 K. Helium boil-off vapor at 0.1 MPa and 4.2 K from the storage dewar is compressed and circulated by the 3-stage compressor. After each stage of compression the helium is cooled to 300 K by an external coolant loop. Helium at 0.8 MPa from the compressor second stage is further cooled by the incoming boil-off vapor and the Zimmerman displacer stages, and is then liquefied and returned to the storage dewar by expansion through the J-T cryostat. The J-T cryostat is a unique, non-clogging design for long-term operation. The Stirling/Zimmerman section is pressurized to 2.0 MPa by the helium compressor third stage to maximize the Stirling cycle efficiency. The regenerators for the four Stirling/Zimmerman stages consist of specially tailored thermal composite materials to achieve high effective heat capacity with low axial conduction losses, void volume, and susceptibility to clogging. The three-stage compressor and Stirling/Zimmerman pistons are driven by a mechanism known as the Ross linkage, which provides optimum Stirling cycle phasing with straight-line travel to minimize side forces and wear.

1.3 Test Plan Scope

The plan presented herein describes the test objectives and approaches to be used to facilitate and demonstrate the development of the proof-of-principles prototype system described above. The planned testing consists of component, subassembly, and system tests intended to evaluate the analyses, design, and performance of the prototype system. Not included are formal inspections and certifications of materials, processes, piece parts, and equipment, or environmental testing, which would otherwise be required to qualify the system for an actual application. It is anticipated that specific test methods and equipment may be refined as the development evolves. All testing is to be performed at General Pneumatics' Western Research Center (GP WRC) in Scottsdale,

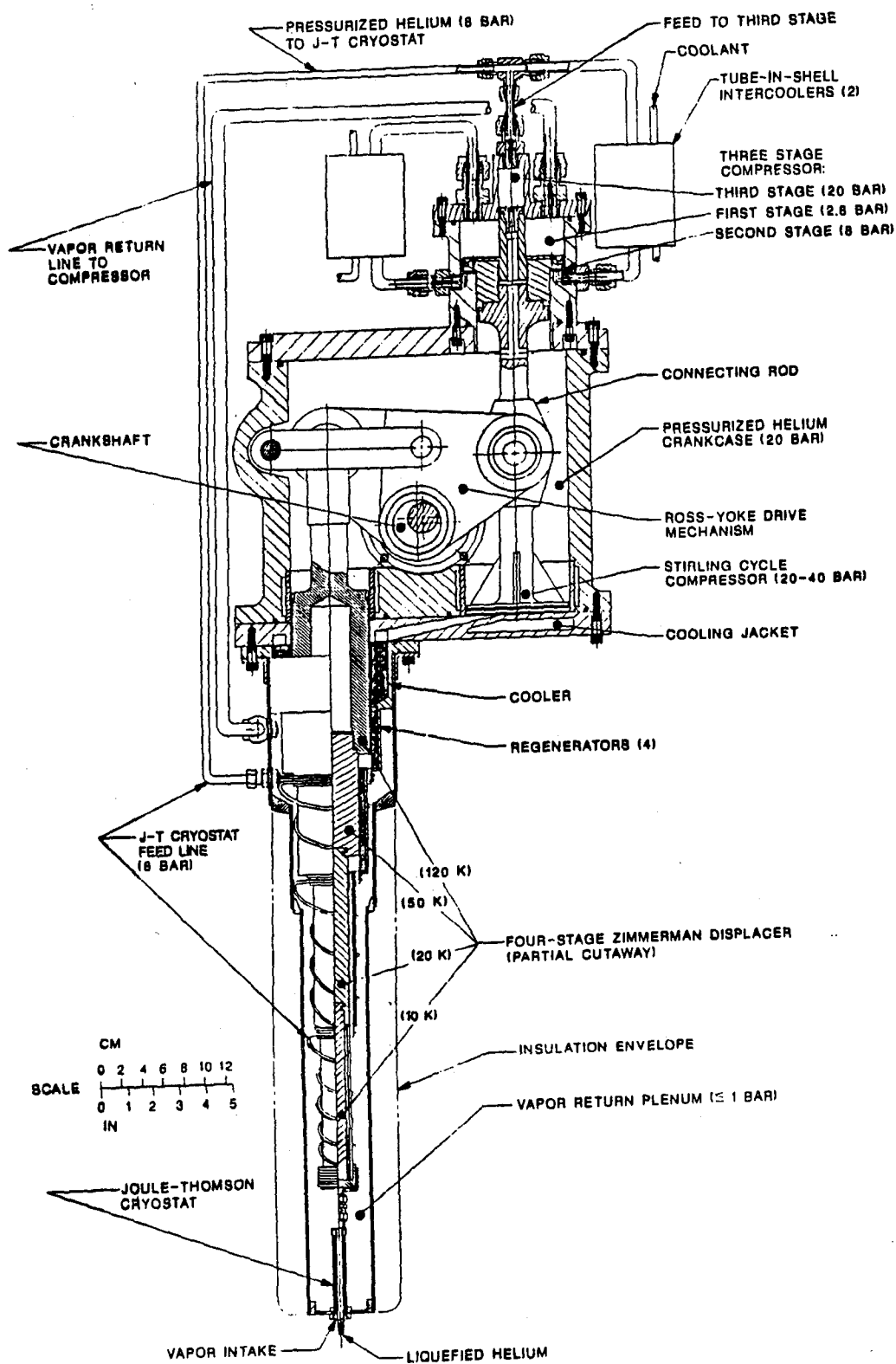


FIGURE 1. HELIUM RELIQUEFIER SYSTEM

Arizona, except for regenerator development testing which is to be carried out at Energy Science Laboratories (ESL) in San Diego, California.

1.4 Government Furnished Equipment

There is no planned requirement for government furnished equipment or facilities. However, any applicable expertise, information, or equipment, such as related to long-life bearings and lubricants for vacuum operation, evaluation of materials for outgassing, fabrication of composite materials, and dewars and instrumentation for cryogenic fluids, which might be made available would be welcomed.

1.5 Applicable Specifications

Due to the purely developmental nature of the project, there are no applicable test or performance specifications other than the Contract, F04611-89-C-0055, and the Contract Data Requirements List included therein.

2.0 TEST OBJECTIVES

2.1 Key Developments

The principal development of the project is that of employing a stepped displacer in a Stirling cryocooler to generate four successive stages of refrigeration down to a temperature of 10 K. Supporting developments include use of composite regenerators to achieve cryogenic thermal capacity with low thermal-fluid losses, incorporation of a non-clogging J-T cryostat for long-term liquefaction of helium, design of a compact three-stage compressor to drive the J-T cryostat and pressurize the Stirling cryocooler, and use of the Ross drive linkage to minimize piston side forces and seal wear.

There are no established analytical models or empirical data for designing a multi-stage Stirling cryocooler to reach 10 K. Even the optimization of single-stage Stirling cryocoolers, which typically operate near 80 K, is not well understood. Dr. J. E. Zimmerman, while working at the National Bureau of Standards, experimentally demonstrated that a stepped displacer in a Stirling cryocooler could reach temperatures down to about 7 K. But Dr. Zimmerman's simple displacer depended on the minimal regenerative thermal capacity inherent in the walls and the helium gas in the annular gaps between the displacer and cylinder, and generated only enough refrigeration to balance the parasitic losses. An objective of the present project is to analytically determine and experimentally verify the sizing of the expansion spaces, pressure cycle, and regenerator capacities to generate sufficient net refrigeration at each stage to cool the flow of helium to the J-T cryostat. Design issues to be tested include: providing an effective

combination of displacements, regenerator capacities, stroke, and speed; minimizing thermal-fluid losses; and maintaining running alignments and seals against pressure and thermal strains.

Effective design of the regenerators is essential to generating the designed refrigeration at each stage. This involves providing adequate thermal capacity without excessive thermal fluid losses, such as due to void volume, axial conduction, and fluid friction, and avoiding susceptibility to clogging. The specific heat capacity and thermal conductivity of conventional materials fall off with cryogenic temperatures, especially below 20 K. This makes it very difficult to effectively couple enough regenerator thermal mass to the helium working fluid. Thermal composite regenerators consist of alternating layers of high conductivity material separated by low conductivity, high capacity material so as to provide effective radial heat exchange with the working fluid with minimal axial conduction and flow passage volume or restriction. Essential provisions to be tested are proper design for adequate thermal capacity, transfer rate, and fluid flow, and selection of materials and bonding for structural and thermal stability and lack of outgassing. For backup contingency and test comparison, conventional regenerators are being designed and fabricated in parallel with the composite regenerators. Regenerators development and component testing are being carried out at ESL. Integration and testing of the regenerators in the Stirling cryocooler will take place at GP WRC.

To reliquefy the helium, the J-T cryostat must provide for near-isenthalpic expansion from the compressor pressure to the storage dewar pressure at the proper flow rate. Conventional J-T cryostats terminate in a simple, very small orifice, which is prone to clogging by trace contaminants in the flow. The J-T cryostat for the subject system has a precision-machined, conical annulus nozzle which is highly resistant to clogging. Key design parameters to be tested are sizing of the nozzle cone angle and flow annulus to produce the required pressure drop at the proper flow rate, and configuration of the coiled finned tubing within the cryostat and the feed line leading to the cryostat to effectively use the cooling available from the incoming boil-off vapor and the Stirling cryocooler. Approximately 90% of the cooling required for the pressurized helium flow, prior to expansion through the J-T nozzle, must be derived from the cold incoming boil-off vapor.

The three-stage compressor must intake helium at approximately 0.1 MPa and 300 K, generate the 0.8 MPa flow to the J-T cryostat, and maintain the 2.0 MPa pressurization of the Stirling cryocooler and crankcase with a minimum of internal leakage and wear. The compressor must also incorporate sufficient cooling to dissipate the heat of compression to the 300 K external coolant. Performance characteristics to be tested include: intake flow; second and third stage output pressure, flow capability, and temperature; input power; piston seals and valves leakage; and inspection for wear.

The purpose of the Ross drive linkage is to reciprocate the pistons of the Stirling cryocooler and the three-stage compressor with straight-line travel so as to minimize piston seal and guide side forces and wear. Metal bellows are incorporated behind the pistons to prevent contaminants, such as lubrication outgassing, from entering the cryocooler or compressor. Critical drive mechanism factors to be tested are: selection, alignment, and lubrication of bearings to minimize drag and wear; and suitability of the metal bellows to withstand reciprocation and pressure differential.

2.2 Organization of Testing

The planned testing is organized to evaluate the separate performance of the regenerators, the J-T cryostat, the three-stage compressor subassembly, and the Stirling/Zimmerman subassembly leading to the combined performance of the integrated system. The regenerators and the J-T cryostat will be tested as individual components. The three-stage compressor will be tested separately for measurements of its pressures, flow capacities, power requirement, and wear. Before installation of the J-T cryostat, the Stirling/Zimmerman subassembly with regenerators will be tested as a complete cryocooler in order to verify operation under actual pressure cycling and cryogenic thermal strains, measure the refrigeration generated at each expansion stage, and check for wear. The J-T cryostat will then be combined with the Stirling/Zimmerman subassembly to confirm the effectiveness of the helium feed line cooling and the liquefaction yield. Finally the three-stage compressor will be added for integrated performance testing of the complete system.

To provide the proper straight-line motion, the Stirling/Zimmerman subassembly and the three-stage compressor subassembly will each be driven by a Ross drive mechanism. This will provide a good basis for evaluating piston seals and guides wear, as well as drive mechanism performance and metal bellows suitability. Each crank-case will be adaptable to allow mounting of either subassembly alone or both together.

A flow diagram of the testing plan is presented in Figure 2.

2.3 Computer Model Correlation

An important objective of the testing is to provide for empirical refinement and verification of a computer model of the multi-stage Stirling cryocooler. The computer model is being developed in coordination with the analysis and design of the system. Once the computer model is confirmed by correlation with test data, it will be used to determine how the system thermodynamic performance might be improved.

The computer model will include design data defining the pistons, cylinders, and regenerators dimensioning and materials, strokes,

1990 | O | N | D | J | F | M | A | M | J | J | A | S | O | N | D | 1991 | J | F | 1992

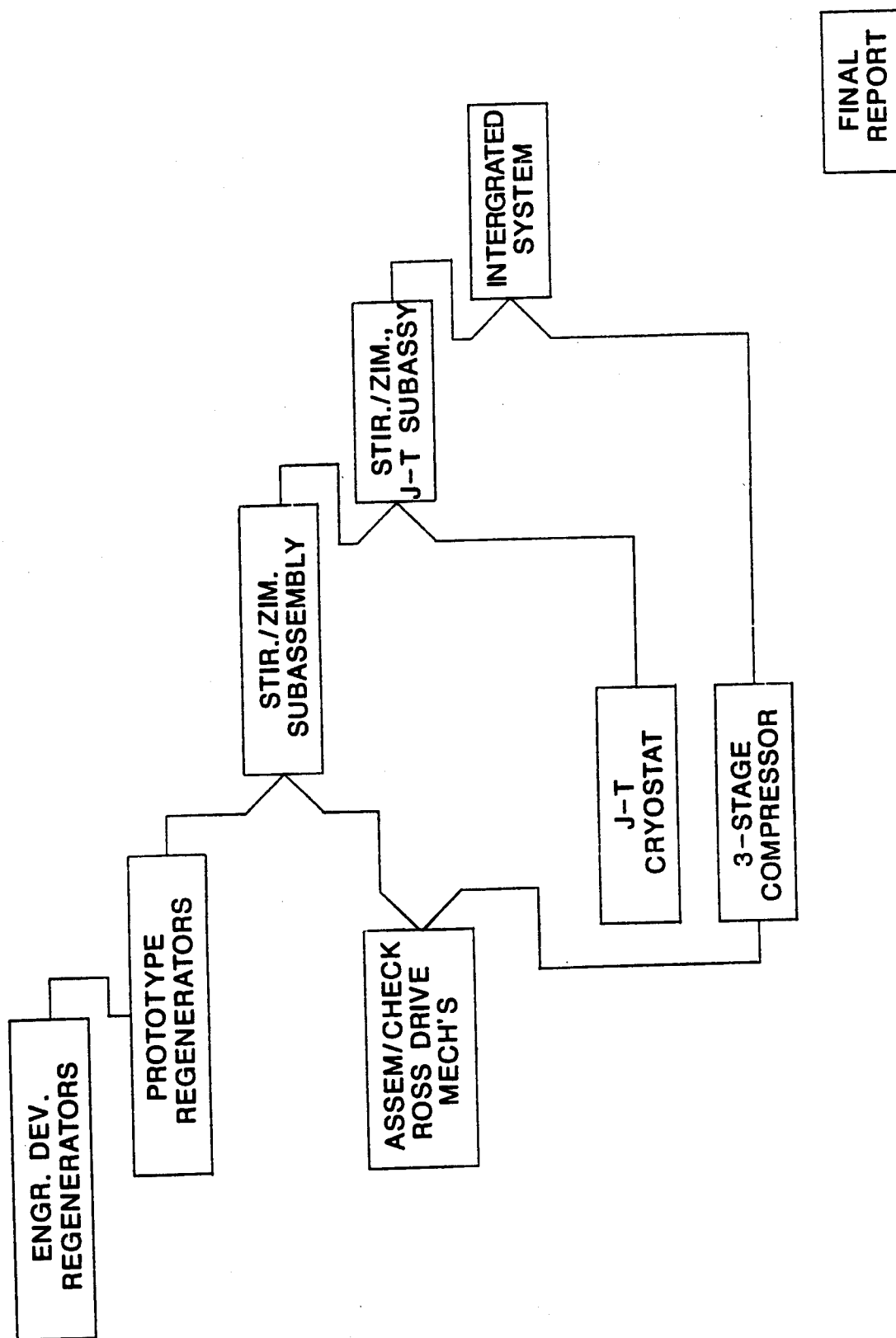


FIGURE 2. TEST PLAN FLOW DIAGRAM

phasing, speed, charge pressure, and assumed temperatures at each stage. The program will calculate the pressure cycle and refrigeration produced at each stage, various parasitic losses, power required, and heat dissipated. Testing of the Stirling/Zimmerman subassembly prior to installing the J-T cryostat will provide data on actual temperatures as affected by heat loads applied at each stage. The measured temperatures will be fed back into the computer model for comparison of the calculated versus applied heat loads. The computer model can then be adjusted to improve the correlation.

3.0 TEST METHODS

3.1 Regenerators

Component testing of the regenerators is to verify their suitability for incorporation into the Stirling/Zimmerman cryocooler, and to characterize their thermal properties for analysis of the cryocooler performance. Development and component testing of the regenerators will be carried out at ESL. Development will include: selection of materials for cryogenic thermal capacity and conductivity, material stability, and outgassing; forming and bonding methods; and computer modeling of thermodynamic performance. Testing of whole regenerators will include:

- resistance to cryogenic thermal shock
- flow pressure loss
- debris generation
- axial thermal conductivity
- radial heat transport rate and time constant using a pulsed heater in the regenerator bore
- heat exchange effectiveness using a single-blow transient test

ESL plans to initially fabricate and test engineering development regenerators to derive performance data and refinements needed, followed by prototype regenerators for installation in the Stirling/Zimmerman cryocooler.

3.2 J-T Cryostat

Component testing of the J-T cryostat is to measure its capability to liquefy helium as related to input pressure, temperature, and flow rate, and to verify its performance match with the three-stage compressor. The cryostat will be separately tested in a vacuum-insulated coldwell, supplied from a pressure-regulated tank of compressed helium, to measure flow rate and liquefaction yield as affected by inlet pressure and temperature. Liquefaction yield will be determined by measuring the power which can be dissipated by an electrical resistance heater in the coldwell without exceeding the helium boiling temperature. The helium flow to the cryostat will be cooled by routing the feed line through successive

dewars of liquid nitrogen, liquid neon, and liquid helium. The temperature of the helium input to the cryostat will be controlled by an electric heater on the feed line at the cryostat inlet. Parameters to be monitored are:

- helium flow rate
- cryostat inlet temperature and pressure (control variables)
- coldwell temperature
- voltage and current to the coldwell heater (control variable)

3.3 Three-Stage Compressor Subassembly

Testing of the three-stage compressor subassembly is to: confirm its capability to provide the proper pressure and flow to the J-T cryostat and maintain pressurization of the Stirling/Zimmerman at the system operating speed; measure its power and cooling requirements; check for internal leakage and wear; and verify the performance of the Ross drive mechanism and the metal bellows seal. The compressor drive mechanism will be the same as that in the completed system except the mounting interface for the Stirling/Zimmerman subassembly will be blanked off. Helium to pressurize the crankcase and to supply the compressor intake will be from a regulated compressed helium tank. Testing will include:

- proof pressure and leak checks
- operating speed (control variable about 300 rpm nominal)
- motor power input
- cooling water flow and temperature
- crankcase operating pressure
- pressure cycling inside the metal bellows (such as due to piston blow-by)
- inlet flow rate to the first stage (control variable to maintain 0.1 MPa inlet)
- pressure and temperature at the inlet and outlet of each stage
- pressure vs. flow rate available from the second and third stages
- inspection of cylinders, valves, and piston seals and guides for wear
- inspection of the drive mechanism and bellows seal for damage
- inspection of outlet filter/traps for wear debris
- accumulated operating time.

3.4 Stirling/Zimmerman Subassembly

Testing of the Stirling/Zimmerman subassembly is to: verify its mechanical design to withstand pressure, thermal strains, and maintain running alignments; measure the temperatures and refrigeration capacities produced at the expansion stages; and provide data for correlation with the multi-stage Stirling computer model. To generate the proper thermal and pressure strains, the subassembly will be operated as a complete cryocooler. This will require insertion of the Zimmerman cylinder into a test coldwell

dewar capable of containing liquid helium and saturated vapor. Liquid helium will be transferred from a commercial portable storage dewar to the test coldwell as needed to maintain saturated vapor in the coldwell.

The subassembly will be driven by a Ross mechanism the same as for the completed system except the mounting interface for the three-stage compressor will be blanked off. The Stirling/Zimmerman and crankcase charge pressure will be maintained from a regulated compressed helium tank. Electric resistance heaters and RTD temperature sensors will be installed at each Zimmerman expansion stage to measure temperature response to heat loads. The heat loads will be systematically applied to one stage at a time to characterize refrigeration capacities, and in combination to simulate cooling the helium flow to the J-T cryostat. Testing will include:

- proof pressure and leak checks
- operating speed (control variable about 300 rpm nominal)
- motor power input
- cooling water flow and temperature
- helium boil-off flow rate from test coldwell, nonoperating and operating
- crankcase operating pressure
- pressure cycling inside the metal bellows (such as due to piston blow-by)
- the Stirling working pressure cycle
- temperatures of the Stirling compression space and each Zimmerman expansion stage
- heat loads at each Zimmerman expansion stage (control variable)
- temperature and pressure start-up stabilizing time at zero applied heat load
- inspection for internal wear or contamination
- inspection of the drive mechanism and bellows seals for damage
- accumulated operating time.

3.5 Combined Stirling/Zimmerman and J-T Subassembly

Testing of the combined Stirling/Zimmerman and J-T subassembly, without the three-stage compressor, is to determine the helium flow rate which can be effectively cooled and liquefied, and the resulting Stirling/Zimmerman temperatures and power dissipation. Testing will be like that for the Stirling/Zimmerman subassembly, with the Zimmerman cylinder and attached J-T cryostat inserted in the test coldwell.

The heaters will be removed from the Zimmerman stages, and the temperature sensors will be placed on the J-T feed line coils at each stage. Flow to the J-T feed line will be from a regulated compressed helium tank. The J-T cryostat and Zimmerman cylinder will be enclosed so as to return the helium flow from the J-T

nozzle back along the cryostat finned tubing and feed line to cool the incoming flow and return to room ambient through a flow meter. The cryostat enclosure will have a heater and temperature sensor at the nozzle end for determining liquefaction yield.

Instrumentation and testing will be the same as for the preceding Stirling/Zimmerman subassembly testing except that applied heat load to the Zimmerman expansion stages will be from the cryostat feed line instead of heaters, and the cryostat liquefaction yield and flow rate will be measured. The results of this test, combined with the three-stage compressor subassembly test, will identify any provisions needed to match the operating speed, pressure, and flow requirements of the subassemblies for system integration.

3.6 System Integration

The last stage of system integration will be to join the three-stage compressor with the Stirling/Zimmerman and J-T subassembly to recirculate the helium through the cryostat and maintain system pressurization. System testing is to verify the compatibility of the subassemblies, determine the system start-up characteristics, and measure liquefaction rate, power input, and cooling requirements.

Instead of expelling the flow from the cryostat into the test dewar, as in an actual application, the cryostat will remain enclosed to recirculate the helium and allow measurement of the liquefaction rate as indicated by heater power absorbed at boiling temperature. Compressor inlet pressure and leakage make-up will be monitored and controlled as necessary through a pressure-regulated line from a compressed helium tank connected to the return flow line to the compressor. Wear debris samples will be collected for examination in in-line filters in the compressor second and third stage outlet lines. Disassembly inspections will be only as needed for trouble investigation or at termination of testing. Instrumentation and testing will include:

- proof pressure and leak checks
- operating speed (control variable about 300 rpm nominal)
- motor power input
- cooling water flow and temperature
- helium boil-off flow rate from the test coldwell with the system nonoperating and operating
- crankcase pressure
- return flow rate to the compressor
- make-up flow rate and pressure to the compressor (control variable about 0.1 MPa nominal)
- output pressures and temperatures of compressor second and third stages
- the Stirling working pressure cycle
- temperatures of the Stirling compression space, the cryostat feed line at each Zimmerman expansion stage, and the return

- flow line at the Zimmerman enclosure exit
- heater power and temperature at the cryostat nozzle enclosure (control variable)
- temperature and pressure start-up stabilizing time at zero and one watt nominal heat load applied to the cryostat
- accumulated operating time.

4.0 TEST EQUIPMENT

The following is a consolidated list of test equipment, most of which is used in multiple tests as described in the preceding section.

- drive motor - Inland RBEH-6201-B02
- motor controller - Inland BDAS-24030-001 servo amplifier and 90A/240V power supply
- digital tachometer with proximity switch - Shimpo DT-3
- system test stand - custom
- system test coldwell - adapt research dewar such as Janis 7 RD
- J-T cryostat test coldwell - custom
- J-T cryostat test precooled dewars (3) - Cole Palmer N-03774-30
- LHe, LNe, LN₂ supply dewars - commercial rental
- LHe level gauge - Andonian A-7
- 8-channel diode RTD cryogenic thermometer - Lakeshore 208
- digital RTD thermometer - Omega 661
- 30-channel RTD, TC and mV hybrid recorder - Yokagawa 8031
- RTD temperature sensors - Lakeshore, various diode and carbon/glass types
- thermocouple temperature sensors - Omega, various types
- turbo vacuum pump - Varian V-80
- mechanical vacuum pump - Varian SD-200
- vacuum gauge controller - Varian 843
- vacuum ionization gauge - Varian 571

vacuum thermocouple gauges - Varian 0531

pressure transducers - CEC 4-390-0125, Dayronic 502 + 15D
Whittaker 100277-1, XTM-190-500G

pressure transducer bridge amplifiers - Gould 747, 757

compressed gas pressure gauges - Ashcroft, Weksler, Norgren,
various ranges

compressed gas pressure regulators - Tescom, Airco, various
ranges

turbine flowmeter - Flow Technology FT6

rotameter flowmeters - Aalborg, Gilmont, various ranges

flexible film heaters - Minco, various

dc power supplies - Sorenson DCR8-12B, RCA WP-704A

digital multimeters - Kiethley 197, Fluke 77

temperature transducer calibrator/readout - Promac DHT-8205

oscilloscope - Tektronix 564 (dual-trace, storage)

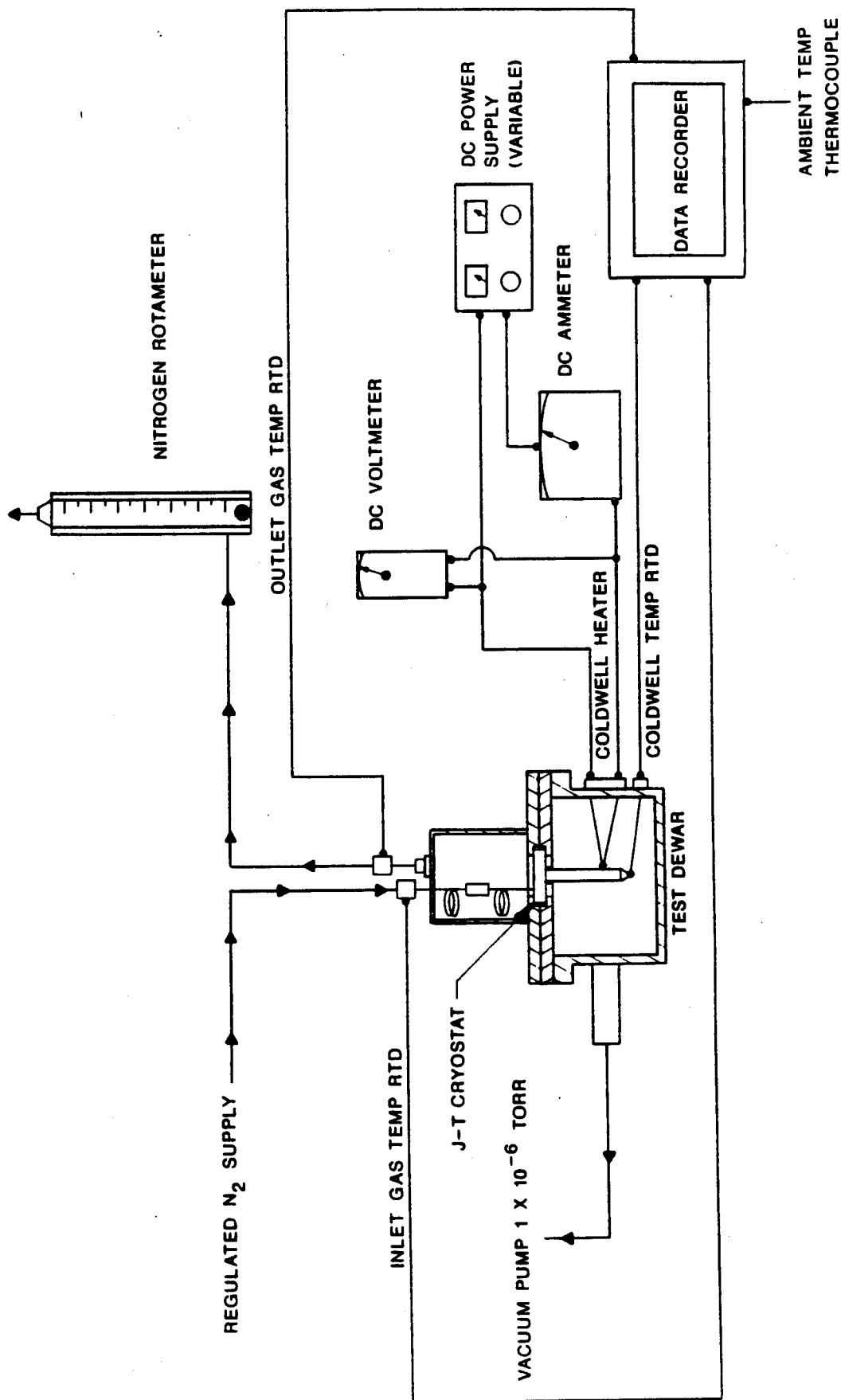


FIGURE 3. J-T CRYOSTAT LEAKAGE/FLOW/PERFORMANCE TEST WITH N₂

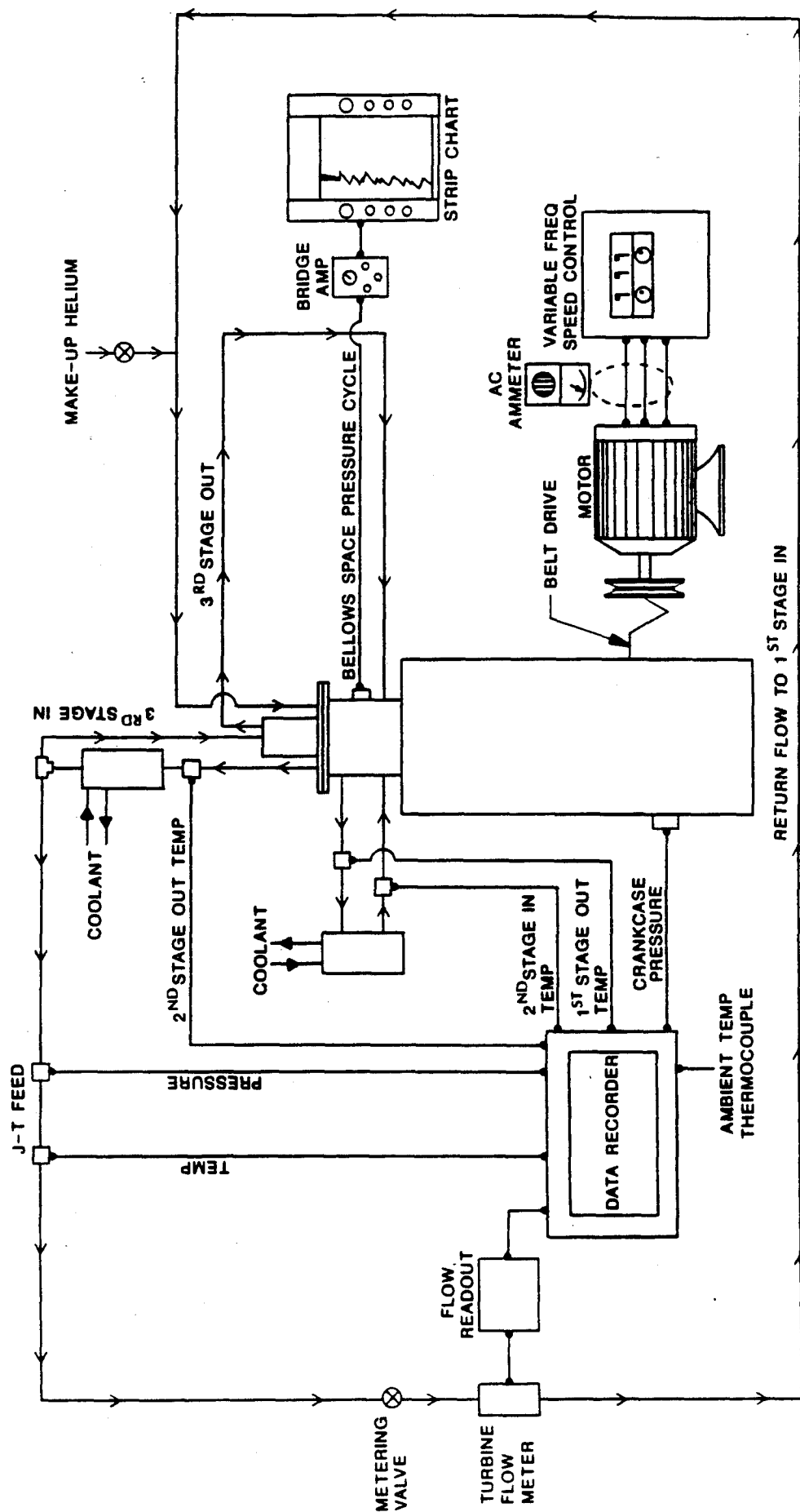


FIGURE 4. THREE-STAGE COMPRESSOR TEST

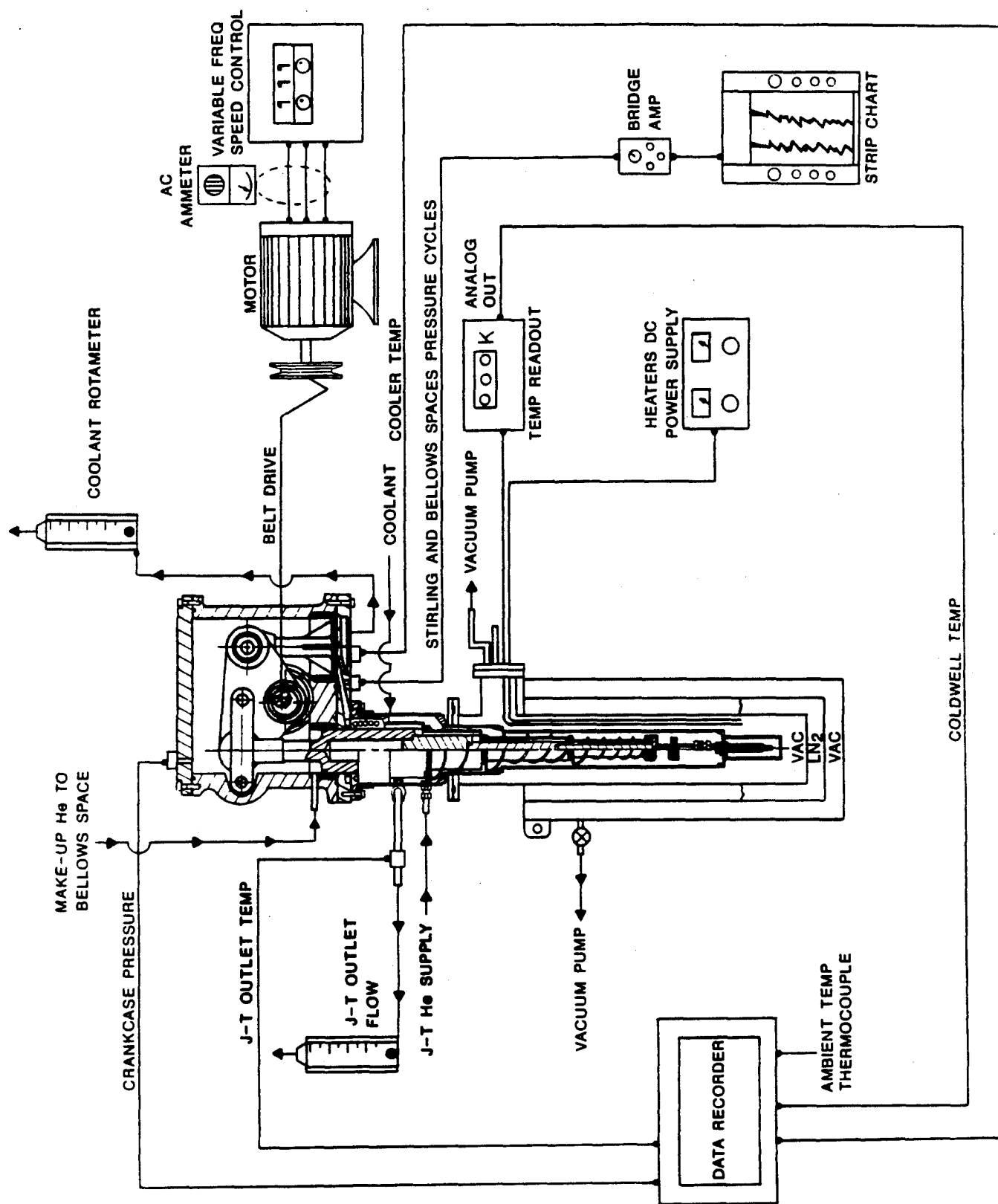


FIGURE 6. STIRLING/J-T SUBASSEMBLY TEST IN DEWAR

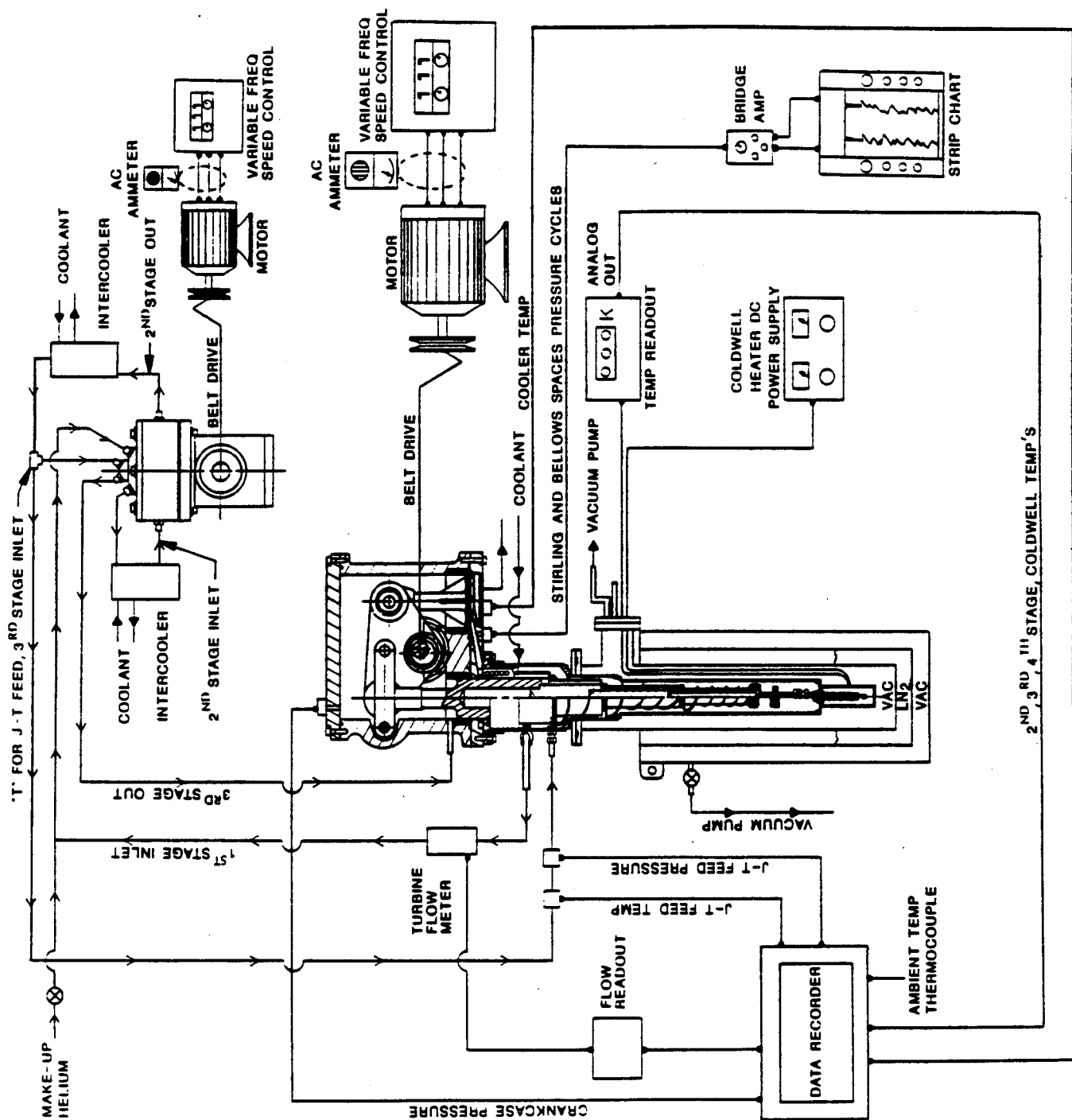


FIGURE 7. INTEGRATED SYSTEM TEST IN DEWAR

DISTRIBUTION LIST

AUL/LSE
Bldg 1405 - 600 Chennault Circle
Maxwell AFB, AL 36112-6424

1 cy

DTIC/OCC
Cameron Station
Alexandria, VA 22304-6145

2 cys

AFSAA/SAI
1580 Air Force Pentagon
Washington, DC 20330-1580

1 cy

PL/SUL
Kirtland AFB, NM 87117-5776

2 cys

PL/HO
Kirtland AFB, NM 87117-5776

1 cy

Official Record Copy

PL/VTPT/Capt Jeff Wiese

2 cys

Dr. R. V. Wick
PL/VT
Kirtland, AFB, NM 87117-5776

1 cy